SISSA
Scuola
Internazionale
Superiore di
Studi Avanzati

Rho GTPases in Glioblastoma Mechanobiology

Thesis submitted for the degree of Doctor of Philosophy

Departerment of Neurobiology

Candidate: Xu Jing

Supervisor: Vincent Torre

.2020.

OFFICE NAME

Via Bonomea, 265
34136Trieste – Italy
T +39 0403787111
E info@sissa.it
sissa.it

"I wish I were a gardener

digging away at the garden with

nobody to stop me from digging."

Rabindranath Tagore

"如切如磋，如琢如磨。"

《诗经》

Abstract

Brain tumors are a source of morbidity and mortality worldwide, especially in children and young adults. Due to the high rates of inherently disabling effects (such as personality changes, visual disturbances, and poor coordination), many patients with brain tumors cannot live independently. Gliomas are one of the most common CNS tumors. Over 70% of gliomas are malignant, of which glioblastoma (GBM, WHO grade IV) is the most common and fatal brain tumor.

The high-grade brain tumor cells (e.g., GBM cells) diffuse into the surrounding healthy tissue and promote a rapid tumor progression. Despite decades of extensive clinical and biological research, the mean survival time of patients with GBM is no more than 15 months following diagnosis. New perspectives and new approaches are needed for a better understanding on GBM progression and ultimately limit GBM invasion and recurrence.

Eukaryotic cell migration is a multi-step process. Cells usually undergo cycles of extending membrane protrusion in the cell front, forming adhesion to interact with the surrounding microenvironment and contracting by actomyosin at the cell rear. Rho GTPases have been reported to play crucial roles in all these steps. Rho GTPases can alter their expression in cancer or cooperate with growth factor receptors to control cell invasion and metastasis. Abnormal expression, organization, and post-translational modification of ECM molecules are observed in solid tumor ECM, further stiffening the tissue ECM. The mechanics and organization of ECM can also regulate or modulate cell migration.

During my PhD study, I have demonstrated that Rho GTPases and mechanical cues play critical roles in the GBM cell invasion. The main results of my thesis are as follows:

1. Rac1 depleting or inhibition dramatically reduces GBM cell invasion and changes their morphology with an abnormal cell cytoskeleton organization, myosin IIa location, and cell adhesion formation.
2. The Erk1/2 signaling is involved in Rac1 induced GBM cell invasion.
3. Inhibition of Rac1 changes GBM cell rigidity and viscosity.

Acknowledgement

It's not easy at my age to decide to go back to school abroad after five years' dwell time. Thanks to SISSA for applying me such a great opportunity. Thanks to my supervisor Vincent Torre, for the continuous support of my PhD study and research, for his kindness, and offering me the chance to go around and learn. Thanks to Prof. Yang Yili, who introduced SISSA to me and always encourage me when I encounter difficulties and frustrations. Thanks to Prof. Marco Lazzarino, for giving me the opportunity to learn AFM in his lab at IOM.

I benefit a lot from seminars and lectures SISSA prepared during my entire Ph.D. study. It's amazing to listen to the lectures hold by John Graham Nicholls, who written 'from neuron to brain,' the first book I read about neuroscience.

I would like to thank my colleagues and friends: Nicola Galvanetto and Zhong Jieye in AFM, Simone Mortal and Li Xiaoyun in live-cell imaging, Song Qin and Xiao Miao in Nanomaterials, Hou Xiaodan, Xu Xin and Liu Yaofu in Cancer biology, Feng Yuan in Bioinformatics, and also Sun Kaiwen in Mathematics, for discussing with me and offering great help. I also would like to thank my classmates and friends in Trieste for all the fun we have had in the four years.

Finally, I would like to thank my family: my parents, my sister, my husband and my little boy, for their love, encouragement and supporting anytime and anywhere.

List of Publications

Peer reviewed publication:

1. Xu, J., et al., Rac1 Promotes Cell Motility by Controlling Cell Mechanics in Human Glioblastoma. Cancers (Basel), 2020. 12(6).

INDEX

Abstract 2

Acknowledgement 3

List of Publications 4

Chapter1. Introduction 6

1.1 Overview of Central Nervous System (CNS) Tumors 6

1.2 Glioblastoma Classification and Therapy 8

1.3 Mammalian Rho GTPases 12

1.4 Mechanosemsitive Piezo ion Channels 24

1.5 Complexities of Extracellular Matrix (ECM) 26

1.6 Mechanical Properties of Single Cells 27

1.7 ECM and Cell Migration 28

1.8 Atomic Force Microscopy 31

Chapter 2. Results 34

2.1 Rac1 Promotes Cell Motility by Controlling Cell Mechanics in Human Glioblastoma 35

2.2 Molecular mechanisms of the blockage of glioblastoma motility 56

Chapter 3. Supplementary Materials 84

3.1 The Effect of the Substrate on GBM Cell Motility 85

3.2 The roles of Piezo1 on GBM cell Response to Substrate 97

Chapter 4. Conclusion and Future Perspectives 106

References 107

Chapter1. Introduction

1.1 Overview of Central Nervous System (CNS) Tumors

CNS tumors are the heterogeneous groups of neoplasms, due to the out-of-control growing of healthy cells in the brain, the spinal cord, meninges or cranial nerves (Table 1) [1]. Although CNS tumors rarely happen in adults, they are still a substantial source of morbidity and mortality worldwide, especially in children and young adults. In 2016, there were approximately 330,000 new cases and 227,000 deaths of CNS cancer globally. Notably, the CNS cancer incidence rate is significantly increased by 17.3% in the decades between 1990 and 2016 [2]. Another serious situation is that CNS cancer was also responsible for approximately 7.7 million disability-adjusted life-years (DALYs) at the global level [2]. Due to the high mortality rates and inherently disabling effects (such as personality changes, visual disturbances and poor coordination), these patients often cannot live independently.

WHO CLASSIFICATION OF TUMOURS OF THE CENTRAL NERVOUS SYSTEM	
Diffuse astrocytic and oligodendroglial tumors	**Ependymal tumors**
WHO II	**Other gliomas**
◆ Diffuse astrocytoma, *IDH*-mutant	**Choroid plexus tumors**
■ Gemistocytic astrocytoma, IDH-mutant	**Meningiomas**
◆ Diffuse astrocytoma, *IDH*-wild-type	**Mesenchymal, non-meningothelial tumors**
◆ Diffuse astrocytoma, not otherwise specified	**Neuronal and mixed neuronal-glial tumors**
◆ Oligodendroglioma, *IDH*-mutant and 1p/19q-codeleted	**Tumors of the pineal region**
◆ Oligodendroglioma, not otherwise specified	**Embryonal tumors**
◆ Oligoastrocytoma, not otherwise specified	**Tumors of cranial an paraspinal nerves**
	Melanocytic tumors
	Lymphomas
WHO III	**Histiocytic tumors**
◆ Anaplastic astrocytoma, *IDH*-mutant	**Germ cell tumors**
◆ Anaplastic astrocytoma, *IDH*-wild-type	**Tumors of the sellar region**
◆ Anaplastic astrocytoma, not otherwise specified	**Metastatic tumors**
◆ Anaplastic oligodendroglioma, *IDH*-mutant and 1p/19q-codeleted	
◆ Anaplastic oligodendroglioma, not otherwise specified	
◆ Anaplastic oligoastrocytoma, not otherwise specified	
WHO IV	
◆ Glioblastoma, *IDH*-wild-type	

- Giant cell glioblastoma,
- Gliosarcoma
- Epithelioid glioblastoma

- Glioblastoma, *IDH*-mutant
- Glioblastoma, not otherwise specified
- Diffuse midline glioma, *H3-K27M* mutant

Other astrocytic tumors

Table 1 The 2016 World Health Organization Classification of Tumors of the Central Nervous System. This table has been abridged and modified from the World Health Organization classification [1].

1.1.1 Risk Factors

Few known risk factors are associated with CNS tumors. Ionizing radiation (e.g., atomic weapon radiation) is the only well established environmental risk factor for primary CNS tumors [3]. Non-ionizing radiation (particular cell phone radiation), hormonal factors, low-frequency magnetic fields, and industrial exposures have shown no clear associations with the risk of CNS tumors [4-8]. Several genetic syndromes are associated with increased the risk of CNS tumors, but less than 5% of primary CNS tumors are due to these predisposition syndromes [9-10]. Studies also showed the inverse correlation between allergic diseases and glioma [11-12]. Still, all these associations remain controversial and additional studies are needed.

1.1.2 Clinical Presentation

Both malignant and benign CNS tumors can present with focal or generalized symptoms. These symptoms depend on the size, type, and location of tumors. Generalized symptoms often reflect increased intracranial pressure, headache, nausea, vomiting and visual disturbances [13-15]. While focal symptoms reflect the intracranial location of tumor, for example, the tumors located in the temporal lobe result in changes in personality.

1.1 .3 Diagnosis and Treatment

Clinical presentation can only provide some clues about whether or which part could be affected by CNS tumors. To diagnose a CNS tumor, the standard imaging test needed is magnetic resonance imaging (MRI) [16-17]. In addition, functional MRI, perfusion MRI, and magnetic resonance spectroscopy may help to evaluate the tumor and plan the treatment. Sometimes, computerized tomography (CT) is recommended to find cancer in other parts of the body. The treatment for a CNS tumor depends on the patient age, the

location and grade of the tumor, and the possible presence of another cancer. Usually, the effective treatments include neurosurgical surgery, and depend on whether the tumor is cancerous or not combined with radiation, and chemotherapy [18].

1.1.4 Pathological Classification

The use of different classification systems creates confusion. It is indispensable to establish a standard system to assess the prognosis and therapy of CNS tumors. Since the last century, the World Health Organization (WHO) has started to establish a pathologic classification and grading system of CNS tumors, which can be accepted and used worldwide. The traditional classification of CNS tumors is based on histological and immunohistochemical phenotype. Histological phenotype depends on hematoxylin and eosin stains to assess the origin and differentiation levels (which also determine the WHO grade of CNS tumors), while immunohistochemical phenotype associates with the expression of lineage-associated proteins and ultrastructural characterization. According to the 2016 version of the WHO classification of CNS Tumors System, molecular parameters are added to enable a more precise tumor categorization. Furthermore, combining epidemiology, clinical signs and symptoms, imaging, prognosis and predictive factors into diagnoses is also necessary [1].

1.2 Glioblastoma Classification and Therapy

Gliomas are one of the most common CNS tumors in adults. These tumors are of neuroectodermal origin and arise from glial or precursor cells [19]. Over 70% of gliomas are malignant, of which glioblastoma (GBM, WHO grade IV) is the most common and fatal brain tumor. According to the *IDH* mutations, GBMs are divided into three types in the 2016 CNS WHO classification of CNS Tumors System (Table1) [1].

1. GBM, *IDH*-wildtype (about 90 % of cases). This GBM subtype typically is defined as ‘primary GBM’-that is, these tumors begin as a Grade IV tumor with no evidence of a pre-existing lower grade precursor and tend to be more aggressive. GBMs that develop de novo predominate in patients over 55 years of age [20].

2. GBM, *IDH*-mutant (about 10 % of cases). This GBM subtype is secondary GBM, which means that these tumors progress from a pre-existing lower-grade astrocytic tumor (Grade II or Grade III). In general, these tumors tend to arise in young patients [21].

3. GBM, not otherwise specified, in which full *IDH* evaluation cannot be performed.

Here I enumerate the main molecules and their signal pathway that involved in GBM. The detail molecular and genetic epidemiology in adult GBM is described below (Table 2):

1. The pentose phosphate pathway: *IDH1* or *IDH2* gene, which encodes cytoplasmic isocitrate dehydrogenase and mitochondrial isocitrate dehydrogenase, respectively. These enzymes can convert isocitrate to α-ketoglutarate and produce NADPH [22].

2. P53 and its regulators: P53 is a tumor suppressor, it is essential for regulating DNA repair and cell division. *TP53* can produce P53 protein. *MDM2* encodes a nuclear localized E3 ubiquitin ligase, and *MDM4* encodes a nuclear protein that has similar structural to MDM2. Both MDM2 and MDM4 can bind the p53 protein and inhibit its activity.

3. PI3K (phosphatidylinositol 3-kinase) signaling: PI3K signaling is essential for many cell activities, such as cell proliferation, cell movement and cell survival. *PIK3CA* gene can produce the catalytic subunit of PI3K, called p110α protein, while *PIK3R1* gene can produce the regulatory subunit of PI3K; the most abundant one is called p85α.

4. Cyclin-dependent pathway genes: *CDK4* and *CDK6* gene encode proteins belonging to the Ser/Thr protein kinase family. These kinases are catalytic subunits of the protein kinase complex and are crucial for cell cycle G1 phase progression. *CDKN2A* gene can encode p16 (INK4A) and p14 (ARF) proteins. The p16 (INK4A) protein binds to CDK4 and CDK6 and regulates the cell cycle, while p14 (ARF) protein can protect p53 from being degenerate. *CDKN2B* gene encodes a cyclin-dependent kinase inhibitor, which forms a complex with CDK4 or CDK6, and prevents the activation of the CDK kinases.

5. Mitogenic RTKs: *EGFR* gene and *PDGFRA* gene encode epidermal growth factor receptor (EGFR) and platelet-derived growth factor receptor alpha (PDGFRA), respectively, which both control many vital cellular processes, such as cell proliferation and cell survival. *MET* gene encodes a member of the receptor tyrosine kinase family of proteins and the product of the proto-oncogene MET.

6. Telomere maintenance: Telomerase enzyme consists of two major components, hTERT and hTR. These two parts then work together as a telomerase enzyme. *TERT* gene encodes the hTERT protein.

7. Chromatin remodeling complexes: *ATRX* gene encodes a protein which may involve in chromatin remodeling.

8. *NF1* (Neurofibromatosis type 1) gene encodes a protein that changes skin coloring and the growth of tumors.

9. MGMT (O6-methylguanine-DNA methyltransferase) repairs DNA damage, methylation of the MGMT promoter silences the MGMT gene.

Characteristic	Glioblastoma, *IDH*-wild type	Glioblastoma, *IDH*-mutant
Genetic	*TERT, TP53, PIK3CA, PIK3R1, NF1, H3F3A-G34* and *PDGFRA1* mutation; *PTEN* mutation or homozygous deletion; *CDKN2A* or *CDKN2B* deletion; *EGFRvIII* rearrangement; *EGFR, PDGFRA, MET, CDK4, CDK6, MDM2, MDM4* amplification	*IDH1* or *IDH2, TP53, ATRX* mutation; *CDKN2A* or *CDKN2B* deletion
Epigenetic	~40% *MGMT*-promoter methylation	~90% *MGMT*-promoter methylation; G-CIMP
Chromosomal	Trisomy 7 or 7q gain; monosomy 10 loss; double minute chromosomes	Trisomy 7 or 7q gain; LOH 17p; Chromosome 10q loss
Median age at diagnosis (years)	59	38
Median overall survival (years)	1.2	3.6

Table2 Common Genetic, Epigenetic and Chromosomal Aberrations Associated with the Major Glioblastoma Entities [23-24]. This table has been abridged and modified from Nat Rev Clin Oncol 14, 434–452 (2017) and Nat Rev Neurol 15, 405–417 (2019). EGFRvIII: EGFR variant III; G-CIMP: glioma CpG-island methylator phenotype (excludes frequent MGMT-promoter methylation).

The treatment of GBM remains a challenge. In order to improve the survival time of patients, lots of efforts are needed to refine neurosurgical techniques, radiotherapy, and the discovery of powerful therapeutic agents. Nowadays, many therapeutic agents have been entering into clinical trials, which mainly target the growth factor receptors and their downstream pathways, cell cycle, epigenetic modulators, angiogenesis, and antitumor immune responses.

Here are some examples:

The inhibitors of tyrosine kinase receptor pathways, which include the EGFR blocker, depatuxizumab

mafodotin, an antibody-drug conjugate [25]; MET antibody, onartuzumab and the inhibitor of both MET, VEGFR2 and AXL, cabozantinib [26-28]; and the oral pan-FGFR (Fibroblast growth factor receptor) kinase inhibitor, JNJ-42756493 [29]. The pan-PI3K inhibitor, buparlisib, is used to block the activation of PI3K/AKT/mTOR signaling [30]. Palbociclib and TG02, a multi-CDK inhibitor mainly targeting CDK9, are used to block the retinoblastoma (pRB) pathway [31-32]. Due to the important role of tumor suppressor p53, many trials are also focused on this pathway [33-34]. TERT is one of the components of the telomerase enzyme, which often mutate in *IDH*-wild type GBM. Eribulin, the inhibitor of tubulin polymerization, also exerts a TERT inhibitory activity [35]. Proteasomes play a central role in degrading unneeded or damaged proteins, and their inhibitors potently induce apoptosis in many types of cancer cells. Marizomib, the brain-penetrant pan-proteasome inhibitor, has been used for clinical trials of GBM [36]. Angiogenesis is the formation of new blood vessels, which can provide nutrients and oxygen for tumor cells to grow and spread. Bevacizumab is used in GBM to block vascular endothelial growth factor (VEGF) for angiogenesis [37-38]. Cilengitide can inhibit the malignancy of GBM by inhibiting specific integrins [39]. TGF (Transforming growth factor)-β is a key molecule responsible for immunosuppression. TGF-β2-specific antisense oligonucleotides and tyrosine kinase inhibitors, galunisertib, are used to block the immunosuppression in GBM [40-42].

MGMT-promoter methylation is ubiquitous in GBM, especially in *IDH*-mutant GBM. Lots of strategies are used to target this change, including:

1) monofunctional methylating agents, temozolomide (TMZ) [43];

2) histone deacetylase inhibitors, panobinostat and valporic acid [44-45];

3) levetiracetam, an AMPA receptor antagonist, can decrease MGMT protein and mRNA expression levels in the cell [46].

Well-known repurposed drugs, which can cross blood-brain-barrier (BBB), also provide a strategy to treat GBM. Propentofylline, a vascular dementia and Alzheimer's disease drug, can target the orphan receptor in the Tumor Necrosis Factor Receptor (TNFR) signaling [47]. Pimozide, an antidepressant and antipsychotic drug, can inhibit protumorigenic activities [48]. Chlorpromazine, an antipsychotic drug, inhibits protumorigenic activities [49]. Metformin, an anti-diabetic drug, can modulate metabolism, lower glucose availability, suppress of insulin-like growthfactor signaling, and specifically inhibit of AMP-activated protein

kinase, which is expected to affect the survival of GBM cells [50].

Immunotherapy is a type of biological therapy that helps patients' immune systems to fight cancer. Regulating the expression of PD-1 and PD-L1 can modulate the response to immune checkpoint blockade [51]. Investigating of dendritic cell (DC) vaccines, activated natural killer (NK) cells and chimeric antigen receptor (CAR) expressing T cells (CAR-T) or CAR-expressing NK cells (CAR-NK) are promising new ways for the treatment of GBM.

Furthermore, improving the efficiency of the drugs delivery across BBB is also important. Such procedures may include using nanobiotechnology-based drug or nanoparticles for drugs delivery.

1.3 Mammalian Rho GTPases

Small GTPases superfamily is formed after the discovery of the Ras oncogene. They are typically between 20-25 kDa. Mammal Rho GTPases comprise a family of 20 members (Table3). Like other GTPases, most of them cycle between an inactive GDP-bound form and an active GTP-bound form. Active GTPases then switch on the downstream signaling events by binding to effectors. This cycling of Rho GTPases between active and inactive states is controlled by guanine nucleotide-exchange factors (GEFs), GTPase-activating proteins (GAPs) and guanine nucleotide-dissociation inhibitors (GDIs) (Figure1) [52-54]. Rho GEFs include two families, which contain either a Dbl-homology (DH) domain (at least 70 members) or a Dock Homology Region (DHR) domain (11 members) [55]. Rho GAPs (70 members in mammals) contain a unique catalytic domain. Both GEFs and GAPs are essential regulators for GTPases activity. GEFs can modify the nucleotide-binding site of G protein and decrease its affinity to the nucleotide. Thus, the nucleotide is dissociated from the G protein and subsequently replaced. In general, the affinity of the G protein for GTP and GDP is similar, so more abundant GTP is needed for the GTP-bond. GTPases can hydrolyze GTP at a very slow rate. However, GAPs can help GTPases to accelerate the GTP hydrolysis rate [56]. Rho GTPases carry either a farnesyl pyrophosphate (FPP) or geranylgeranyl pyrophosphate (GGPP) at their C-terminus for their localization and interaction [57]. Rho GDIs (3 members in mammals) can recognize the inactive GTPases and remove them from the membrane [58]. Besides, Rho GTPases signaling can also be regulated by gene expression, the post-transcriptional (e.g., micro RNA) and post-translational modifications. For example, lipid modifications determine Rho GTPases localization, phosphorylation and sumoylation

regulate GTPases activity, and ubiquitylation modulate their protein levels (Figure1) [59-60].

Furthermore, Rho GTPases are critical linkers in many chemokine receptors and growth factor receptors signaling pathways. The spatial and temporal segregation of their active state can efficiently regulate their function. Currently, Rho GTPases play important roles in regulating neuronal development, morphogenesis, cell-cycle progression, gene expression, cytoskeleton dynamics, vesicle trafficking, cell division, migration and adhesion [61-65].

Subfamilies	Rho GTPase	GTPase activity	Prenylation	Expression pattern
Rho	RhoA	Yes	GG	Ubiquitous
	RhoB	Yes	GG, F	Ubiquitous
	RhoC	Yes	GG	Ubiquitous
RhoD/Rif	RhoF (Rif)	Yes	GG, F	Hematopoietic system
	RhoD	Yes	F	Skin, esophagus
Rnd	Rnd1	No	F	Brain, liver, lung
	Rnd2 (RhoN)	No	F	Brain, testis
	Rnd3 (RhoE)	No	F	Widespread
Rac	Rac1	Yes	GG	Ubiquitous
	Rac2	Yes	GG	Hematopoietic system
	Rac3	Yes	GG	Brain, testis
	RacG	Yes	GG	Hematopoietic system
Cdc42	Cdc42	Yes	GG	Ubiquitous
	RhoQ (TC10)	Yes	F	Ubiquitous
	RhoJ (TCL)	Yes	F	Female tissues, smooth muscle, lung
Wrch/Chp	RhoU (Wrch-1)	Yes, but high intrinsic GEF	No	Ubiquitous
	RhoV (Wrch-2, Chp)	Yes, but high intrinsic GEF	No	Esophagus, skin
RhoH	RhoH (TTF)	No	GG, F	Hematopoietic system
RhoBTB	RhoBTB1	No	No	Placenta, skeletal muscle, kidney, testis
	RhoBTB2		No	Lung, brain, small intestine

Table 3 The Rho GTPase Family [66]. Grouping based on similarity of the GTPase domain. Rho GTPase: gene name (alternative name). GTPase activity: Rho GTPases without GTPase activity are constitutively active. Prenylation: GG (Geranylgeranylation), F (Farnesylation).

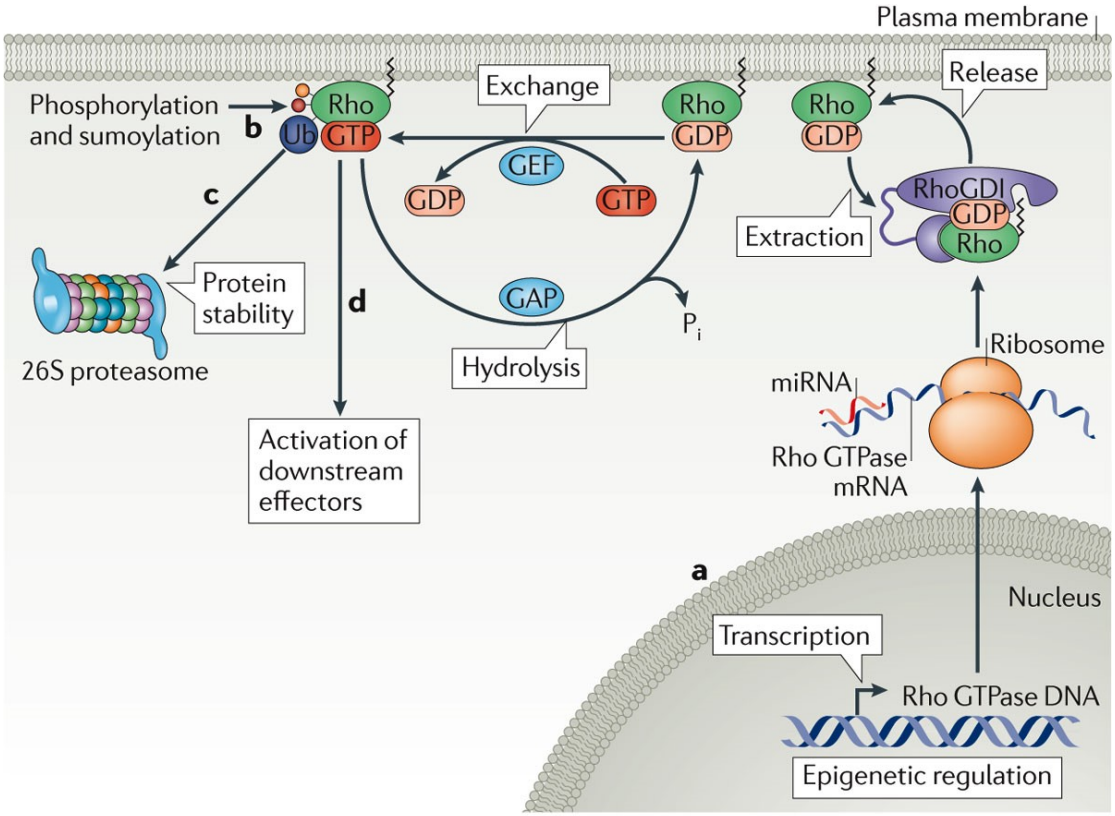

Figure 1 Overview of Rho GTPase Regulation [59]. The route from Rho GTPase protein expression to effector protein activation is tightly regulated. Guanine nucleotide exchange factors (GEFs), GTPase-activating proteins (GAPs) and guanine nucleotide dissociation inhibitors (GDIs) constitute the classic regulatory proteins that regulate the GTPase cycle. GEFs activate Rho GTPases by catalysing the exchange of GDP for GTP, whereas GAPs greatly stimulate the intrinsic GTPase activity of Rho GTPases and inactivate them. GDIs extract prenylated Rho GTPases from the membrane by binding the isoprenoid moiety and sequester them away in the cytoplasmic compartment. Unconventional mechanisms of regulating Rho GTPases are becoming more apparent. (a) Rho GTPase expression can be controlled at the transcriptional level by epigenetics and at the translational level by the action of microRNAs (miRNAs). (b) Post-translational covalent modifications of Rho GTPases, including phosphorylation and sumoylation, can result in the activation or inactivation of Rho GTPases, depending on the cellular context. (c) Protein levels of Rho GTPases can be acutely regulated by the ubiquitin–proteasome system. (d) The combination of classical and unconventional regulatory mechanisms ensures the appropriate spatiotemporal activation of the Rho GTPases during various cellular processes, including regulation of cytoskeletal dynamics, cell polarity and survival.

1.3.1 Actin Dynamics

In eukaryotic cells, actin dynamics are regulated by the coordination of polymerization factors (e.g., Arp2/3 and formin), filament severing and capping proteins (Figure2). Briefly, Cdc42-GTP directly targets N-WASP (Wiskott-Aldrich syndrome protein) or Toca-1 (transducer of Cdc42-dependent actin assembly) and exposes N-WASP C-terminal site for Arp2/3 binding and activation [67-68]. WAVE complex consists of five components: Sra1/Cyfip1 (or the ortholog PIR121/Cyfip2), Nap1/Hem2/Kette (or the ortholog Hem1), Abi2

(or the orthologs Abi1 and Abi3), HSPC300/Brick1, and WAVE1/SCAR (or the orthologs WAVE2 and WAVE3) [69]. Rac promotes the disassembly of the WAVE complex by directly targeting of Nap125 and PIR121. Nap125 and PIR121 subsequently release the inhibition of WAVE and allow it approaching the Arp2/3 complex [69].

Mammalian cells can also use diaphanous-related formin (DRF), such as mDia1or mDia2, for actin polymerization. Once a Rho-GTP binds to mDia1, it will relieve the auto-inhibitory interaction of mDia1, which then exposes an FH2 domain for binding the barbed end of actin filament and an FH1 domain to deliver profilin/actin for filament elongation [70]. Cofilin can regulate actin dynamics by stimulating both depolymerization and polymerization. As an actin-filament severing protein, activated cofilin applies more uncapped barbed ends for actin polymerization and filament elongation [71]. Phosphorylation of cofilin leads to its inactivation. LIM kinase (LIMK), one of the downstream effectors of the PAK family, can stimulate cofilin phosphorylation. However, the PAK family is a group of Rac/Cdc42-dependent kinases [72-73]. Rho can also phosphorylate cofilin in a Rho kinase (ROCK)-LIMK dependent way to stabilize actomyosin filaments [74]. In addition, Rho promotes assembly of contractile actomyosin filaments through a ROCK-dependent way. ROCK can inactivate the myosin light chain (MLC) phosphatase by phosphorylating it and subsequently leads to increased phosphorylation of MLC [75].

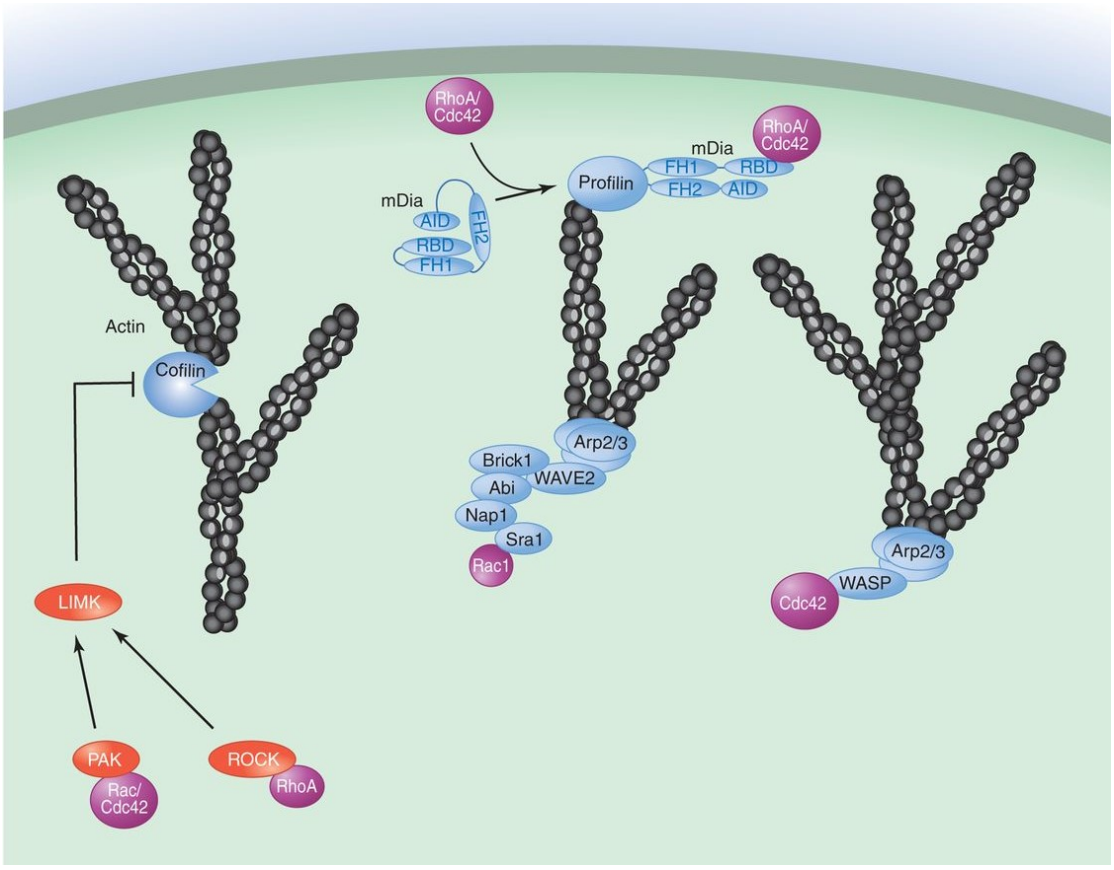

Figure 2. Regulation of Actin Dynamics by Formins and Arp2/3 in Cellular Protrusions [76]. The Rho GTPases Rac, RhoA, and Cdc42 regulate actin dynamics at the leading edge via their effects on the activities of formins (mDia), Arp2/3 complex, and LIM kinase (LIMK). Arp2/3 nucleates actin branches that are seen in broad protrusions. Its activity is regulated by Cdc42 and Rac1, which act on WASP/WAVE-containing protein complexes. Rac and Cdc42 also act on PAK, which phosphorylates LIM kinase, which in turn regulates cofilin, a severing protein. Finally, RhoA acts on mDia1 and Cdc42 acts on mDia2 to promote actin polymerization using a processive capping mechanism. RhoA also activates profilin, which binds to actin monomers and increases the rate of polymerization. These GTPases are activated in a clear temporal sequence near the leading edge. AID, autoinhibitory domain; FH, formin homology domains; RBD, Rho-GTPase-binding domain.

1.3.2 Microtubule Cytoskeleton

Microtubules are essential for cell polarity and the distribution of intracellular organelles. Op18/stathmin family promotes disassembly and inhibits polymerization of microtubules [77]. These proteins can be phosphorylated at Ser16 and, in turn, to an inactivation state mediated by Cdc42/Rac-dependent activation of PAK [78]. In neurons, collapsin response mediator protein-2 (CRMP-2) can promote microtubule assembly though binding tubulin heterodimers. Rho can inactivate CRMP-2 mediated by ROCK phosphorylated CRMP-2 [79]. In migrating fibroblasts, Rho promotes the formation of stabilized microtubules by mDia without changing actin cytoskeleton [80]. Moreover, Rho GTPases can regulate the activities of

many microtubules plus end-binding proteins to define cell shape and polarity [81-83].

1.3.3 Gene Expression

Rho activation can promote the translocation of MAL from the cytoplasm to the nucleus by the actin cytoskeleton, which then help serum response factor (SRF) for gene transcription [84]. CDC42/Rac/Rho GTPases can regulate the JNK and p38 MAP kinase and NFκB signaling pathway and play import roles [85-88].

1.3.4 Cell Cycle

During cell cycle G1, Rho GTPases can stimulate cyclin D1 transcription, cyclin E expression and regulate the levels of the Cdk2 inhibitors, $p21^{cip1}$ and $p27^{kip1}$ [89-97]. During cell cycle mitosis, Rho can control the positioning of the centrosomes by actomyosin filaments [98]. In C.elegans, Cdc42 can directly target Par6 to regulate the positioning of the spindle by Par6/aPKC/Par3 and Par1/Par2 complex [99]. Cdc42-specific effecter mDia3 is one of the kinetochore's key components, which is very important for spindle microtubules and chromosomes interaction [100]. Furthermore, Rho plays a crucial role in contractile ring function and cleavage furrow during cytokinesis [101-103]. The roles of Rho GTPases in the cell cycle are also showed in Figure 3.

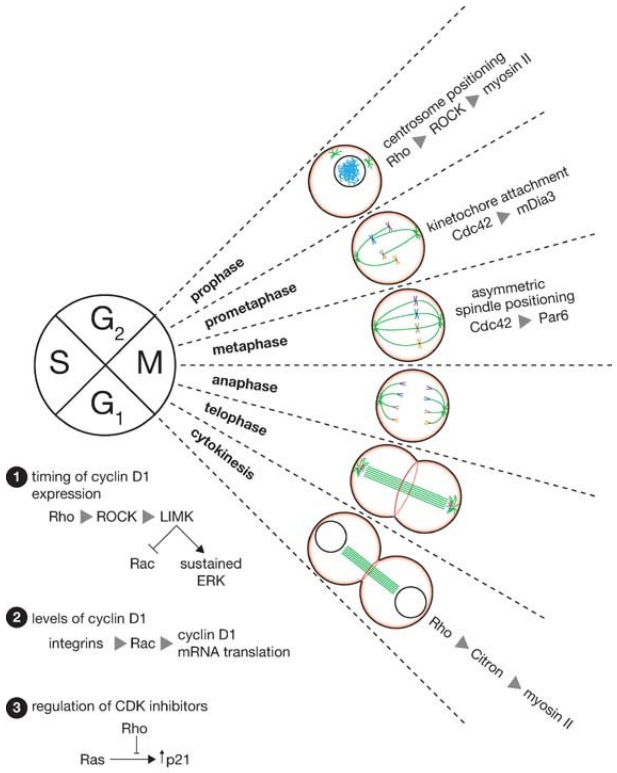

Figure 3 Rho GTPases and the Cell Cycle [61]. Rho GTPases control multiple aspects of M phase and G1 progression. The signaling pathways are shown for the relevant stages. Microtubules, green; actin, red; condensed chromosomes, blue.

1.3.5 Cell Polarity

Three protein complexes, Par6/aPKC/Par3, Dlg/Lgl/scribble, and Crumbs/PALS1/PATJ, have been implicated in epithelial morphogenesis [104]. Cdc42 can directly target Par6 and involve morphogenesis via regulating Par6/aPKC/Par3 alone or together with the other two complexes [105].

1.3.6 Cell Migration

Current concepts of cell migration are well established in regular cell culture. So far, the best understandable form is two-dimensional (2D) migration, which means cells cultured and migrated on flat glass or plastic. Mostly, eukaryotic cell migration is a multistep process that cells usually undergo cycles of extending membrane protrusion in the cell front, forming adhesion to interact with the surrounding microenvironment and coupled with the actomyosin-based contraction [106-107].

Protrusion

Membrane protrusions at the leading edge of cells include filopodia and lamellipodia. Filopodia are

finger-like protrusions that contain parallel bundles of actin filaments in the direction of protrusion (Figure 4). Lamellipodia are thin branched actin sheets, which can both protrude and retract (Figure 4). Filopodia or lamellipodia protrusions at the leading edge depend on actin filaments growth, which then helps to push the front of the cell forward [52, 108-109]. As mentioned above, actin polymerization is stimulated by Rho family GTPases.

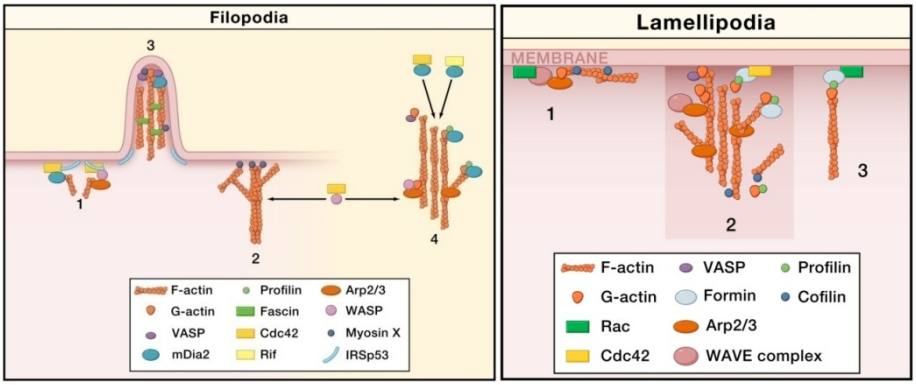

Figure 4. Filopodia [52]. A model for filopodium formation is as follows: (1) IRSp53 initiates filopodia by bending the membrane and recruiting Cdc42 and Cdc42 targets, mDia2 and WASP/N-WASP, which then stimulate actin polymerization. (2) Actin filaments could also be provided from lamellipodia, where Myosin X could cluster WASP/Arp2/3-nucleated actin filaments. (3) Filopodia subsequently extends through the addition of actin monomers (G-actin) onto actin filaments (F-actin). VASP, Myosin X, and mDia2 are localized to the tip of filopodia. Myosin X moves dynamically in filopodia and could contribute to delivery of proteins to the filopodial tip. (4) Actin polymerization in filopodia is nucleated by mDia2 in concert with VASP, which delivers actin monomers to the filopodial tip. Profilin binds to and provides actin monomers directly to mDia2. Cdc42 and Rif stimulate mDia2-mediated actin polymerization, and Cdc42 also stimulates WASP/Arp2/3-driven polymerization.**Lamellipodia [52].** A model for lamellipodium formation is as follows: (1) Severing of actin filaments by cofilin provides free actin filament barbed ends, which act as sites for actin polymerization and subsequently Arp2/3-mediated nucleation of new filaments. (2) In conditions of steady-state lamellipodial extension, actin polymerization in lamellipodia is nucleated by the Arp2/3 complex, generating a branched actin filament network. The Arp2/3 complex is activated by the WAVE complex, which in turn is activated at the membrane by Rac1. Formins extend Arp2/3 complex-generated filaments. Formins are activated by Cdc42, Rac1, and probably other Rho GTPases. Actin monomers (G-actin) are provided to formins by profilin. VASP also contributes to actin filament extension. Cofilin severs and depolymerizes older actin filaments in the network. (3) Formins can also nucleate actin filaments independent of the Arp2/3 complex, generating unbranched filaments.

Adhesion

'Nascent adhesions' to the substrate are formed beneath the extending lamellipodium. Integrin-mediated adhesions are the best studied (Figure 5) [110]. These adhesions transmit forces at the leading edge and are released at the cell rear during cell migrations [111]. These steps are mediated by actin polymerization and myosin II activity through Rho-family GTPases [112-113]. Nascent adhesions mature to focal adhesions

in response to force transmission by actomyosin stress fibers. Adhesion disassembly occurs at both the front and rear of the cell. Disassembly occurs most prominently at the lamellum–lamellipodium interface and retraction area. Disassembly associated with retraction seems dependent on a Rho GTPase- and myosin II-activity [114].

The molecules that reside in adhesions are more than 150. Some molecules can regulate Rho-family GTPases for cell migration, for example, focal adhesion kinase (FAK)/paxillin signaling module. Paxillin is a signaling adapter. It enters adhesions as they form and remains there until they disassemble [115]. FAK and Src mediate phosphorylation of paxillin on Y31 and Y118, this then allows paxillin to bind a number of molecules such as Crk/p130Cas, FAK/Src, and Ras GAP, and conformationally activate the molecules including Src, FAK, paxillin, and p130 Cas. Among paxillin binding proteins, P130Cas recruits Rac GEF Dock180; GIT1 and GIT2 can bind to Cdc42 and Rac GEF Pix [116-118]. Activated Src and FAK can inhibit or activate RhoA activity by regulating p120RasGAP-p190RhoGAP complex and p190RhoGEF and PDZRhoGEF, respectively [119].

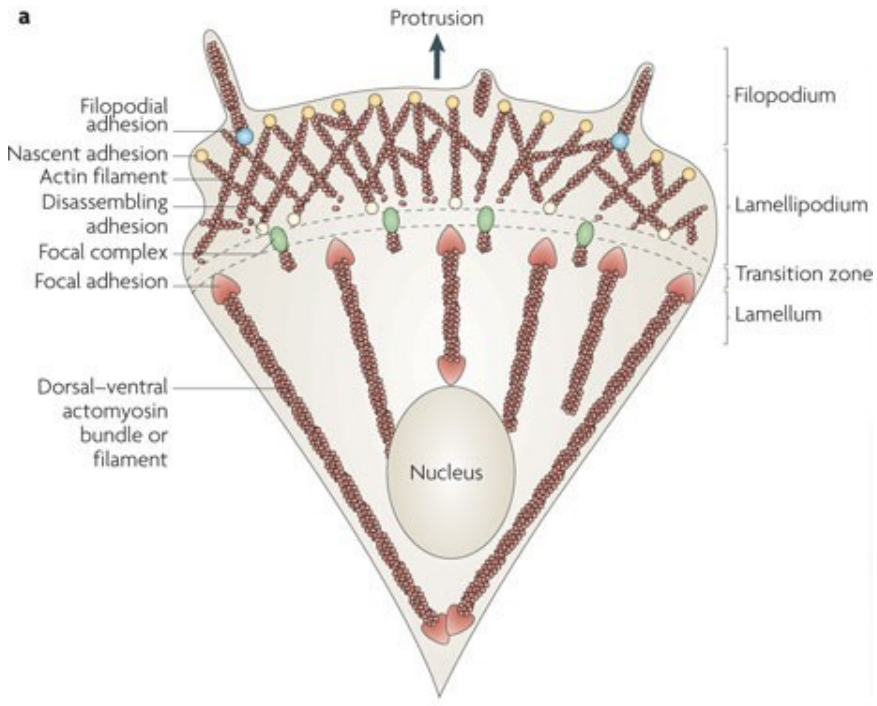

Figure 5 Adhesions in Migration Cell [114]. Adhesion is closely coupled with the protrusions of the leading edge of the cell (filopodia and lamellipodia). Adhesions (nascent adhesions) initially form in the lamellipodium (although adhesions may also be associated with filopodia) and the rate of nascent adhesion assembly correlates with the rate of protrusion. Nascent adhesions

either disassemble or elongate at the convergence of the lamellipodium and lamellum (the transition zone). Adhesion maturation to focal complexes and focal adhesions is accompanied by the bundling and cross-bridging of actin filaments, and actomyosin-induced contractility stabilizes adhesion formation and increases adhesion size.

Contraction

Rho A can promote both cell adhesion disassembly and cell retraction at the rear of the cell. It also activates ROCK to stimulate myosin II activity by phosphorylating myosin RLC and inhibiting myosin phosphatase, promoting actomyosin stress fibers assembly and function.

1.3.7 Atypical and Other Rho-family GTPases

The atypical Rho GTPases consist of four subfamilies: RhoU/RhoV subfamily, RhoH subfamily, Rnd subfamily, and RhoBTB subfamily. RhoU can bind to the SH3 domains of Grb2 through its N-terminal domain and be phosphorylated by Src [120-121]. Both RhoU and RhoV can bind to the PAK family kinases and affect actin cytoskeleton and adhesion dynamics [122-123]. RhoH predominantly expresses in haematopoietic tissues [124]. RhoH is GTPase-deficient and therefore is constitutive in the GTP-bound form. RhoH can regulate murine haematopoietic progenitor ability and T-cell differentiation [125-126]. In addition, RhoH can antagonize the activity of other Rho GTPases, such as Rac1 and RhoA [127-128]. Rnd1, Rnd2 and Rnd3 proteins are also GTPase deficient [129]. Rnd1 and Rnd3 mainly locate in membranes and can antagonize the activity of RhoA [130-131]. Rnd2 mainly locate in the cytoplasm. Rnd can regulate their activity through gene expression, protein phosphorylation and their localization. Phosphorylation allows Rnd proteins to bind to 14-3-3 proteins. Raf mediates Rnd3 expression and regulates the actin cytoskeleton [132]. RhoBTB1 and RhoBTB2 contain BTB domain. It is important for the formation of Cullin-ring ubiquitin ligases (CRLs, E3 ubiquitin ligases) [133-134]. RhoBTB1 and RhoBTB2 can localize at the membrane vesicles. RhoBTB2 is involved in transporting vesicular stomatitis virus glycoprotein (VSVG) and affects the cell cycle, apoptosis, cytoskeleton and membrane trafficking [135]. The more information about Rho proteins and their effectors and functions are shown as follows (table 4):

RHO protein	Effectors	Effector protein type	Function
RHOA, C	ROCK I, II	Kinase	Actomyosin contraction, transformation, transcription (SRF)
		Scaffold	Actin polymerization, transcription (SRF),

			microtubules
	PRK1/PKN	Kinase	Endocytosis, p38γ MAPK activation, transcription (MEF2C)
	Citron	Kinase	Cytokinesis
RHOB	PRK1/PKN	Kinase	EGFR trafficking, motility and cell adhesion
RHOD	Unknown	-	Vesicle transport
RND1, 2, 3/RHOE	Unknown	-	Antagonist of RHOA
RHOG	Kinectin	Scaffold	Microtubule binding
	Unknown	Unknown	RAC1 and CDC42 activation
RHOH	Unknown	-	Implicated in tumours of myeloid origin
RIF	Unknown	-	Actin organization
CHP	PAK	Kinase	JNK activation
WRCH1	PAK	Kinase	JNK activation, morphological transformation
RAC1, 2, 3	PAK1, 2, 3	Kinase	JNK activation, transformation
	MLK2, 3	Kinase	JNK activation2–
	PAR6	Kinase	Cell polarity, transformation
	p67*PHOX*	Enzyme	NADPH oxidation, transcription (NFκB)
	IQGAP1, 2	Scaffold/GAP	Adherens junctions
	POSH	Scaffold	JNK activation, transcription (NFκB)
	IRSp53	Scaffold	Actin polymerization
CDC42	PAK1, 2, 3, 4	Kinase	JNK activation, transformation
	MLK2, 3	Kinase	JNK activation
	PAR6	Scaffold	Cell polarity, transformation
	N-WASP, WASP	Scaffold	Actin organization
	MRCK1, 2	Kinase	Actin organization
TC10 (TCL)	PAK	Kinase	JNK activation
	WASP	Scaffold	Actin polymerization
	PIST136	Scaffold	?
	?	?	GLUT4 translocation, glucose uptake

Table 4 RHO Proteins, Their effectors and Functions [136]. CHP, CDC42 homologue protein; EGFR, epidermal growth-factor receptor; GLUT4, glucose transporter 4; IQGAP, IQ-motif-containing GTPase-activating protein; IRS, insulin-receptor substrate; JNK, JUN N-terminal kinase; MAPK, mitogen-activated protein kinase; MEF2C, myocyte-enhancer factor 2C; MLK, mixed-lineage kinase; NF-κB, nuclear factor of κB; PAK, p21-activated kinase; PAR, partitioning defective; PIST, PD2 domain protein interacting specifically with TC10; PKN, protein kinase N; POSH, plenty of SH3 domains; PRK, protein-kinase-C-related kinase; RIF, RHO in filopodia; ROCK, RHO-associated coiled-coil-forming kinase; SRF, serum response factor; WASP, Wiskott–Aldrich syndrome

protein; WRCH, WNT-responsive CDC42 homologue.

1.3.8 Rho GTPase in Cancer

The Altered expression of Rho GTPase in Cancer: RhoA seems to act as a tumor suppressor gene because this gene is rarely amplified but often deleted in many cancer types [66]. Some mutational hotspots of RhoA are described in the TCGA database. However, among them constitutively active mutants, RhoA G14V and RhoA Q63L, and "fast cycling" mutation RhoAF30L, are not found, indicating that direct mutational activation of RhoA is not crucial for tumor formation. RhoB gene is amplified, while the RhoC gene is deleted in many cancer types. Rac1 is amplified in many cancers types, which seems to act as a tumor promoter [66]. Several Rac mutations, such as the hotspot at P29, can increase the activity of Rac1 in melanoma and uterine cancer [66]. Cdc42 can be amplified, deleted or mutated, which is highly dependent on tumor type [66]. The rest members of the Rho GTPase family also involve human cancers. For example, Rac3, RhoU and RhoD are mostly amplified, whereas RhoBTB2 and RhoV are often deleted in many cancer types.

Rho proteins and RAS: Rho GTPases are required for RAS transformation [136]. For example, mutants of RhoA, RhoG, Rac1, TC10 and CDC42 regulate RAS-induced fibroblast transformation [137]. Rac2 is required for the hyperproliferation of RAS activated mast cells [138]. In RAS-transformed cells, RAS can regulate the activation of Rac1 and RhoA, which depend on the cancer type [106, 139].

Rho proteins and growth factors: the abnormal signal of EGF, hepatocyte growth factor (HGF), lysophosphatidic acid (LPA), platelet-derived growth factor (PDGF) and transforming growth factor-β (TGF-β) can transmit into cell though Rho proteins in tumorigenesis [136].

Rho proteins in invasion and metastasis: losing the epithelial polarity is the first step of tumorigenesis. However, Cdc42/Rac/PAK can regulate cell polarity [140]. Rho proteins, such as RhoA, play important roles in cell-cell adhesions and are supposed to involve in the epithelial-mesenchymal-transition (EMT). Rho proteins and their effectors play critical roles in cell motility. RhoA and Rac1 can regulate the levels of MMPs or their antagonists, tissue inhibitors of metalloproteinases (TIMPs), to remodel the ECM for cell migration [141-143].

Rho proteins and cell-cycle control: Rac1 and Cdc42 can mediate the expression of cyclin D1, and RhoA signaling can down-regulate the levels of CDKIs $p21^{WAF1}$ and $p27^{KIP1}$ [96-97].

1.4 Mechanosemsitive Piezo ion Channels

Piezo family proteins, including Piezo1 and Piezo2, are mechanically activated calcium-permeable ion channels and convert physical force into biochemical information [144]. Such mechanical stimulations include poking, stretching and shear stress. Piezo1 is highly expressed in epithelial tissues, including lungs, bladder, pancreas skin, and blood vessels, while Piezo2 is mostly expressed in cells of neuronal origin, for example, sensory dorsal root ganglia [144].

Piezo1 is a large membrane protein (~2500 amino acids) contains 36 transmembrane domains and functions as three pore-forming units (Figure 6). Details of this channel's structure and gating have been partly shown based on studies of mouse Piezo1 (Figure 7) [145-147].

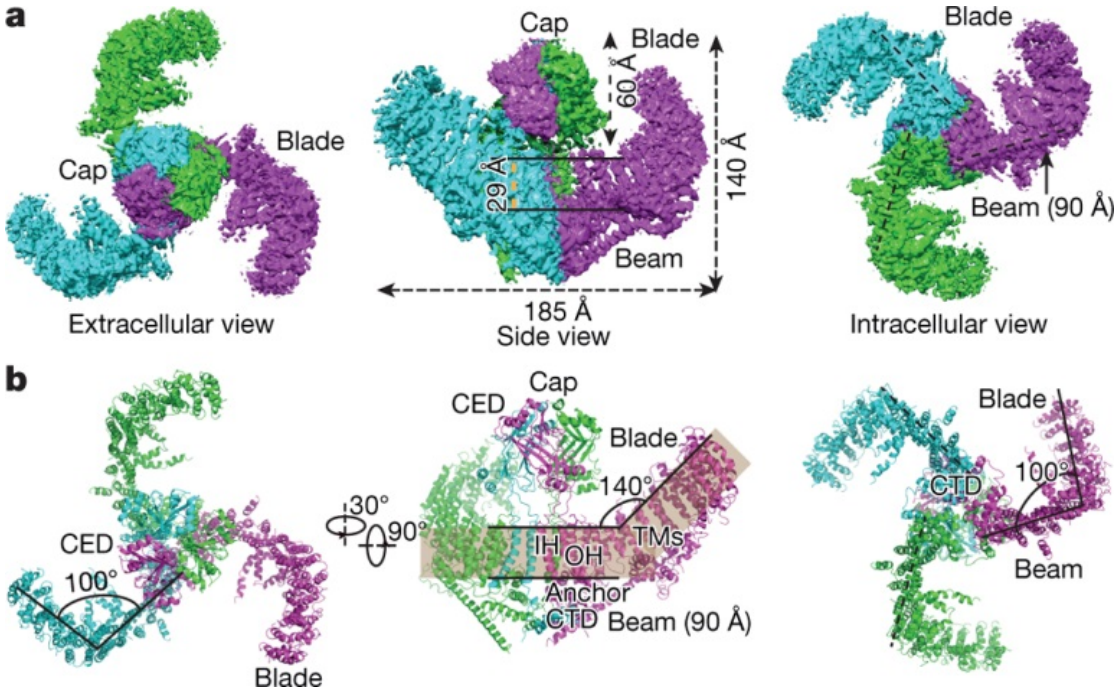

Figure 6 Overall Structure of Mouse Piezo1 [147]. **a**, The indicated view of the sharpened map (6σ contour level) filtered to a resolution of 3.97Å, with each subunit colour-coded and the major domains labelled. **b**, Cartoon models with each subunit colour-coded. In the middle panel, the peripheral blade of the front subunit is omitted for a better view of the curvature of the TM helices. The shadow area indicates a planar and a potentially curved membrane plane where TM helices reside.

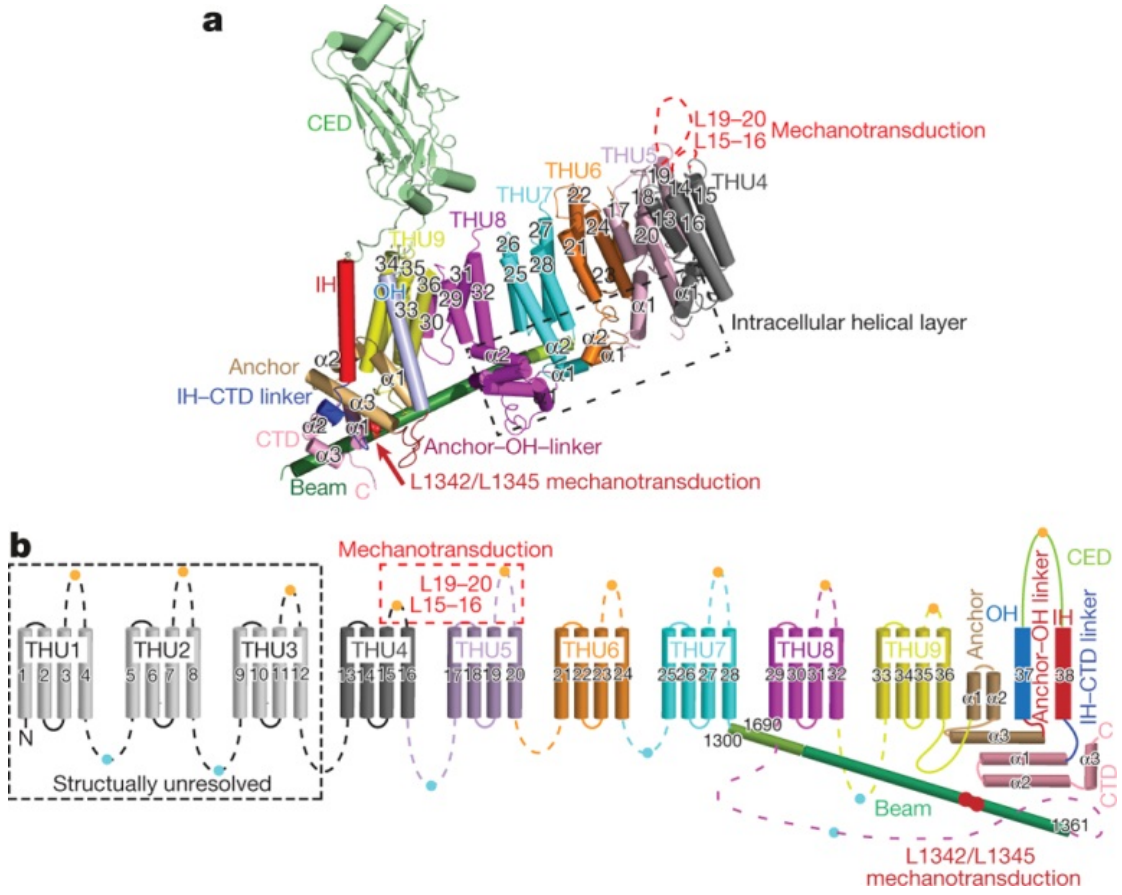

Figure 7 Repetitive THUs and a 38-TM Topology Model [147]. **a**, Cartoon model showing cylindrical helices displays one subunit, with individual THUs and major structural domains labelled. The functionally characterized extracellular loops of TM15–TM16 (L15–16) and TM19–TM20 (L19–20) are shown in red dashed lines, and residues L1342 and L1345 in the beam are shown by red spheres. **b**, A 38-TM topology model, colour-coded to match the cartoon models in **a**. Some intracellular helices shown in **a** are omitted for better illustration of the THUs and beam features. Yellow dots mark the experimentally verified extracellular loops, and blue dots indicate loops that contain residues that can be cross-linked to residues in the intracellular loops of TM28–TM29 and TM32–TM33.

Both Piezo 1 and Piezo 2 have been shown to play crucial roles in many processes. Gain-of-function (GOF) and loss-of-function (LOF) mutations in Piezo1 are associated with dehydrated hereditary stomatocytosis and lymphatic malformation, respectively [148-149]. While GOF and LOF mutations in Piezo 2 are associated with distal arthrogryposis and the defects in touch perception and proprioception, respectively [150-151]. Recently reports also show that Piezo1 controls epithelial cell numbers. In crowded regions, Piezo1 forms large cytoplasmic aggregates triggering extrusion and apoptosis. In sparse regions, it localizes to both of the plasma membrane and cytoplasm to trigger cell division [152-153]. Piezo1 plays functions in both development and adult physiology by shear stress sensing and the determination of the vascular structure [154]. Piezo1 suppresses the PKA activity in a phosphodiesterase 1 (PDE1)-dependent way during

cells transition from unconfined to confined spaces [155]. In addition, Piezo1 has also been shown to participate in endothelial inflammation [156], serotonin synthesis [157], axon growth [158], demyelination [159] and innate immunity [160]. Piezo1 is overexpressed in glioma and associated with glioma aggression [161]. The expression of Piezo1 is also positively correlated with the degree of peritumoral brain edema in GBM patients [162]. It seems that Piezo1 is an ideal new prognostic biomarker for glioma patients [163].

1.5 Complexities of Extracellular Matrix (ECM)

The ECM serves as physical scaffolding for the cellular constituents and is required for tissue morphogenesis, differentiation and homeostasis. The main molecular components of the ECM are proteoglycans (PGs) and fibrous proteins [164-165]. PGs are composed of glycosaminoglycan (GAG) chains covalently linked to a specific protein core. They can be classified into three main families: small leucine-rich proteoglycans (SLRPs), modular proteoglycans and cell-surface proteoglycans [164]. PGs can form into a hydrated gel, fill into the major part of the extracellular interstitial space, and have a wide variety of functions [165]. The main fibrous proteins include collagens, elastins, fibronectins (FNs) and laminins, and the most abundant one is collagen. Collagen constitutes the main structural element of the ECM, which provides tensile strength and plays important roles in cell adhesion, chemotaxis and migration, and tissue development [166]. FN can direct the ECM organization and mediate cell attachment and other functions [167-168].

Normal tissue ECM is a relaxed meshwork composed of collagens and elastin fibers, together with FN and surrounding with PGs hydrogel. This network allows ECM to resist a wide range of tensile stresses. ECM is a highly dynamic entity. Its precise orchestration is crucial to maintain its normal function. For example, it can coordinate the function of fibroblast metalloproteinases (MMPs), tissue inhibitors of metalloproteinases (TIMPs) and other enzymes (e.g., LOX and transglutaminases). [169-171].

ECM Change in Tumor

In many solid tumors, ECM often expresses high levels of fibrillar, collagens, fibronectin, elastin, and laminins. Abnormal organization and post-translational modification of ECM molecules are also observed in tumor ECM. In myofibroblasts, copious quantities of deposited collagen and elastin fibers are reoriented and crosslinked by lipoxygenase and transglutaminase, which further stiffen the tissue ECM [172-174]. Linear

collagen fibrils provide a prognostic marker for low cancer survival in invasive human breast cancers [175]. In addition, this collagenous matrix activates series of stress associated signaling, such as FAK. A large degree of cancer-associated fibroblasts (CAFs) can be observed in tumor ECM [176]. These alterations can support tumor cells by paracrine stromal cell-derived factor-1 (SDF1) and TGFβ signals and act as a positive-feedback loop to potentiate tumor growth and survival.

1.6 Mechanical Properties of Single Cells

The elastic properties of different type of somatic cells are shown largely different. Some of them are very soft, such as neuronal cell types (0.1–0.2kPa), while some of them are much stiffer, such as bone and muscle cell types (up to 100 kPa) [177-178]. The same cell type is also observed to have differences in mechanical properties. For example, superficial-zone chondrocytes are approximately twice stiffer than the middle- or deep-zone chondrocytes cells [179]. Furthermore, the differences in mechanical properties can even be found when comparing cells in spread to spherical state. For example, the module of human spread osteoblasts is 6.5 kPa; however, this number can change into 2.6 kPa in spherical osteoblasts [179]. Different regions of the cell have different mechanical properties, too [180]. Finally, individual cell stiffness is inextricably linked to their intracellular components.

Cytoskeleton components mainly include microfilaments, intermediate filaments, and microtubules. Microfilaments are linear polymers of actin subunits, which are used to polymerize or depolymerize within minutes and facilitate cell motility. They can act to resist tension, maintain the positioning of organelles and provide overall resistance to deformation. Intermediate filaments have six types and serve as an elaborate network in cells. They can extend from the nucleus to the plasma membrane. This network plays crucial roles in helping cytoskeletal elements, organelles, and the cell membrane connect. Like microfilaments, they also resist tension. Microtubules are polymers of tubulin. They serve to transport intracellular components and also contribute to overall cellular structure and behavior. Opposed to microfilaments and intermediate filaments, they resist compression. In addition, there are also a number of nucleocytoskeletal proteins, including lamins A, B1, B2, and C, spectrin, kinesin, plectin, emerin, SUN proteins, and KASH proteins, which link the nucleus to the cytoskeleton [181-182]. The cell membrane contributes to cellular mechanical behavior mainly due to its largely connected to the cytoskeleton. The nucleus and organelles can also influence both local and whole-cell mechanical property measurements. However, all these cellular

mechanical cues always change over time.

Researchers have repeatedly observed that invasive cells are less rigid than benign or less invasive cells [183]. Cross et al. showed that malignant cells were >70% softer than cells from normal tissue [184].The mechanical changes of invasive cells are presumable because lowering stiffness facilitates cell invading surrounding tissues and has been attributed to a distinct cytoskeletal organization. Mechanical phenotyping can identify the architectural features of cells quickly without the need for labeling. Thus, it has great potential to become a new technology in cancer diagnostics. Chemicals that can affect the components of the cytoskeleton or nucleus can dramatically change cellular mechanical properties [185]. Lots of chemotherapeutic drugs target at modifying the architecture of the cytoskeleton [186]. Cell mechanics can be used to monitor the effects of chemical treatment and have the potential to screen for drug sensitivity.

1.7 ECM and Cell Migration

Tissue features, such as mechanics and organization of the ECM, can regulate or modulate cell migration. However, tissues are not purely materials and usually exhibit complex, time- and rate-dependent behaviors. Thus, it is better to focus on the local properties of the ECM.

1.7.1 ECM Elastic Modulus

The physical deformability (elastic modulus) of different tissues is largely different (Table 5). Cells sensing the rigidity of ECM (well-known as mechanotransduction) mainly depends on the actomyosin-based contractility and integrin-based adhesions or other cell-surface links (such as syndecan clustering) [187-189]. Mechanosensitive proteins, including adhesion adaptor protein talin and vinculin, nucleoskeletal lamin, and mechanosensitive ion channels (such as piezo1) and their downstream factors, are also involved in mechanotransduction [111, 190]. For example, if strong adhesion and high tension are within cells, the force will activate Src family kinases and their downstream signaling, including Rac1 and repressor/activator protein 1 homologue (RAP1; also known as RAP1A) [191-192]. Subsequently, RhoA can be activated by Rho GEF, ARHGEF1 and ARHGEF12 [193]. DIAPH family proteins, the effectors of RhoA, can also recruit Src family kinases and lead positive feedback for this signaling [194-195]. Furthermore, the increased activity of Src family kinases can also increase the expression of MMPs [196]. However, FAK activation inside the focal adhesions can promote their disassembly, mediated by Erk-, dynamin- and calpain

2-signaling [115, 197-198].

Tissue	Stiffness
Brain	<1 kPa
Loose collagen (dermis/breast)	0.2–2.0 kPa
Muscle	12 kPa
Basement membrane	250–500 kPa
Tendon	1.4–2.2 GPa
Cortical bone	15 GPa

Table 5 Elastic Modulus Range Present in Macromolecular Tissue Structures [199]. Glycosaminoglycan (GAG)-rich stroma surrounding cell networks, such as brain tissue, is soft (below 1.0 kPa); loose fibrillar collagen type-I- and type-III-based porous protein networks, such as dermis and breast, scale typically between 0.2 and 2 kPa. Thicker, more crosslinked collagen bundles in muscle are substantially stiffer (12 kPa), which reaches the low GPa range in tendons. Basement membranes consisting of collagen type-IV and laminins have a stiffness in the higher kPa range, with at least double the stiffness on the epithelial side compared to the stromal side. The stiffness of calcified tissue, including cortical bone, can go up to 15 GPa.

Cells can detect differing substrate rigidity, so-called durotaxis. Focal adhesions detect stiffness changes and transmit this information to the cytoskeleton, promoting actin polymerization and microtubule polarized for directional cell migration [200-201]. At shorter timescales, the mechanisms of this rapid process are mostly dependent on post-translational modifications. At longer timescales, there areincreasing expressions of many myosin components, which are regulated by Yorkie homologue (YAP), translin-associated zinc-finger protein (TAZ) and myocardin-like protein (MKL; also known as MRTF) [202-203]. This increased expression of myosin components will help cells to generate more force on stiffer surfaces. Nucleus structure plays an important role in this stepbecause the depletion of lamin A prevents such transcriptional response [204].

1.7.2 ECM Topology

ECM topology defines mechanical cell-migration interfaces, including 1D tracks or fibrils, 2D sheets and 3D ECM. The surfaces that cells encounter during the migration can be divided into continuous and discontinuous surfaces. On continuous surfaces, such as on 2D sheets, cells predominantly use lamellipodia for membrane protrusion [205]. On discontinuous surfaces, cells push the membrane forward by generating hydrostatic pressure because of the lake of ECM for adhesion traction. Unlike 2D migration, cells in 1D migration share multiple features of 3D migration. For example, topological effects, such as 1D and 3D matrix ridges, can prevent perpendicular actin protrusions, which lead cells to adopt a polarized morphology

and rapid migration [206]. During cell migration, the ECM surfaces can influence the curvature of the cell membrane. Bar proteins can detect this change and promote them to bind to the membrane and recruit F-actin for cells to migrate rapidly [207-208].

1.7.3 ECM Confinement

During cell migration, the levels of confinement are mediated either by the ECM or by surrounding cells. In this situation, cell migration is not dependent on the changes in ECM chemistry and rigidity. They use filopodia or hydrostatic pressure to drive membrane blebs to push cell membrane forward [209-210]. In confined environments, Rac1/Arp2/3 mediated lamellipodia and cell-matrix adhesion, is less required, while actomyosin contractility is more needed [211-214]. Whether cells can deform sufficiently to squeeze through the confined environment mostly depends on the size and mechanical properties of nucleus. The nucleoskeletal protein lamin A/C is a pivotal contributor to the stiffness of the nucleus [215]. Finally, the levels of lamin A/C and the function of myosin determine cells the capacity to squeeze through small constrictions [215-216]. In addition, in order to adapt the mechanochemical complexity of ECM, cells can also extensively remodel ECM by physical or biochemical factors to facilitate their migration. For example, if cell migration is prevented by small pores (pores smaller than the nuclear limit), in this case, cells can secrete proteases, typically as MMPs, to cleave ECM components and create migration tracks [142, 196].

1.7.4 Cellular Responses to ECM

Cells can exhibit complex responses to mechanical cues during migration. These responses include actin polymerization, actomyosin contractility, cell adhesions and their dynamics. The categories of 3D cell migration are mainly including (Table 6):

Migration mode	Role of cell-substrate adhesions	Role of cell contractility	Necessary environmental conditions	Characteristic cell polarization	Notes
Pseudopodial	Adhesions required	Migration occurs under conditions of both high or low levels of RHOA, depending on matrix pore size	Sites for cell adhesion	Polarized PIP3, RAC1 and CDC42 at the leading edge	Speed often unchanged upon inhibition of contractility
Lobopodial	Adhesions	High RHOA levels	Linearly elastic 3D	Nonpolarized	Efficient migration

	required		matrix	cortactin, PIP3, RAC1 and CDC42	following CDC42 or RAC1 knockdown
Bleb-based amoeboidal (A2 blebbing)	Low adhesion	High RHOA levels	Pore size larger than the nuclear limit on migration	Myosin II accumulation at the cell rear	Speed typically reduced upon ROCK inhibition
Protrusion-based amoeboidal (A1 blebbing	Low adhesion	Low RHOA levels	Pore size larger than the nuclear limit on migration	Retrograde actin flow localized to small protrusion at the leading edge	Activation of cell contractility converts A1 blebbing to A2 blebbing
Osmotic engine	Low adhesion	RHOA dispensable	Full confinement	Polarized aquaporins and ion transporters at the leading edge	Occurs even if actin polymerization is disrupted

Table 6 Summary of Confined Cell Migration Modes [217].

Current techniques for measuring the mechanical properties are listing as below (Table 7):

Technique	Mechanical Properties	Typical applied force range
Atomic force microscopy	Elastic and viscoelastic properties of a local region or a whole cell	pN-μN
Microbead rheometry	Elastic and viscoelastic properties of a local region	pN
Optical tweezers and traps	Membrane elasticity, whole-cell deformability	fN-pN
Micropipette aspiration	Elastic and viscoelastic properties of a local region or a whole cell	pN-nN
Fluid-based deformation cytometry	whole-cell deformability	pN

Table 7 Summary of Conventional Approaches to Testing Biomechanical Properties [218].

1.8 Atomic Force Microscopy

AFM was invented by Gerd Binnig in 1986 [219]. It is an extremely high-resolution scanning-probe microscope with a resolution of nanometer. The basic parts of AFM include a cantilever, a photodiode and a focused laser (Figure 8). The cantilever can move by the control of piezo and contains a sharp tip, which interacts with the sample surface and transmits the force for cantilever bending. The vertical bending of the cantilever is measured by thelaser beam with thephotodiode. AFM can be used for topographic imaging and force measurement. For imaging, AFM enables to image almost any type of surface using contact modes

and provides a true 3-D surface profile. For force measurement, AFM can perform force spectroscopy to measure many different forces, including adhesion strength, magnetic forces and mechanical properties.

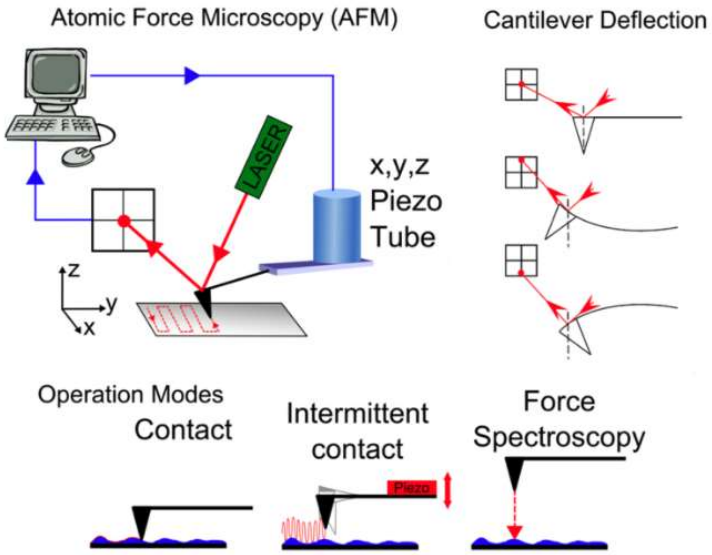

Figure 8 Schematic Representation of Basic Parts and Working Principle of AFM. https://covalentmetrology.com/afm/.

Force spectroscopy is a set of techniques that can be used to study the interactions and the binding forces between the individual molecules. In AFM, force spectroscopy is performed at one single point each time. The step is that cantilever approaches and interacts with the sample surface, and then withdraws (Figure 9). The cantilever deflection vs. piezo movement is measured, and the Hertz model is always used to determine Young's modulus.

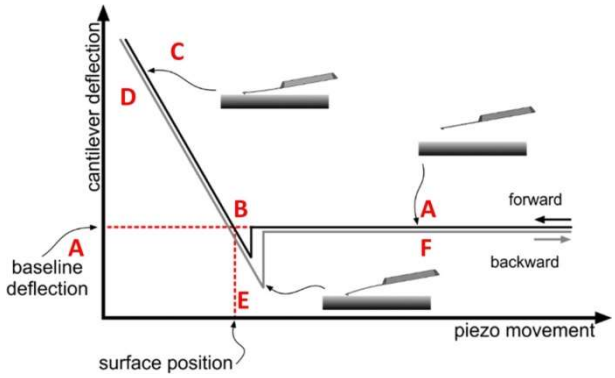

Figure 9. A Model Force Curve of Cantilever Deflection vs. Piezo Movement. https://www.nanosurf.com/en/support/afm-modes-overview/force-spectroscopy. The force curve can be divided in different segments where A-C (black line) refers to motion where the tip is approaching the surface and D-F (gray line) is when the tip is retracting from the surface. The gray line has been given an artificial offset for illustrative purposes:

Cantilever is approaching the surface.

Cantilever snaps into contact with the sample.

Repulsive portion: the tip and sample are in contact and bends up upon further movement of the z-piezo.

Repulsive portion on withdrawal: the tip is now unbending while being withdrawn from the surface.

Pull-out: the tip gets “stuck” in an adhesive dip before it is able to emerge from the adhesion at the interface.

The cantilever has returned to its unperturbed state while the z-piezo further increases the tip sample distance.

Chapter 2. Results

This section is about the paper published and paper in preparation during my PhD. It was accomplished by me and my collaborators under the supervision of Prof. Vincent Torre and his collaborators.

I investigated the roles of Rac1 in GBM infiltration. I confirm that Rac1 is involved in GBM infiltration and show that during Rac1 depleting or inhibition:

1) GBM cells dramatically reduce their invasion ability.

2) GBM cells change their morphology accompanies with a reorganization of the cell cytoskeleton, abnormal myosin IIa location and cell adhesion formation.

3) There is a rapid suppression of Erk1/2 phosphorylation according to EHT 1864 inhibition in GBM cells.

4) GBM cells increase in the rigidity and viscosity in response to EHT 1864 inhibition.

I actively participated in and made a major contribution to all these works.

2.1 Rac1 Promotes Cell Motility by Controlling Cell Mechanics in Human Glioblastoma

Jing Xu, Nicola Galvanetto, Jihua Nie, Yili Yang* and Vincent Torre*

cancers

MDPI

Article

Rac1 Promotes Cell Motility by Controlling Cell Mechanics in Human Glioblastoma

Jing Xu [1,2], Nicola Galvanetto [1], Jihua Nie [1,3], Yili Yang [2,*] and Vincent Torre [1,2,3,4,*]

1 International School for Advanced Studies (SISSA), 34136 Trieste, Italy; jixu@sissa.it (J.X.); nicola.galvanetto@sissa.it (N.G.); jnie@sissa.it (J.N.)
2 Joint Laboratory of Biophysics and Translational Medicine, Suzhou Institute of Systems Medicine (ISM)- International School for Advanced Studies (SISSA), Suzhou 215123, China
3 School of Radiation Medicine and Protection, State Key Laboratory of Radiation Medicine and Protection Medical College of Soochow University, Suzhou 215123, China
4 Cixi Institute of Biomedical Engineering, Ningbo Institute of Materials Technology and Engineering Chinese Academy of Sciences, Ningbo 315201, China
* Correspondence: yangyl@ism.pumc.edu.cn (Y.Y.);torre@sissa.it (V.T.)

Received: 21 May 2020; Accepted: 2 June 2020; Published: 23 June 2020

Abstract: The failure of existing therapies in treating human glioblastoma (GBM) mostly is due to the ability of GBM to infiltrate into healthy regions of the brain; however, the relationship between cell motility and cell mechanics is not well understood. Here, we used atomic force microscopy (AFM), live-cell imaging, and biochemical tools to study the connection between motility and mechanics in human GBM cells. It was found thatRac1 inactivation by genomic silencing and inhibition with EHT 1864 reduced cell motility, inhibited cell ruffles, and disrupted the dynamics of cytoskeleton organization and cell adhesion. These changes were correlated with abnormal localization of myosin IIa and a rapid suppression of the phosphorylation of Erk1/2. At the same time, AFM measurements of the GBM cells revealed a significant increase in cell elasticity and viscosity following Rac1 inhibition. These results indicate that mechanical properties profoundly affect cell motility and may play an important role in the infiltration of GBM. It is conceivable that the mechanical characters might be used as markers for further surgical and therapeutical interventions.

Keywords: Rac1; cell motility; cell mechanics; cytoskeleton; cell adhesion

1. Introduction

Glioblastoma (GBM; World Health Organization grade IV glioma) is the most common and incurable primary brain tumor. Its infiltration ability is largely responsible for the failure of existing therapies. Despite significant progress in developing targeted agents and immunotherapies, the prognosis of patients with GBM has not been improved markedly. Current GBM treatments focus on neurosurgical resection followed by radiation and chemotherapy. Unfortunately, the median survival time of patients with GBM is less than fifteen months [1,2]. Novel diagnostic strategies and tools to rapidly determine the response of individual GBM to drugs are highly desirable to improve patient survival.

Rho GTPases are known to be at the basis of infiltration, regulating the dynamics of the cytoskeleton and cell adhesion and providing a fine adjustment of cell movements [3,4]. In migrating cells, Rac1 is well known for its function in lamellipodia formation, which serves as a major driving force of cell movement [5,6]. Rac1 mediates actin polymerization though WAVE family proteins and activates the Arp2/3 complex for branched actin filament formation in lamellipodia [7–9]. Rac1 is also involved in fast plasma membrane movements, such as cell membrane ruffling and

vesicular transport [6,10]. Interestingly, deregulation of Rac1 has been recently found in a variety of cancers [11–13]. It has also been shown that increased Rac1 activation promotes cancer cell proliferation, migration, and metastasis [3,14,15]. However, how aberrant Rac1 activation plays a role during GBM migration is still not fully understood.

Similar to most other Rho GTPases, Rac1 usually switches between two conformations with GDP and GTP and mediates activation. Their intrinsic GTPase activity coupled with GAPs stimulates GTP hydrolysis and leads to the inactive state, which is then extracted from the cell membrane under the influence of guanine nucleotide exchange inhibitors (GDIs) [16]. The small molecule EHT 1864 binds to Rac1 with a high affinity and blocks Rac1 interaction with its effectors (guanine nucleotide-associated effectors to Rac1) both in vivo and in vitro [17]. Therefore, EHT 1864 is a powerful probe to evaluate the function of Rac1.

The mechanical properties of single cells are inextricably linked to their intracellular components. Cells usually change their mechanical properties during development and disease. Most malignant cells have been reported to be softer than normal tissue cells [18,19]. Drugs that affect the cytoskeleton or cell architecture are often used to treat cancer or other cellular diseases [20–22]. Among these drugs, paclitaxel, dexamethasone, and daunorubicin modify the mechanical phenotypes of cells [23,24]. However, further studies are still needed to understand how these intracellular components, such as the cytoskeleton and cell architecture, contribute to cell mechanical properties.

In this study, we blocked Rac1 activation by gene knockdown and Rac-specific inhibitor EHT 1864 to investigate how and to what extent Rac1 mediates GBM cell motility. We focused our attention on Rac1 regulating plasma membrane movements and the dynamics of the cytoskeleton and cell adhesions during GBM migration. We also examined which downstream effectors of Rac1 are important in GBM motility. AFM was used to explore the relationship between cell infiltration and cell mechanics in the presence or absence of Rac1 inhibition.

2. Results

2.1. Rac1 Is Essential for GBM Motility

Rac1 is the Rho GTPase family member that is mostly expressed in gliomas, and its level of expression correlates with patient survival outcome (Figure S1a,b). In this study, three types of typical GBM cell lines, U87 (glioblastoma multiforme grade IV), U251 (glioblastoma-astrocytoma grade III–IV), and T98G (glioblastoma multiforme grade IV), were used to study motility and associated changes. GBM cells display strong invasion properties, and these cells efficiently migrate through narrow pores (~8 μm) or invade into a three-dimensional Matrigel matrix. To investigate whether Rac1 is required for GBM cell invasion, small interfering RNA (siRNA) specifically against Rac1 was used to knockdown its expression in U87, U251, and T98G cells (Figure 1a and Figure S1c). Knockdown of Rac1 prevented the invasive phenotype of all these GBM cells (in U87 cells, 37.5 ± 13% in siRNA#1 group and 56.2 ± 11% in siRNA#2 group; in U251 cells 19.4 ± 16% in siRNA#1 group and 34 ± 17% in siRNA#2 group; and in T98G cells 65.7 ± 26% in siRNA#1 group and 66.8 ± 20% in siRNA#2 group passed through ~8μm pores coated with Matrigel, Figure 1c,d). The small EHT 1864 (M.W. 581.47) blocks the binding of guanine nucleotide-associated effectors to Rac1 [17]. To further detect the role of Rac1 in GBM motility, a concentration of 10 μM EHT 1864 was chosen because it had a limited effect on GBM cell viability (Figure S1g). The levels of active Rac1 were assessed using an active GTPase pull-down assay. As shown by immunoblotting measurements in GBM cells, incubation with EHT 1864 for 1 or 2 h reduced the levels of Rac1-GTP (Figure 1b). Upon inhibition, the invasion ability of these cells was reduced (21 ± 13% of U87 cells, 50 ± 13% of U251 cells, and 21 ± 23% of T98G cells passed through the pores, Figure 1e,f).

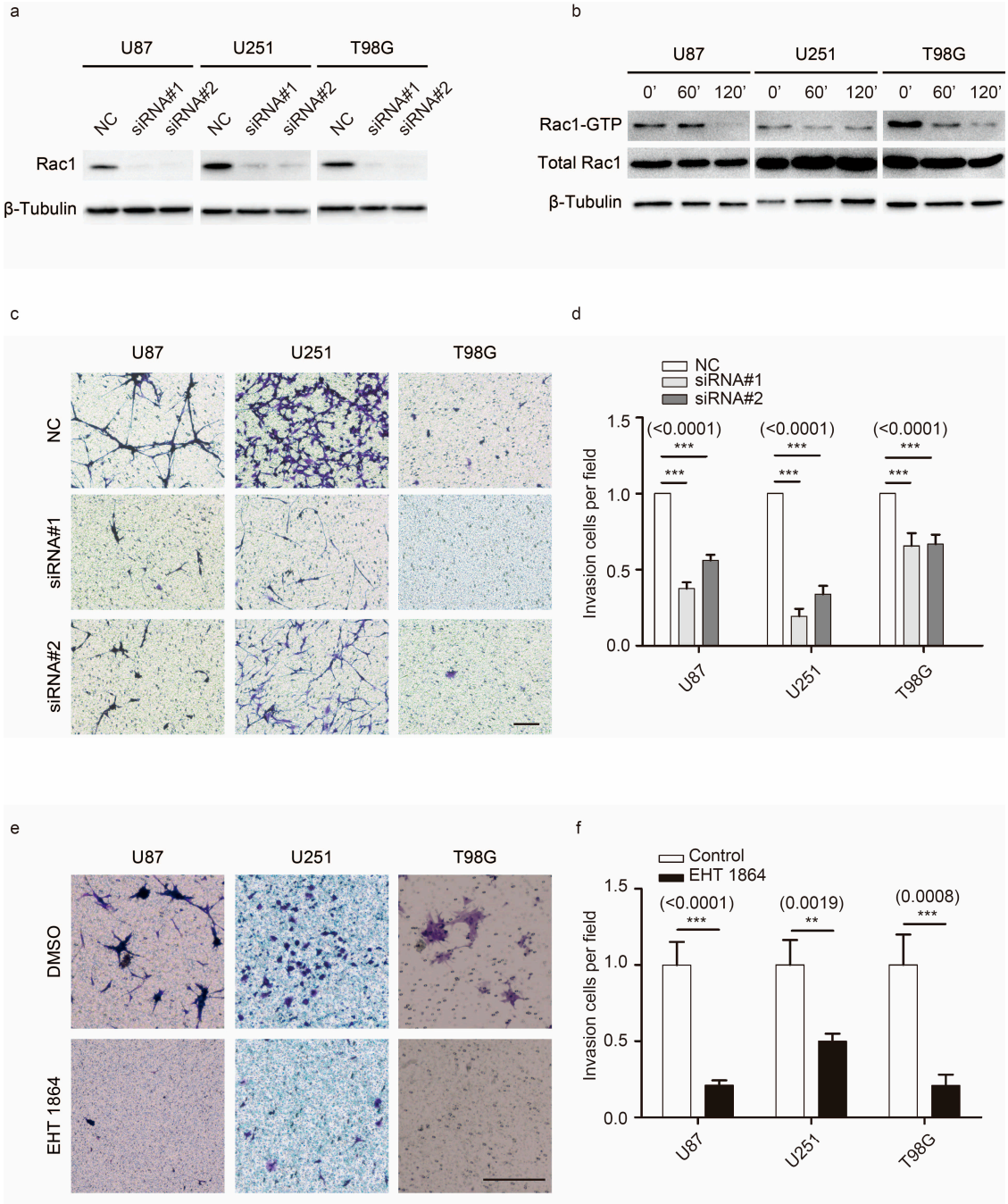

Figure 1. Rac1 is essential for glioblastoma (GBM) invasion. (**a**) Western blot analysis for Rac1 expression in U87, U251, and T98G cells 48 h after treating with siRNAs against Rac1 and negative control (NC).(**b**) The levels of Rac1-GTP (upper panel) with or without EHT 1864 treatment for 1 h or 2 h were concentrated by PAK-GST pull down assay and detected by Rac1 antibody. The expressions of total Rac1 protein (middle panel) and β-tubulin were also detected. (**c**,**e**) Invasion trans well assays were carried out to detect the invasion ability of U87, U251, and T98G cells uponRac1 knockdown (**c**) and 10 μM EHT 1864 treatments (**e**). (**d**,**f**) Cell invasion ability was calculated by counting the number of cells per field. ***: $p < 0.001$, **: $p < 0.01$. Scale bar: 1000 μm. Uncropped blots are shown in Figure S6.

We next tested the role of Rac1 in the motility of GBM cells using live cell imaging. A stable mCherry-U87 cell line was established by using LV_Pgk1p-mCherry to visualize GBM movements. U87 cells usually quickly change their shape during movement (Figure 2a upper panel, Video S1).

Upon Rac1 inhibition, U87 cells became rounder (Figure 2a lower panel, Video S2) and reduced their spreading area (Figure 2b). Trajectories of individual cells were used to quantify motility differences following EHT 1864 treatment (Figure 2c,d). We verified that Rac1 inhibition of GBM significantly reduced the velocity of U87 cells (Figure 2e).

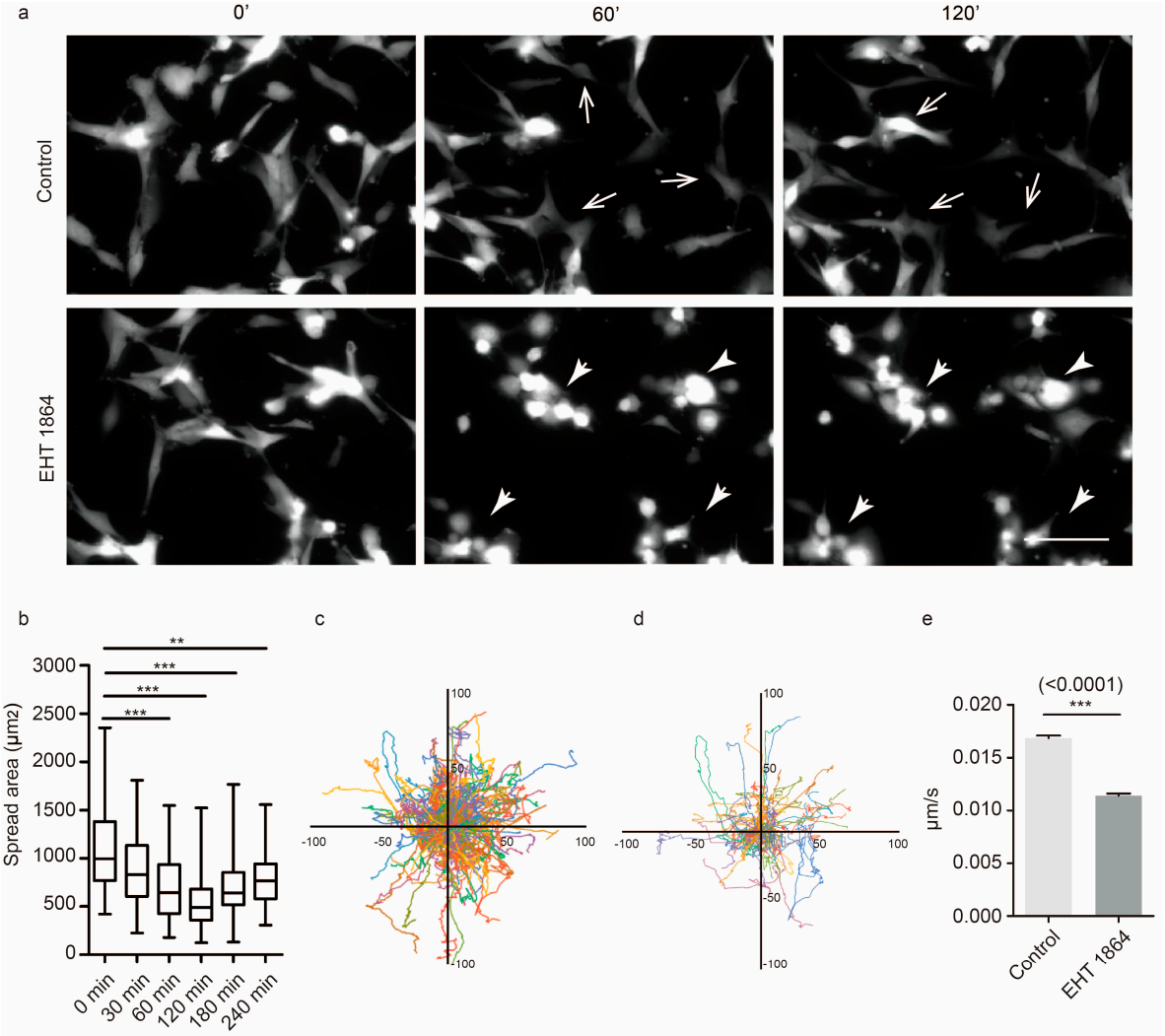

Figure 2. Rac1 activity affects random movement. (**a**) Time-lapse images of U87-mCherry cells. After 4 h recording, cells were incubated with EHT 1864 and recorded for another 4 h. Open arrow indicates cells that rapidly move, and the solid arrow indicates cells that slowly move. (**b**) U87-mCherrycell spreading areas were quantified using the ImageJ program (NIH) after EHT 1864 added for 30, 60, 120, 180, and 240 min. (**c,d**) Cell trajectories of normal U87 cells (**c**) and EHT 1864-treated U87 cells (**d**) for 4 h; each color represents the trajectory of an individual cell, and the starting positions of each cell were registered to the center of the plot. (**e**) The mean velocity of U87-mCherry cells was recorded for 4 h and analyzed using the ImageJ program (NIH). Recordings of U87-mCherrycell movement are shown in Videos S1 and S2. Cell number: 277 cells in control group and 241 cells in EHT 1864 treated group. ***: $p < 0.001$, **: $p < 0.01$. Scale bar: 100 µm.

2.2. Rac1 Signaling Regulates Myosin IIa Localization

In the leading edge, cells quickly formed membrane ruffles and protrusions for cell movement. U87 and U251 cells usually exhibited epithelial-like morphology and formed lamellipodia in front of cell. However, knockdown of Rac1 led to cell morphological changes and the formation of long protrusions (Figure 3a,b and Figure 4). Inhibition ofRac1 signaling by EHT 1864 also showed that Rac1 was

involved in the formation of membrane ruffles and protrusions (Figure S2, Video S3), polymerization of stress actin fibers (Figure S3, Videos S4 and S5), and tubulin (Figure S4) in lamellipodia.

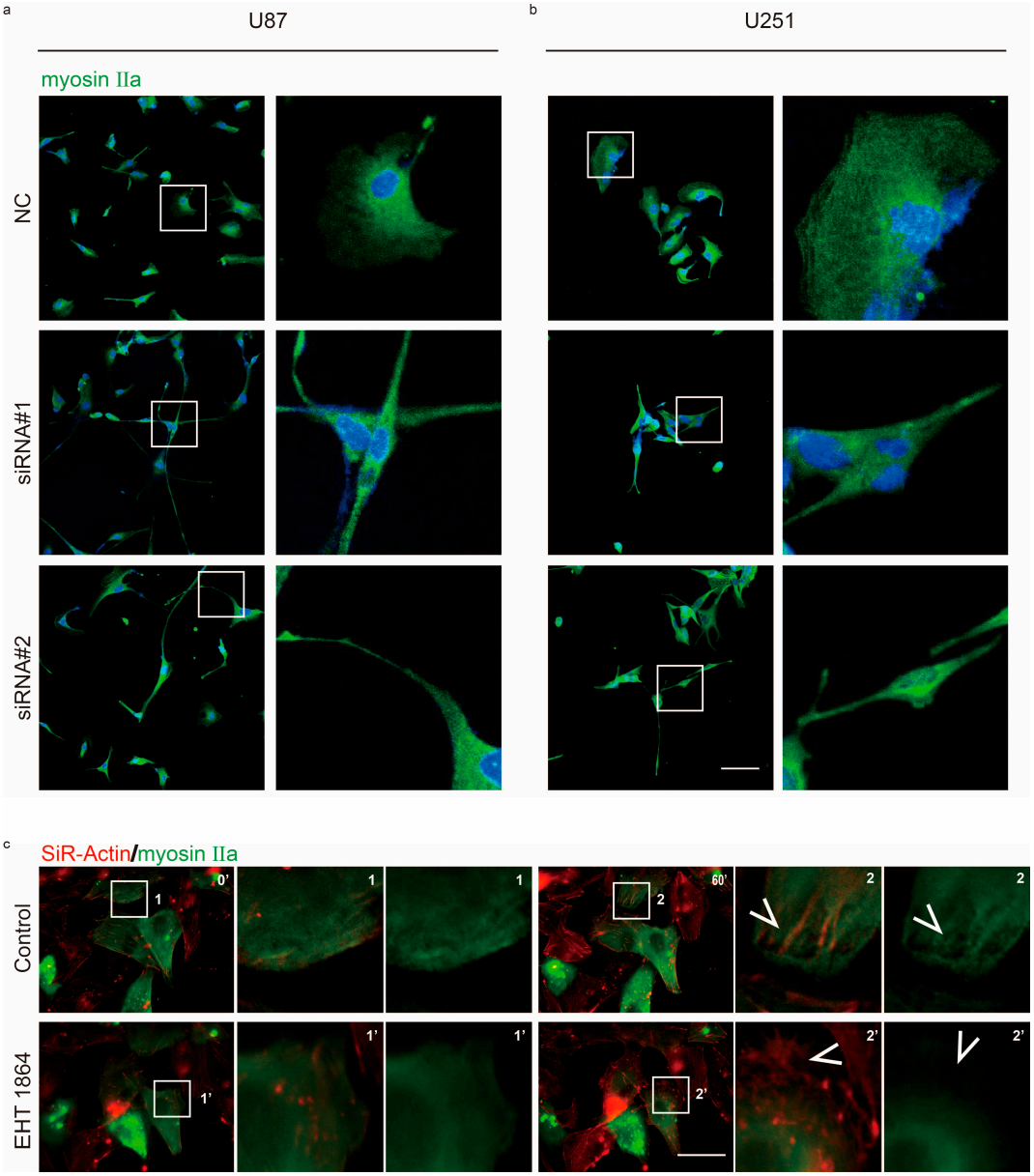

Figure 3. Rac1 regulates myosin IIa localization. (**a,b**) Confocal sections of U87 and U251 cells depleted of Rac1 48 h post-transfection and stained for myosin IIa (green). (**c**) Time-lapse images of SiR-actin staining and myosin IIa-GFP-expressing U87 cells. After 60 min, 10 µm EHT 1864 was added and recorded for another 60 min. Arrows indicate actin fibers and myosin IIa localization in the protrusion. Recordings are shown in Videos S6 and S7. Scale bar: 50 µm.

Non-muscle myosin II is an actin-binding protein and plays an important role in cell contraction during cell migration. Rac1 activation allows GBM cells to change their shape for their movement (Videos S1 and S2). We were interested whether Rac1 signaling regulates myosin II during cell movement. Immunoblotting analysis indicated that, following Rac1 knockdown or inhibition, myosin IIa phosphorylation levels did not significantly change (Figure S5). However, we found that myosin IIa usually represented a gradient from the cell rear to the leading edge in normal U87 and U251 cells. After Rac1 depletion, this gradient changed, and myosin IIa also exhibited a significant degree in the

newly formed, long protrusions (Figure 3a,b). Furthermore, myosin IIa rarely localized in the leading region according to EHT 1864 inhibition (Figure 3c, Videos S6 and S7).

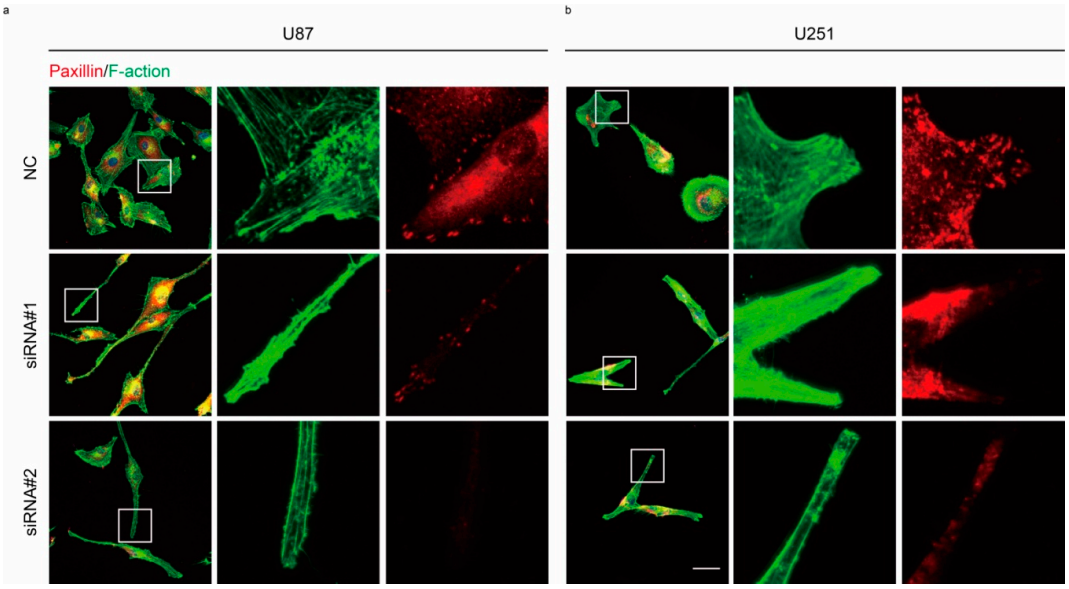

Figure 4. Rac1 is involved in cell adhesion formation. (**a**,**b**) Confocal sections of U87 and U251 cells depleted of Rac1 48 h post-transfection and stained for phalloidin (green) and Paxillin (red). Scale bar: 50 µm.

2.3. Rac1 Signaling in Cell Adhesion Formation

Inhibition of Rac1 activity disrupted lamella formation and induced a reduction in cell motility. We next analyzed the formation of cell adhesions in GBM. Cell adhesions form at the leading edge of protrusions and disassemble at both the leading edge and at the rear of the cell. These events are at the basis of cell migration. Depletion of Rac1 in U87 and U251 allowed cells to form long, thin cellular protrusions, where cells were rich in actin filaments and exhibited lack of Paxillin spots (Figure 4a,b). To determine whether Rac1 activity is involved in the rapid assembly and disassembly of adhesions, U87 cells expressing mCherry-Lifeact-7 and Paxillin-GFP were used. In this way, we monitored the dynamics of adhesions and actin organization using live cell imaging (Figure 5a, Videos S8 and S9). Recordings lasted approximately 15 min, and one frame was digitized every 10 s. Analysis of these recordings showed four distinct adhesion types: assembly type, in which a single assembly event was observed within 15 min; disassembly type in a single disassembly event was seen; stable type, in which the adhesion spot remained stable; and turnover type, which showed both assembly and disassembly events (Figure 5f). Our data show that in U87 GBM cells, after adding EHT 1864 for 2 h, more adhesion spots were stable, while both disassembly and turnover types were less frequent (Figure 5a,f). Although the number of adhesions (Figure 5b), the area of adhesions (Figure 5c) and the assembly rate (Figure 5d) was less affected by the addition of EHT 1864, the disassembly rate (Figure 5e) were less affected by the addition of EHT 1864, the disassembly rate (Figure 5e) was dramatically decreased, concomitant with a blockage of actin filament collapse (Figure 5a). Furthermore, the lifetime of turnover adhesions did not exhibit a detectable difference between each group (Figure 5i); however, both the assembly and disassembly rates of these adhesions were significantly slower than the rates in control conditions (Figure 5g–j), which explains why the portion of turnover type was low following Rac1 inhibition.

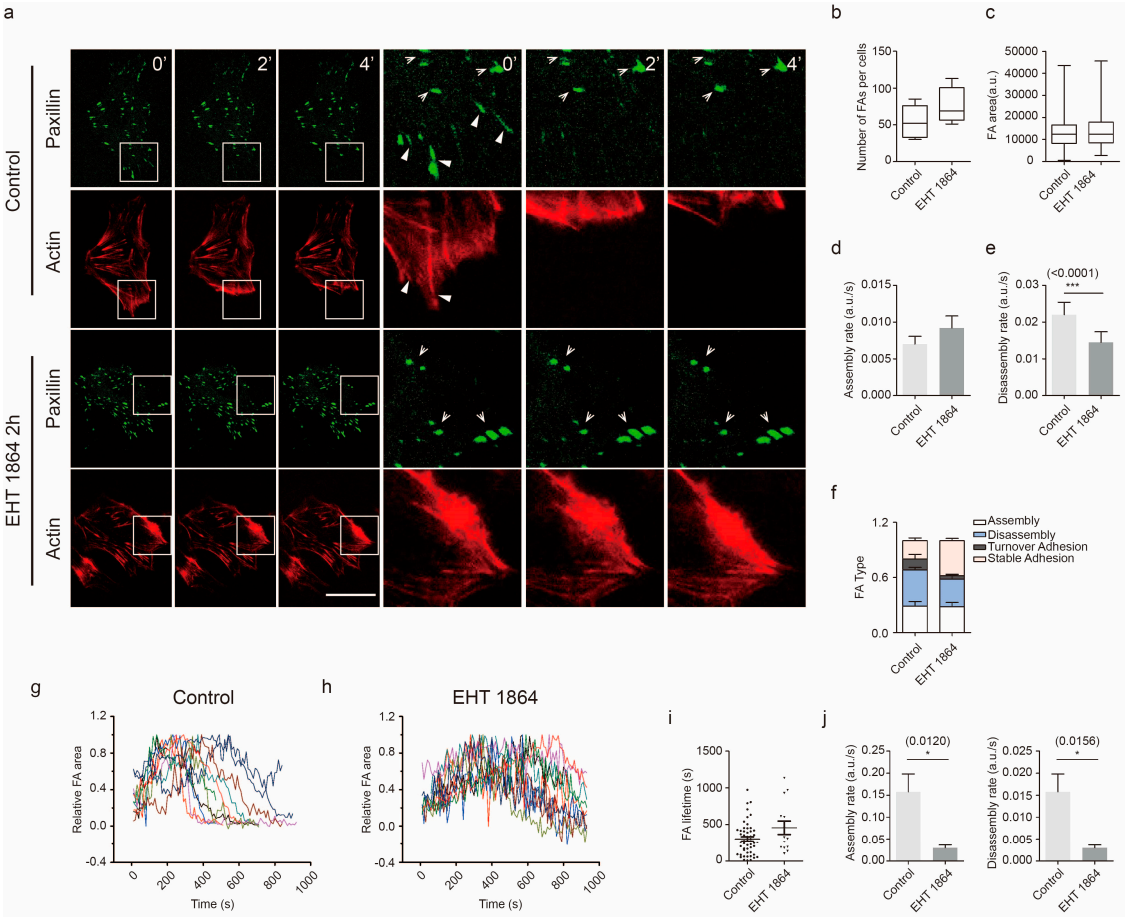

Figure 5. Rac1 signaling controls cell adhesion dynamics. (**a**) U87 transfected with Paxillin (green) and mCherry-Lifeact-7 (red) were imaged by time-lapse microscopy at 10 s intervals for 15 min. Time-lapse images of U87 cells after 1 h of incubation with DMSO or EHT 1864, respectively. Closed arrow indicates disassembly type, and open arrow indicates cell stable adhesion. Histograms of the total cell adhesion number (**b**), adhesion area (**c**), adhesion assembly rate (**d**), and disassembly rate (**e**) and adhesion type proportion ratio in the normal and EHT 1864-treated groups (**f**). (**g–h**) Typical curves of dynamic turnover adhesions in both the control group (**g**) and EHT 1864 group (**h**). (**i**) Lifetime of turnover adhesions in the normal and EHT 1864-treated groups. (**j**) Histograms of the assembly rate and disassembly rate of turnover adhesions in the normal and EHT 1864-treated groups. Recordings are shown in Videos S8 and S9. Scale bar: 20 μm. Tracking cell adhesion numbers: 395 in the control group and 407 in EHT 1864-treated group. ***: $p < 0.001$, *: $p < 0.05$.

2.4. Rac1 Activates Erk to Mediate Cell Adhesion Dynamics

The mitogen-activated protein kinase (MAP kinase)/Erk cascade promotes Paxillin phosphorylation [25]. Inhibition of the Erk1/2 upstream regulator MEK1/2 constitutively abolishes active Rac1-induced EMT in ovarian cancer cells [26]. Our data showed that inhibition of Rac1 contributes to impaired Paxillin disassembly and turnover of cell adhesions. We then investigated whether Erk1/2 is involved in Rac1 signaling that regulates the dynamics of cell adhesion. Immunoblotting analysis indicated that, following Rac1 inhibition, Erk1/2 phosphorylation levels were diminished within 30 min and up to 120 min in a time-dependent manner after EHT 1864 was added (Figure 6). These results show that the Erk1/2 pathway may be involved in Rac1 regulation of GBM cell motility.

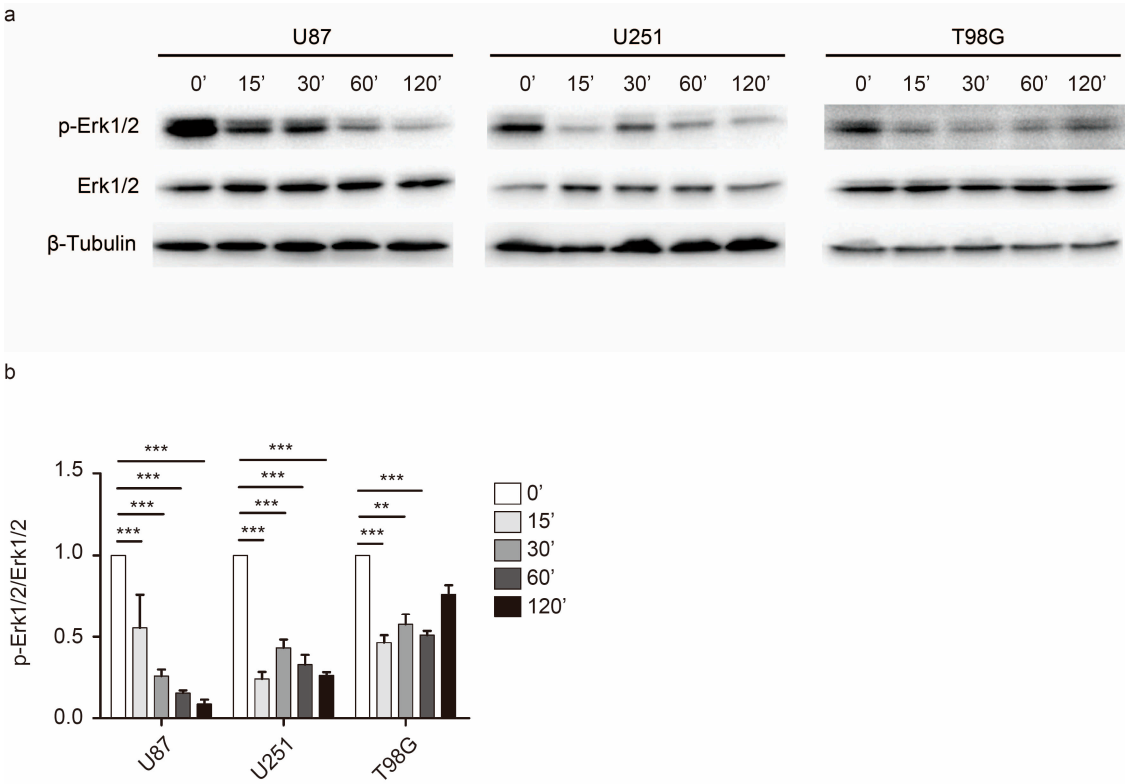

Figure 6. Rac1 regulates cell motility in Erk1/2 dependent way in GBM. (**a**) Western blot analysis of the level of phosphorylation of Erk1/2 in U87, U251 and T98G cells when responding to EHT 1864. (**b**) Histograms of the expression levels of phosphorylated Erk1/2 compared to total Erk1/2 in response to EHT 1864. ***: $p < 0.001$, **: $p < 0.01$. Uncropped blots are shown in Figure S7.

2.5. Characterization of the Mechanical Properties in Response to Rac1 Inhibition

Several works have shown that the elastic properties of cancer cells are correlated with malignant transformation [18,26,27]. The cell cytoskeleton, especially the actin cytoskeleton, is the key regulator for maintaining cell shape and mechanics [28,29]. Changes in cytoskeletal organization and cell shape during migration were observed in response to Rac1 inhibition (Figure 2b, Figures S3 and S4). We further decided to detect the elastic properties of GBM cells, and single-cell force spectroscopy (SCFS) measurements were performed using AFM (Figure 7a,b). Cell elasticity values were obtained by fitting the approaching part of the recorded F–D curves using the Hertz–Sneddon model and calculating the Young's modulus (E) of each cell (Figure 7c,d). Quantitative analysis showed that, following Rac1 inhibition, the Young's modulus of GBM cells increased from 0.84 ± 0.53 kPa to 1.12 ± 0.70 kPa (Figure 7e). Cellular viscosity can be used to characterize the fluidity or ease of movement inside cells, which is an important mechanical property of live cells. We hypothesized that, following the inhibition of Rac1, the viscosity of GBM could be changed. The viscosity of GBM cells was obtained following the procedure described by Achu Yango et al. using AFM (Figure 7f–i) [30]. Consistent with the elasticity changes, the viscosity of live GBM cells also increased from 193.59 ± 152.16 Pa × s to 257.15 ± 187.82 Pa × s following Rac1 inhibition (Figure 7j). The increased viscosity observed here is consistent with the view that, following inhibition of Rac1, the whole cell interior reorganizes and is less fluid and more rigid.

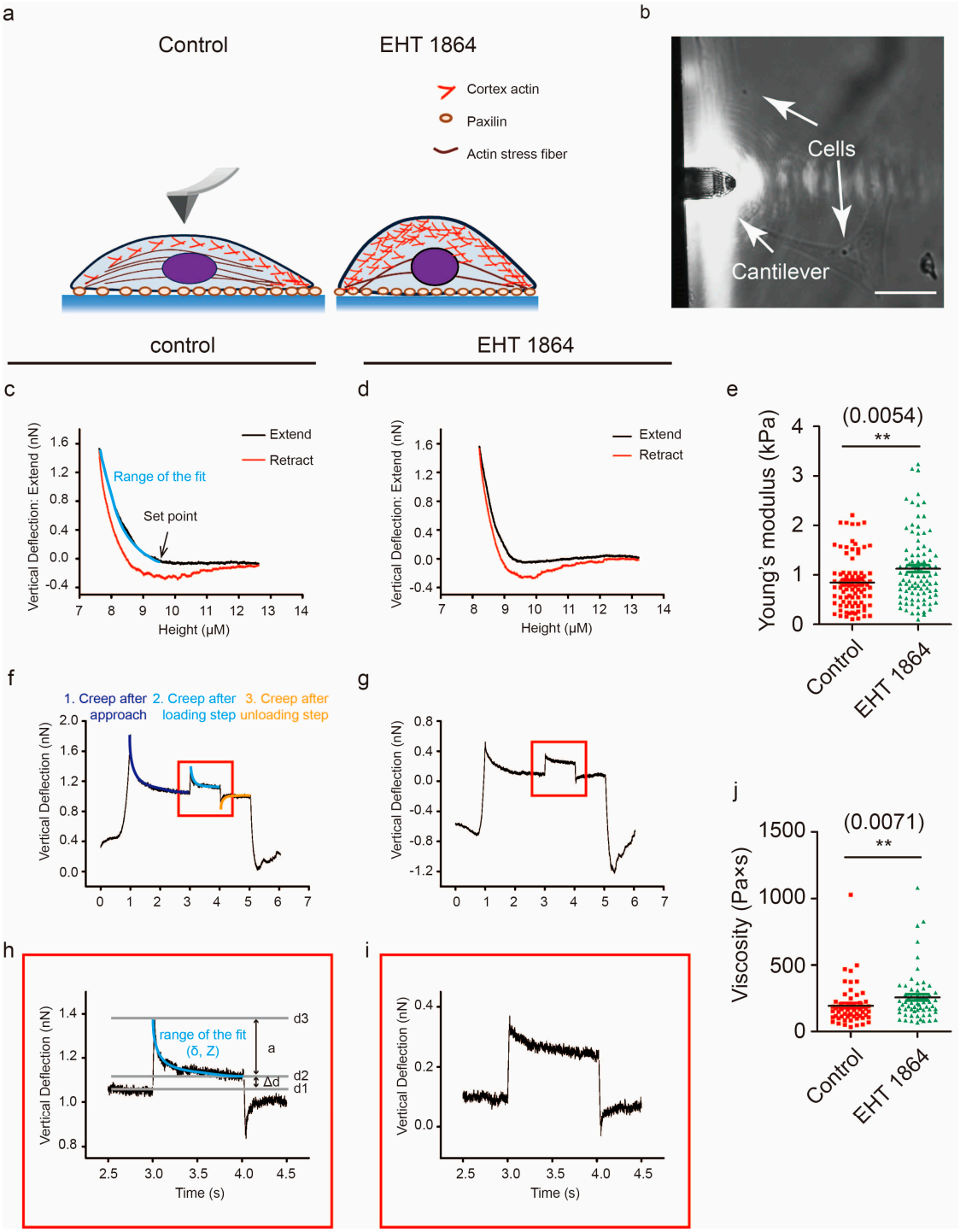

Figure 7. Rac1 activation affects the mechanics of GBM cells. (**a**) Diagrams illustrate the method of application of external force. (**b**) Image showing the AFM detection of the cell mechanical properties of a single living cell. (**c,d**) Exemplary force curve recorded on a U87 cell with (**d**) and without (**c**) EHT 1864 incubation for 1–2 h. The black solid line represents the approach curve, and the Young's modulus (E) was calculated by fitting the approach curve of each cell. (**e**) Histograms of the associated Young's modulus E for U87 cells with and without EHT 1864 treatment. (**f–i**) Typical creep curve responses to a cell after applying the z step. The z height is first ramped as in a conventional force curve (approach ramp) and then kept constant for 1 s. (**j**) Histograms of the viscosity value of U87 cells with and without EHT 1864 treatment. Cell number: 95 in control group and 101 in EHT 1864-treated group for Young's modulus; 64 in control group and 66 in EHT 1864-treated group for viscosity. **: $p < 0.01$; scale bar: 25 μm.

3. Discussion

In the present study, we confirmed that Rac1 is involved in GBM infiltration. We showed that Rac1 depletion or inhibition leads to the following: I. GBM cells dramatically reduce their invasion ability; II. GBM cells change their morphology accompanied with a reorganization of the cell cytoskeleton, abnormal myosin IIa location, and cell adhesion formation; III. there is a rapid suppression of Erk1/2 phosphorylation according to EHT 1864 inhibition; and IV. this was accompanied by an increase in the rigidity and viscosity of GBM cells.

Upregulation of Rac1 has been recently reported in various kinds of cancers and is correlated with poor overall survival of patients with glioma (Figure S1a,b). Recent works report that Rac1 plays a very important role in cancer cell proliferation and survival. In our study, knockdown of the expression of Rac1 in U87, U251, and T98G cells did not significantly affect cell viability (Figure S1f), which indicates that Rac1 promotes glioma progression mainly by another way. Regarding GBM, in particular, U87 cells were observed in a co-culture condition with healthy neurons and glia, and visual inspection revealed a remarkable feature: GBM cells had a much higher motility than healthy neurons and glial cells [31]. Activated Rac1 induced the formation of membrane ruffles and cell protrusion at the leading edge of migrating cells [11,32]. Knockdown of Rac1 in both U87 and U251 showed that cell lacked lamellipodium, instead of forming long, thin cell protrusions (Figure 3a,b and Figure 4). In the presence of Rac1 inhibitor EHT 1864, cells showed frequent membrane protrusions but without ruffle activity (Figure S2 and Video S3). Activated Rac1 allows WAVE to stimulate Arp2/3-actin polymerization activity in the lamellipodium [33]. Abnormal ruffles and shrinkage of the cell body suggest that Rac1 inactivation causes a reorganization of actin in GBM cells. Using SiR-actin and SiR-tubulin to label cytoskeleton filaments, we found that Rac1 inhibition caused defects in actin organization and tubulin direction (Figures S3 and S4 and Videos S4 and S5).

Impaired disassembly of cell adhesion affects cell migration in murine embryonic fibroblasts (MEFs); however, constitutive activation of Rac1 shows no detectable effect on adhesion disassembly [25]. Here, we found that Rac1 depletion in GBM cells promoted the formation of long, thin protrusion sand lack of Paxillin spots (Figure 4a,b). Furthermore, inhibition of Rac1 by EHT 1864 disrupted the disassembly of cell adhesion concomitant with defects in the actin web and switched the proportion of stable cell adhesion complex (Figures 5a and 4e,f, Videos S8 and S9). These results demonstrate that Rac1 plays different roles in different cell types in regulating cell adhesion formation. In migrating cells, non-muscle myosin II can bind to actin and lead to cell contraction that increases cell membrane protrusion at the leading edge and inhibits protrusion at the rear of the cell [34,35]. Our results indicated that there were no detectable changes in myosin IIa activity (Figure S5). Myosin IIa exhibited a high degree of long, thin protrusions of Rac1-depleted GBM cells, which maybe the reason for these cells losing their polarity for fast movement. Myosin IIa rarely emerged at the leading stage according to EHT 1864 inhibition (Figure 3, Video S6 and S7). This demonstrates a lack of forces that induce contraction and breakage of cell–matrix adhesions at the rear mainly due to the abnormal distribution of myosin IIa. Donna J. Webb and colleagues demonstrated that Erk and MLCK activated the phosphorylation state of Paxillin, which further regulates adhesion disassembly [25]. Here, we found a rapid decrease in the phosphorylation level of Erk1/2 (Figure 6), suggesting that Rac1 also regulates the dynamics of cell adhesion through the Erk signaling pathway.

Previous studies have reported that cancer cells are softer than normal cells [18,19], which allows metastatic cells to squeeze their shape through the extracellular matrix. The mechanical properties have also been used to evaluate cancer progression and the reaction to drugs [27]. The mechanical properties depend primarily on the cytoskeleton, and it is expected that the decreased value of cell elasticity (Figure 7c–e) caused by Rac1 inhibition is associated with the disruption of cytoskeleton organization inside GBM cells (Figures S3 and S4). Viscosity is a measure of fluid resistance, and the inhibition of Rac1 causes an increase in viscosity, i.e., a decrease in the fluidity of the cell (Figure 7f–j). These results indicate that cell mechanical properties change according to pharmacologic treatment, and these changes are associated with cell motility in GBM cells.

4. Materials and Methods

4.1. Cell Lines

Human GBM cell lines U87, U251, T98G (all from ATCC), and U87 stably transfected with LV_Pgk1p-mCherry were cultured at 37 °C, 5% CO_2 in DMEM medium supplemented with 10% FBS and penicillin/streptomycin. Cell cultures were routinely subcultured every two days by trypsinization using standard procedures. U87 stably transfected with LV_Pgk1p-mCherrywere provided by the laboratory of Prof. Antonello Mallamaci from the International School of Advanced Studies.

4.2. Gene Silencing

siRNAs against Rac1 and the negative control (NC) were purchased from Shanghai GenePharma Co., Ltd (Shanghai, China). Target sequences for siRac1 were as follows: siRac1#1, 5′-CUACUGUCUUUGACAAUUATT-3′ and 5′-UAAUUGUCAAAGACAGUAGTT-3′; siRac1#2, 5′-GAGUCCUGCAUCAUUUGAATT-3′ and 5′-UUCAAAUGAUGCAGGACUCTT-3′.

siRNAs were transiently transfected into U87, U251, or T98G cells by Lipofectamine™ RNAiMAX (Invitrogen, Carlsbad, CA, USA) according to the manufacturer's instructions.

4.3. Immunofluorescent Staining and RT-PCR

Cells were fixed with 4% PFA for 20 min and permeabilized with 0.1% TritonX-100 for 20 min. Cells were then incubated with primary antibody and secondary antibody. The following primary antibodies were used: anti-myosin IIa (1:200, Cell Signaling Technology, Danvers, MA, USA) and anti-Paxillin (1:200, Abcam, Cambridge, UK). Phalloidin (1:2000, Invitrogen) was used to detect F-actin.

Total RNA was extracted using Trizol® (Invitrogen), according to the manufacturer's instructions, and then was reverse-transcribed by PrimeScript™ reagent kit (TaKaRa, Kusatsu, Japan). PCR reaction was done using SUBR® Premix Ex Taq™ (TaKaRa). RAC1 primer sequence was 5′-AAGCTGAC TCCCATCACCTATCCG-3′ and 5′-CGAGGGGCTGAGACATTTACAACA-3′.

4.4. Cell Proliferation Assay

A total of 5×10^3 cells were plated in 96-well plates. After 12 h culture, cells were transfected with Rac1-siRNA and NC-siRNA and cultured for another 48 h. Cell growth was measured by a colorimetric CCK-8 assay (Sigma-Aldrich Co, St. Louis, MO, USA).

A total of 2.5×10^4 cells were plated in 96-well plates. After 12 h culture, cells were treated with different concentrations of EHT 1864 2HCL (Sellekchem, Houston, TX, USA) for another 24 h, and then CCK-8 measurement followed.

4.5. Cell Transfection and Live Cell Imaging

Cells were plated at a density of 1×10^5 cells/mL into 35 mm confocal dishes and incubated overnight. SiR-actin and SiR-tubulin (cytoskeleton, Denver, CO, USA) staining were used to detect the dynamics of actin and tubulin cytoskeleton following the protocol provided by the manufacturer. Transient transfections of mCherry-Lifeact-7 and paxillin-GFP were carried out with Lipofectamine™ 2000 (Invitrogen) using the protocol provided by the manufacturer. Twenty-four hours after transfection, cells were used for the live cell imaging assay. mCherry-Lifeact-7 was a gift from Michael Davidson (Addgene plasmid # 54491; http://n2t.net/addgene:54491; RRID:Addgene_54491).

For the live cell imaging assay, cells were maintained at 37 C, 5% CO_2 in chambers in culture medium on an inverted microscope (Nikon, Tokyo metropolis, Japan) with a motorized stage (Prior Scientific, Cambridge, UK) controlled by Simple PCI software (Compix). Stable U87-mCherry cells were used to detect the cell shape, and velocity changes with and without EHT 1864 and time-lapse image series were acquired at 1 min intervals using a 20 × 1.4 NA objective lens (Nikon). SiR-actin, SiR-tubulin, mCherry-Lifeact-7, and Paxillin-GFP fluorescence time-lapse image series were acquired at 1 s to 2 min

intervals using a 40 × or 60 × 1.4 NA objective lens (Nikon). Cells were treated with 10 μM EHT 1864 to detect the role in cytoskeleton organization and dynamics of cell adhesions.

4.6. Tracking Assays and Data Analysis

Tracking of cell migration was performed over a period of 4 h. Individual cells were tracked by repeated selection of cells in movie frames and manual tracing of migration pathways with Image J software.

Individual cell adhesions were tracked similar to the cell tracking procedure. We then fit the curves of 'adhesion assembly' or 'adhesion disassembly' by Origin software using Slogistic1 function, and we obtained the *k*/-*k* value as the rate of assembly or disassembly. To calculate the lifetime of turnover adhesions, we separated the curves into two parts and fit them individually.

4.7. Active Rac1 Pull-Down Assay and Western Blot

Cells were plated at a density of 2×10^6 cells/well in 10 cm and grown to 70–80% confluence. The cells were then incubated with 10 μM EHT 1864 for 15, 30, 60, and 120 min. Cells were washed with cold PBS and lysed in IP lysis buffer (20 mMTris pH 7.4, 150 mM NaCl, 5 mM $MgCl_2$, 0.5% NP-40, 10% glycerol, pH 7.4) supplemented with a protease inhibitor cocktail (Sigma-Aldrich Co, St. Louis, MO, USA). After normalization, lysates were incubated with 20 μg PAK-PBD agarose for 60 min at 4 °C with rotation, and then the beads were collected for Western Blotting analysis.

Equal amounts of total protein were boiled for 5 min in 5× sample buffer and fractionated by 12% SDS-PAGE. Samples were then transferred to PVDF Membranes (Millipore, Danvers, MA, USA). Immunoblots were detected using the ECL System (Millipore) with horseradish peroxidase-conjugated secondary antibodies (Sigma-Aldrich Co, St. Louis, MO, USA). The following first antibodies were used: anti-Rac1 (Abcam, Cambridge, UK), anti-p-Erk1/2 (Cell Signaling Technology, Danvers, MA, USA), and anti-Erk1/2 (Cell Signaling Technology, Danvers, MA, USA).

4.8. Transwell Assay

To detect cell invasion, transwell chambers were pre-coated with 200 μL of a 0.8 mg/mL Matrigel suspension and dried at 37 °C. Cells were starved overnight in DMEM medium, 5×10^5 cells in DMEM medium were added to the top chambers of 12-well transwell plates (Nunc; 8 μm pore size), and 15% FBS DMEM medium was added to the bottom chambers. After 48 h incubation, top (non-migrating) cells were removed, and bottom (migrating) cells were fixed with 4% PFA and stained with 5% crystal violet.

4.9. Force Spectroscopy of Living Cells and Data Analysis

Single-cell force spectroscopy (SCFS) measurements were performed by using a commercial AFM (JPK Instruments, Berlin, Germany) mounted on top of an Axiovert 200 inverted microscope (Olympus, Japan). We used rectangular low-stress SiN cantilevers terminated with a silicon pyramidal tip (APPNANO, Mountain View, CA, USA). Those cantilevers are characterized by a nominal spring constant k = 0.0084 N/m; the tip height was 4–6 μm, while the radius of curvature at the tip apex was <25 nm. The cells were incubated 37 °C using a temperature-controlled BioCell chamber (JPK Instruments, Berlin, Germany) during the measurements. Cell elasticity values were obtained by fitting the approaching part of the recorded F–D curves using the Hertz–Sneddon model and calculating the Young's modulus (E) of each cell through JPK software. Cell viscosity measurements were obtained as previously described [36]. Briefly, the z voltage was kept constant for 2 s after approaching the sample, the z height was increased by a small amount (0.5 nN) and kept for 1 s, and then it was withdrawn again after 1 s.

4.10. Statistical Analysis

Differences between groups were assessed by Student's *t* test, one-way ANOVA, or two-way ANOVA test. GraphPad Prism was used for all statistical analyses. The differences of RT-PCR, WB, and CCK-8 were evaluated by two-way ANOVA. The differences in cell mobility, mechanics, and adhesion dynamics were evaluated by a Student's *t* test followed by a Mann–Whitney test. The difference of cell spreading area was evaluated by one-way ANOVA followed by a Kruskal–Wallis test. The results are presented as the mean ± SEM of at least three independent experiments.

5. Conclusions

Our study demonstrates that there is a close relationship between cell mechanics and invasiveness of GBM cells. In GBM cells, downregulation of Rac1 is associated with low cell motility by regulating the dynamics of the cytoskeleton and cell adhesion. Rac1 activation also adjusts the rigidity and viscosity of GBM cells. It takes only a few minutes to measure the single-cell mechanics, which is a much shorter time compared to the typical original assays. Here, we suggest that cell mechanics can be used as a novel and convenient strategy for surgical and therapeutical interventions in the future.

Supplementary Materials: The following are available online at http://www.mdpi.com/2072-6694/12/6/1667/s1, Figure S1: (**a**) Rac1 expression in GBM tissue compared with non-GBM tissue (The Y-axis represent log2 (TPM+1), red box represent GBM tissue and grey box represent non-GBM tissue). (Data are from GEPIA: gepia.cancer-pku.cn) (**b**) Overall survival of GBM patients with low Rac1 expression and high Rac1 expression. (Data are from GEPIA: gepia.cancer-pku.cn) (**c**) mRNA levels of Rac1in U87, U251, and T98G GBM cells were analyzed by RT-PCR after Rac1-siRNA and NC-siRNA were transfected for 48 h. (**d**) Cell viability of U87, U251, and T98G GBM cells was evaluated by using the CCK-8 assay after Rac1 knockdown for 48 h. (**e**) Cell viability of U87, U251, and T98G GBM cells was evaluated by using the CCK-8 assay after incubation with different concentrations of EHT 1864 for 12 h. ***: $p < 0.001$, **: $p < 0.01$, *: $p < 0.05$, Figure S2: Phase contrast time-lapse microscopy recording of U87 cells at 2 min intervals for 1 h. After 1 h recording, 10 µm EHT 1864 was added and recorded for another 1 h to observe cell membrane movement. The red arrow indicates cell membrane ruffles, and the yellow arrow indicates cell membrane protrusion. U87 cell recordings are shown in Video S3. Figure S3: SiR-actin staining of U87 cells was imaged by time-lapse microscopy at 2 min intervals for 30 min. After 30 min recording, 10 µm EHT 1864 was added and recorded for another 30 min to observe actin organization. The red arrow indicates actin assembly fibers in the protrusion, and the yellow arrow indicates actin disassembly fibers in the protrusion. Recordings of actin dynamics are shown in Videos S4 and S5. Figure S4: SiR-tubulin staining of U87 cells was imaged by time-lapse microscopy at 2 min intervals for 30 min. After 30 min recording, 10 µm EHT 1864 was added and recorded for another 30 min to observe tubulin organization. The red arrow indicates tubulin assembly in the protrusion, and the yellow arrow indicates tubulin disassembly. Figure S5: Western blot analysis of the level of phosphorylation of myosin IIa in U87, U251, and T98G cells in response to Rac1 depletion by siRNA and inhibited by EHT 1864, Figure S6. The whole Western Blot for Figure 1, Figure S7. The whole Western Blot for Figure 6, Video S1: Random movement of U87-mCherry cells in control condition. Video S2: Random movement of U87-mCherry cells incubated with EHT 1864. Video S3: Phase contrast microscopy recording of U87 cells incubated without (left) and with (right) EHT 1864. Video S4: Recording of SiR-actin staining of U87 cells in control conditions. Video S5: Recording of SiR-actin staining of U87 cells incubated with EHT 1864. Video S6: Recording of SiR-actin staining (red) and myosin IIa transfected (green) U87 cells in control conditions. Video S7: Recording of SiR-actin staining (red) and myosin IIa transfected (green) U87 cells incubated with EHT 1864. Video S8: Recording of dynamics of cytoskeleton and cell adhesion in U87 cells in control conditions. Video S9: Recording of dynamics of cytoskeleton and cell adhesion in U87 cells incubated with EHT 1864.

Author Contributions: J.X.: Conceptualization, Data curation, Formal analysis, Investigation and Writing—Original draft; N.G.: Software and Writing—Review & Editing; J.N.: Writing—Reviewing and Editing; Y.Y.: Supervision and Writing—Reviewing and Editing; V.T.: Funding acquisition, Supervision, Writing—Reviewing and Editing. All authors have read and agreed to the published version of the manuscript.

Funding: This work was supported by funds from Regione Friuli-Venezia Giulia (FVG) (Italy) for the project "GLIOBLASTOMA—Infiltrazione nei gliomi: nuovo target terapeutico" and the 3315 Innovative Teams Program of Ningbo—China, Zhejiang Provincial Natural Science Foundation of China under grant no. LQ17C100001, the Natural Science Foundation of Ningbo City under grant no. 2017A610256.

Acknowledgments: The authors thank Beatrice Pastore for technical assistance, Kaiwen Sun for data analysis support, and Qin Song, Miao Xiao, and Xiaoyun Li for useful discussions.

Conflicts of Interest: The authors declare no conflict of interest.

References

1. Stupp, R.; Mason, W.P.; van den Bent, M.J.; Weller, M.; Fisher, B.; Taphoorn, M.J.; Belanger, K.; Brandes, A.A.; Marosi, C.; Bogdahn, U.; et al. Radiotherapy Plus Concomitant and Adjuvant Temozolomide for Glioblastoma. *New Engl. J. Med.* **2005**, *352*, 987–996. [CrossRef] [PubMed]
2. Stupp, R.; Hegi, M.E.; Mason, W.P.; van den Bent, M.J.; Taphoorn, M.J.; Janzer, R.C.; Ludwin, S.K.; Allgeier, A.; Fisher, B.; Belanger, K.; et al. Effects of Radiotherapy with Concomitant and Adjuvant Temozolomide Versus Radiotherapy Alone on Survival in Glioblastoma in a Randomised Phase Iii Study: 5-Year Analysis of the Eortc-Ncic Trial. *Lancet Oncol.* **2009**, *10*, 459–466. [CrossRef]
3. Chan, A.Y.; Coniglio, S.J.; Chuang, Y.Y.; Michaelson, D.; Knaus, U.G.; Philips, M.R.; Symons, M. Roles of the Rac1 and Rac3 Gtpases in Human Tumor Cell Invasion. *Oncogene* **2005**, *24*, 7821–7829. [CrossRef] [PubMed]
4. Parri, M.; Chiarugi, P. Rac and Rho Gtpases in Cancer Cell Motility Control. *Cell Commun. Signal* **2010**, *8*, 23. [CrossRef] [PubMed]
5. Chi, X.; Wang, S.; Huang, Y.; Stamnes, M.; Chen, J.L. Roles of Rho Gtpases in Intracellular Transport and Cellular Transformation. *Int. J. Mol. Sci.* **2013**, *14*, 7089–7108. [CrossRef] [PubMed]
6. Ridley, A.J.; Paterson, H.F.; Johnston, C.L.; Diekmann, D.; Hall, A. The Small Gtp-Binding Protein Rac Regulates Growth Factor-Induced Membrane Ruffling. *Cell* **1992**, *70*, 401–410. [CrossRef]
7. Blanchoin, L.; Amann, K.J.; Higgs, H.N.; Marchand, J.B.; Kaiser, D.A.; Pollard, T.D. Direct Observation of Dendritic Actin Filament Networks Nucleated by Arp2/3 Complex and Wasp/Scar Proteins. *Nature* **2000**, *404*, 1007–1011. [CrossRef]
8. Goley, E.D.; Welch, M.D. The Arp2/3 Complex: An Actin Nucleator Comes of Age. *Nat. Rev. Mol. CellBiol.* **2006**, *7*, 713–726. [CrossRef]
9. Takenawa, T.; Miki, H. Wasp and Wave Family Proteins: Key Molecules for Rapid Rearrangement of Cortical Actin Filaments and Cell Movement. *J. Cell Sci.* **2001**, *114*, 1801–1809.
10. Ridley, A.J. Rho Gtpases and Actin Dynamics in Membrane Protrusions and Vesicle Trafficking. *Trends Cell Biol.* **2006**, *16*, 522–529. [CrossRef]
11. Malliri, A.; van der Kammen, R.A.; Clark, K.; van der Valk, M.; Michiels, F.; Collard, J.G. Mice Deficient in the Rac Activator Tiam1 Are Resistant to Ras-Induced Skin Tumours. *Nature* **2002**, *417*, 867–871. [CrossRef] [PubMed]
12. Kissil, J.L.; Walmsley, M.J.; Hanlon, L.; Haigis, K.M.; Bender Kim, C.F.; Sweet-Cordero, A.; Eckman, M.S.; Tuveson, D.A.; Capobianco, A.J.; Tybulewicz, V.L.; et al. Requirement for Rac1 in a K-Ras Induced Lung Cancer in the Mouse. *Cancer Res.* **2007**, *67*, 8089–8094. [CrossRef] [PubMed]
13. Kazanietz, M.G.; Caloca, M.J. The RacGtpase in Cancer: From Old Concepts to New Paradigms. *Cancer Res.* **2017**, *77*, 5445–5451. [CrossRef] [PubMed]
14. Gastonguay, A.; Berg, T.; Hauser, A.D.; Schuld, N.; Lorimer, E.; Williams, C.L. The Role of Rac1 in the Regulation of Nf-Kappab Activity, Cell Proliferation, and Cell Migration in Non-Small Cell Lung Carcinoma. *Cancer Biol. Ther.* **2012**, *13*, 647–656. [CrossRef]
15. Yang, W.H.; Lan, H.Y.; Huang, C.H.; Tai, S.K.; Tzeng, C.H.; Kao, S.Y.; Wu, K.J.; Hung, M.C.; Yang, M.H. Rac1 Activation Mediates Twist1-Induced Cancer Cell Migration. *Nat. Cell Biol.* **2012**, *14*, 366–374. [CrossRef]
16. Etienne-Manneville, S.; Hall, A. Rho Gtpases in Cell Biology. *Nature* **2002**, *420*, 629–635. [CrossRef]
17. Shutes, A.; Onesto, C.; Picard, V.; Leblond, B.; Schweighoffer, F.; Der, C.J. Specificity and Mechanism of Action of Eht 1864, a Novel Small Molecule Inhibitor of Rac Family Small Gtpases. *J. Biol. Chem.* **2007**, *282*, 35666–35678. [CrossRef]
18. Cross, S.E.; Jin, Y.S.; Rao, J.; Gimzewski, J.K. Nanomechanical Analysis of Cells from Cancer Patients. *Nat. Nanotechnol.* **2007**, *2*, 780–783. [CrossRef]
19. Remmerbach, T.W.; Wottawah, F.; Dietrich, J.; Lincoln, B.; Wittekind, C.; Guck, J. Oral Cancer Diagnosis by Mechanical Phenotyping. *Cancer Res.* **2009**, *69*, 1728–1732. [CrossRef]
20. Liu, J.; Zhang, D.; Luo, W.; Yu, Y.; Yu, J.; Li, J.; Zhang, X.; Zhang, B.; Chen, J.; Wu, X.R.; et al. X-Linked Inhibitor of Apoptosis Protein (Xiap) Mediates Cancer Cell Motility Via Rho Gdp Dissociation Inhibitor (Rhogdi)-Dependent Regulation of the Cytoskeleton. *J. Biol. Chem.* **2011**, *286*, 15630–15640. [CrossRef]
21. Olson, M.F.; Sahai, E. The Actin Cytoskeleton in Cancer Cell Motility. *Clin. Exp. Metastasis* **2009**, *26*, 273–287. [CrossRef] [PubMed]

22. Yamazaki, D.; Kurisu, S.; Takenawa, T. Regulation of Cancer Cell Motility through Actin Reorganization. *Cancer Sci.* **2005**, *96*, 379–386. [CrossRef] [PubMed]
23. Jordan, M.A.; Wilson, L. Microtubules and Actin Filaments: Dynamic Targets for Cancer Chemotherapy. *Curr. Opin. Cell Biol.* **1998**, *10*, 123–130. [CrossRef]
24. Kavallaris, M. Microtubules and Resistance to Tubulin-Binding Agents. *Nat. Rev. Cancer* **2010**, *10*, 194–204. [CrossRef] [PubMed]
25. Dia, V.P.; Pangloli, P. Epithelial-to-Mesenchymal Transition in Paclitaxel-Resistant Ovarian Cancer Cells Is Downregulated by Luteolin. *J. Cell Physiol.* **2017**, *232*, 391–401. [CrossRef] [PubMed]
26. Darling, E.M.; Di Carlo, D. High-Throughput Assessment of Cellular Mechanical Properties. *Annu. Rev. Biomed. Eng.* **2015**, *17*, 35–62. [CrossRef]
27. Taatjes, D.J.; Quinn, A.S.; Rand, J.H.; Jena, B.P. Atomic force microscopy: High resolution dynamic imaging of cellular and molecular structure in health and disease. *J. Cell Physiol.* **2013**, *228*, 1949–1955. [CrossRef]
28. Fletcher, D.A.; Mullins, R.D. Cell Mechanics and the Cytoskeleton. *Nature* **2010**, *463*, 485–492. [CrossRef]
29. Zhang, T. Cytoplasmic Motion Induced by Cytoskeleton Stretching and Its Effect on Cell Mechanics. *Mol. Cell Biomech.* **2011**, *8*, 169–193.
30. Yango, A.; Schape, J.; Rianna, C.; Doschke, H.; Radmacher, M. Measuring the Viscoelastic Creep of Soft Samples by Step Response Afm. *Soft Matter* **2016**, *12*, 8297–8306. [CrossRef]
31. Xiao, M.; Li, X.; Song, Q.; Zhang, Q.; Lazzarino, M.; Cheng, G.; Ulloa Severino, F.P.; Torre, V. A Fully 3D Interconnected Graphene-Carbon Nanotube Web Allows the Study of Glioma Infiltration in Bioengineered 3D Cortex-Like Networks. *Adv. Mater* **2018**, *30*, e1806132. [CrossRef]
32. Nobes, C.D.; Hall, A. Rho, Rac, and Cdc42 Gtpases Regulate the Assembly of Multimolecular Focal Complexes Associated with Actin Stress Fibers, Lamellipodia, and Filopodia. *Cell* **1995**, *81*, 53–62. [CrossRef]
33. Eden, S.; Rohatgi, R.; Podtelejnikov, A.V.; Mann, M.; Kirschner, M.W. Mechanism of regulation of WAVE1-induced actin nucleation by Rac1 and Nck. *Nature* **2002**, *418*, 790–793. [CrossRef] [PubMed]
34. Even-Ram, S.; Doyle, A.D.; Conti, M.A.; Matsumoto, K.; Adelstein, R.S.; Yamada, K.M. Myosin Iia Regulates Cell Motility and Actomyosin-Microtubule Crosstalk. *Nat. Cell Biol.* **2007**, *9*, 299–309. [CrossRef] [PubMed]
35. Vicente-Manzanares, M.; Zareno, J.; Whitmore, L.; Choi, C.K.; Horwitz, A.F. Regulation of Protrusion, Adhesion Dynamics, and Polarity by MyosinsIia and Iib in Migrating Cells. *J. Cell Biol.* **2007**, *176*, 573–580. [CrossRef] [PubMed]
36. Webb, N.J.; Donais, K.; Whitmore, L.A.; Thomas, S.M.; Turner, C.E.; Parsons, J.T.; Horwitz, A.F. Fak-SrcSignalling through Paxillin, Erk and Mlck Regulates Adhesion Disassembly. *Nature* **2004**, *6*, 154–161.

Supplementary Materials

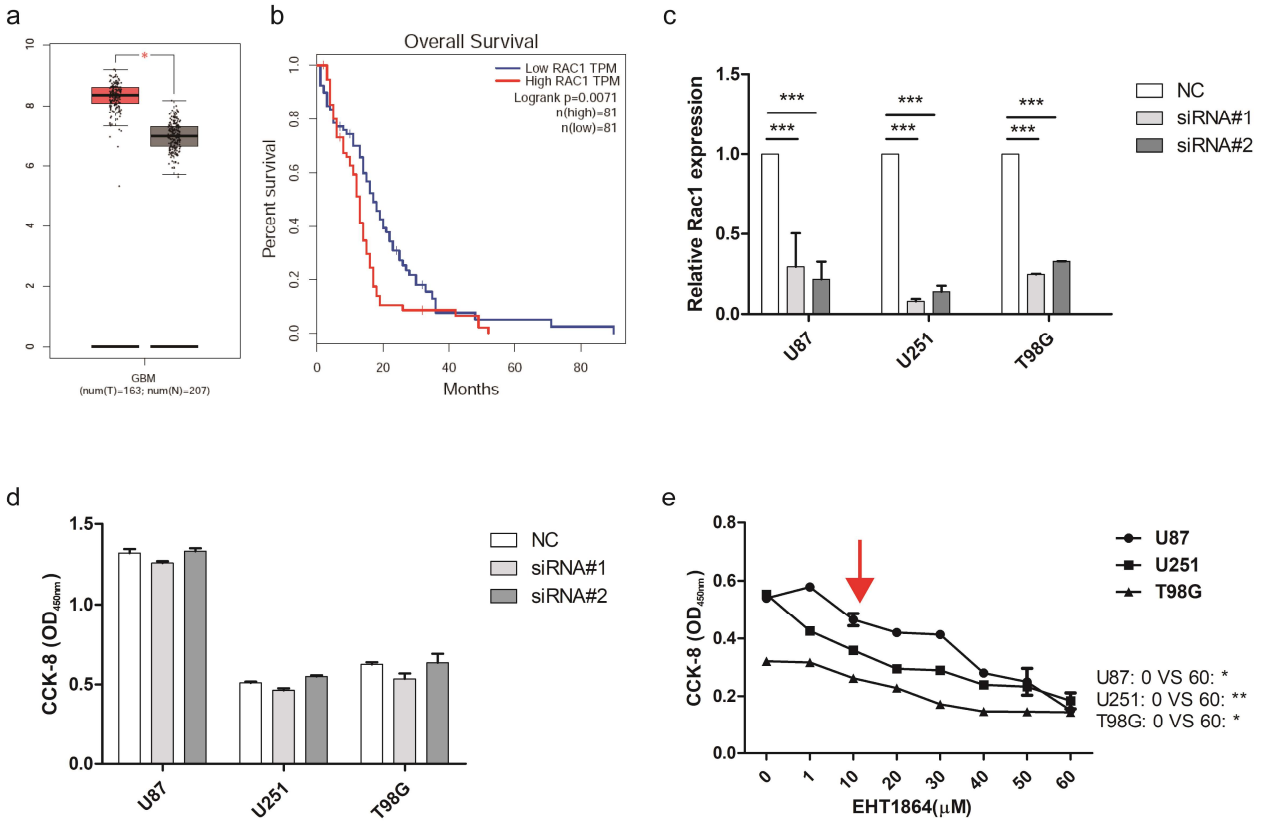

Figure S1: (a) Rac1 expression in GBM tissue compared with non-GBM tissue (The Y-axis represent log2 (TPM+1), red box represent GBM tissue and grey box represent non-GBM tissue). (Data are from GEPIA: gepia.cancer-pku.cn) (b) Overall survival of GBM patients with low Rac1 expression and high Rac1 expression. (Data are from GEPIA: gepia.cancer-pku.cn) (c) mRNA levels of Rac1 in U87, U251, and T98G GBM cells were analyzed by RT-PCR after Rac1-siRNA and NC-siRNA were transfected for 48h. (d) Cell viability of U87, U251, and T98G GBM cells was evaluated by using the CCK-8 assay after Rac1 knockdown for 48h. (e) Cell viability of U87, U251, and T98G GBM cells was evaluated by using the CCK-8 assay after incubation with different concentrations of EHT1864 for 12 h. ***: p<0.001, **: p<0.01, *: p<0.05.

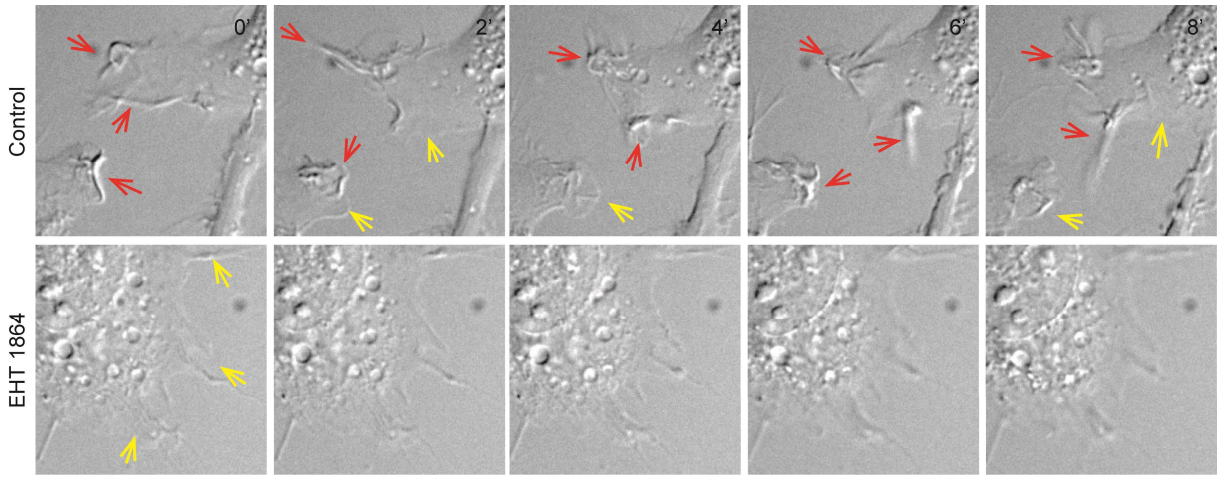

Figure S2: Phase contrast time-lapse microscopy recording of U87 cells at 2min intervals for 1h. After 1h recording, 10µm EHT1864 was added and recorded for another 1h to observe cell membrane movement. The red arrow indicates cell membrane ruffles, and the yellow arrow indicates cell membrane protrusion. U87 cell recordings are shown in Video S3.

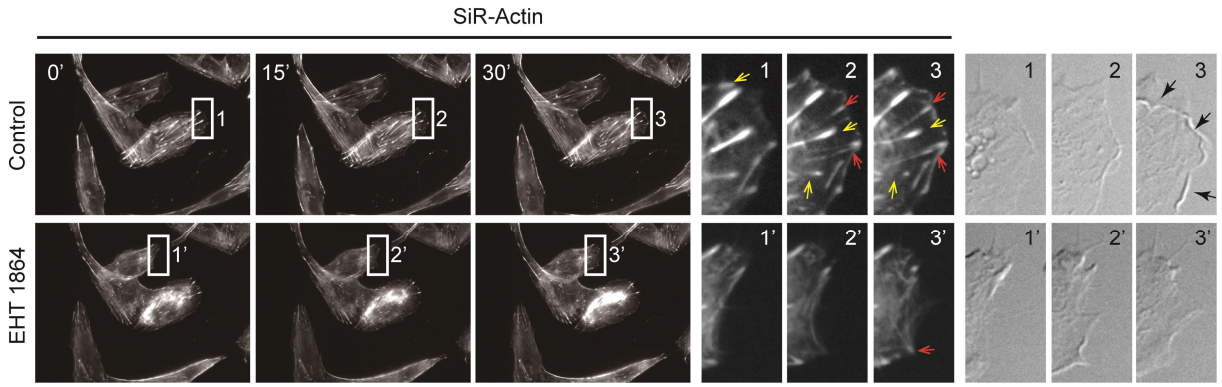

Figure S3: SiR-actin staining of U87 cells was imaged by time-lapsemicroscopy at 2min intervals for 30min. After 30min recording, 10µm EHT 1864 was added and recorded for another 30min to observe actin organization.The red arrow indicates actin assembly fibers in the protrusion, and the yellow arrow indicates actin disassembly fibers in the protrusion. Recordings of actin dynamics are shown in Videos S4 and S5.

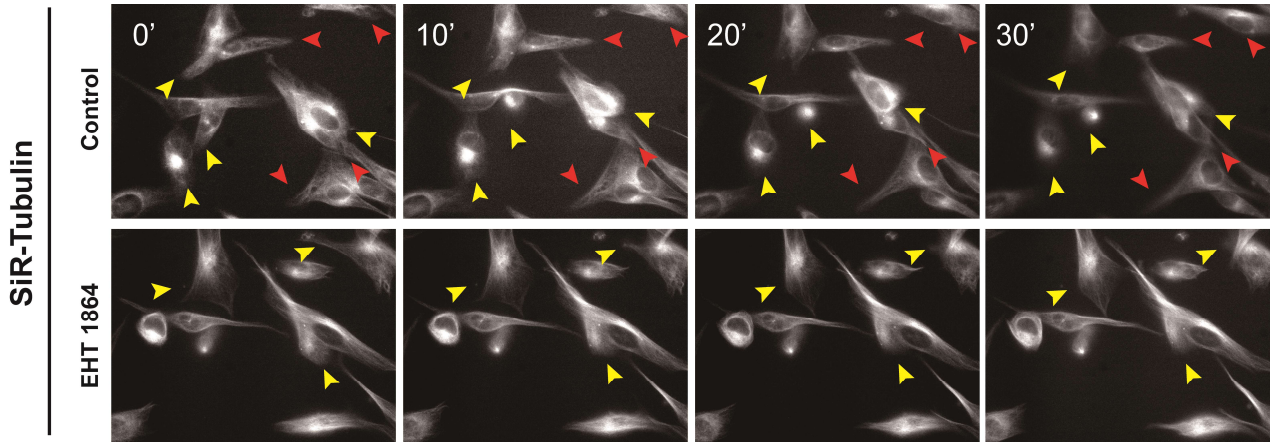

Figure S4: SiR-tubulin staining of U87 cells was imaged by time-lapse microscopy at 2min intervals for 30min. After 30min recording, 10µm EHT 1864 was added and recorded for another 30min to observe tubulin organization. The redarrow indicates tubulin assemblyin the protrusion, and the yellow arrow indicates tubulin disassembly.

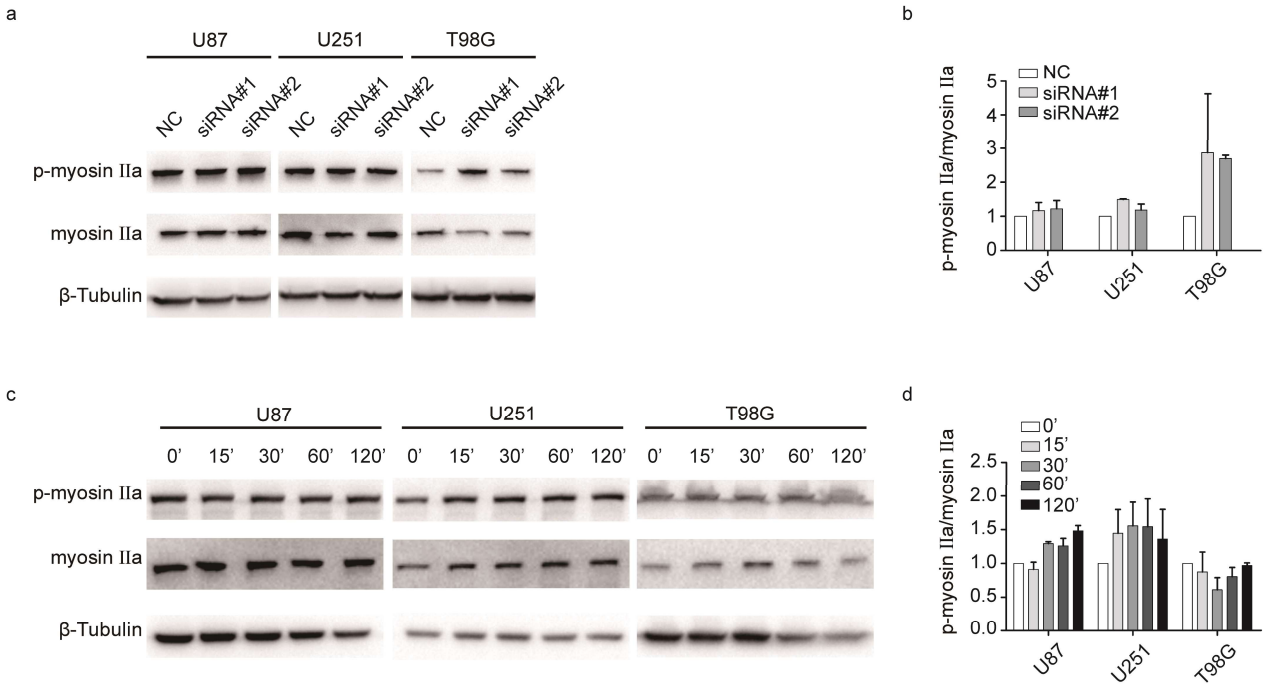

Figure S5: Western blot analysis of the level of phosphorylation of myosin IIa in U87, U251, and T98G cells in response to Rac1 depletion by siRNA and inhibited by EHT 1864.

In collaboration with Alessandra Magistrato at SISSA and her student we performed an investigation of the action of three inhibitors of the small GTPases Rac1 and Cdc42. I performed the transwell assay of U87 cells undergoing Rac1 inhibition by EHT 1864 (Figure 2 and Figure 3A).

In what follow I have reported a very preliminary draft of the manuscript, which we will complete hopefully before the end of the present year.

2.2 Molecular mechanisms of the blockage of glioblastoma motility

Abstract

Glioblastoma (GBM) is the most common and lethal brain tumor. GBM have a remarkable degree of motility and are able to infiltrate in the healthy brain. In order to perform a rational-based drug-repositioning study we have used known inhibitors of two small Rho GTPase, Rac1 and Cdc42, which are upregulated in GBM and are involved in signaling processes underlying the orchestration of the cytoskeleton and therefore in cellular motility. The selected inhibitors (R-ketorolac and ML141 for Cdc42 as well as R-ketorolac and EHT 1864 for Rac1) have been successfully employed to reduce the infiltration propensity of the GBM. All-atoms simulations have unprecedentedly disclosed the binding poses of these drugs on the target proteins, providing a rationale at atomic-level of detail of their non-competitive inhibition mechanism.

Introduction

Glioblastoma (GBM; World Health Organization grade IV glioma) is the most common and lethal intrinsic tumor. Unlike other solid tumor cell types, GBM invades the surrounding brain and in contrast with other kind of cancers, GBM rarely metastasizes to other organs [1]. Although several attempts, for instance using several drugs such as bevacizumab or immunotherapies [2-4], have been made to stop and counteract GBM infiltration, GBM treatment is still mainly focused and primarily limited to surgical resection followed by concurrent radiation therapy with some chemotherapic reagent such temozolomide [5, 6]. GBM represents one of the most comprehensively genomically characterized cancer types [7, 8], leading to recognition of groups of tumors defined by four distinct transcription profiles (proneural, neural, classical, and mesenchymal). Mutations leading to the transformation of healthy astrocytes into malignant glioma and/or GBM [6] are very diverse and indeed there are at least the four above mentioned different transcription profiles at the basis of brain tumors.

The molecular mechanisms at the basis of cellular motility are similar in all cells and in healthy cells and neurons as well as in malignant GBM. The process of polymerization of actin filaments is the main source of cellular motion and protrusion, which is regulated and controlled by several proteins such as Actin related protein 2/3 complex (Arp2/3), cofilin, formin and molecular motors, such as myosin, dynein, controlling different features of cellular motility [9]. A key role in cellular motility and migration is played by the small GTP-ases, which are presented in all migrating cells. Rho family GTPase has distinct and specific roles in the regulation of growth, maintenance and retraction of growth cones (GCs) [10]. The mammalian typical Rho GTPase family consists of three subfamilies, Rho subfamily (RhoA, RhoB and RhoC), Rac subfamily (Rac1, Rac2, Rac3 and RacG) and Cdc42 subfamily (Cdc42, RhoQ and RhoJ) [11]. RhoA, Rac1 and Cdc42 are well-studied members of Rho GTPase family controlling distinct cytoskeletal elements. Activation of Rac1 stimulates actin polymerization to form lamellipodia [12], Cdc42 induces the polymerization of actin to form filopodia and Rho regulates the bundling of actin filaments into stress fibers and the formation of focal adhesion complexes[13].

The GTP-binding proteins of Rho family are activated by a variety of growth factors, cytokines, adhesion molecules, hormones, integrins, G-proteins and the other biologically active substances [14, 15]. Biochemical approaches have shown that Rho GTPase also involves crosstalk. Depending upon the

concentration and localization of these Rho GTPases, mammalian cells show different morphology, movement and behavior [16]. GTPase work via a cyclic mechanism in which they pass from an active guanine triphosphate (GTP) bound form, to an inactive Guanine Diphospate (GDP) bound form after the GTP hydrolysis occurs fostered by the GTPase-activating protein (GAP), in which the GEF enhance the exchange of the GTP/GDP nucleotide.

At the basis of the present manuscript there is the biological observation that the cellular motility - allowing cells to move, migrate and infiltrate - is in essence very similar in all kind of cells and is primarily based on the orchestration of the cytoskeleton and of a variety of adhesion molecules. The proteins involved in these biological processes as well as their inhibitors are known and in the present manuscript we focus on three inhibitors of cellular motility, i.e. ML141, EHT 1864 and R-Ketorolac. These inhibitors will be employed to monitor their ability to reduce cellular motility. Complementarily, Molecular Dynamics (MD) simulations have been instrumental to have a better understanding of their binding mode and mechanisms of the action of these inhibitors from an atomic-level perspective. Our outcomes remark the importance of abrogating the cellular mobility in infiltrative tumor types like GBM, and provide a fundamental advance in understanding the mechanism of small molecules inhibitors of Rho GTPase, which are of pivotal importance to devise novel more effective drug-candidates.

Results

According to The Cancer Genome Atlas (TCGA) (cancergenome.nih.gov), the analysis of the expression level of proteins involved cellular motility in normal tissue and GBM is herereported in Figure 1A and C for Rac1 and Cdc42 and showing that Rac1 and Cdc42 are both upregulated in primary and recurrent tumors. The overexpression of these two proteins is strongly related to a negative outcome of the patient (Figure 1 B and D). Cdc42 and Rac1 are primarily involved in cellular motility [17] and their upregulation leads to a higher infiltration ability of malignant GBM to invade the healthy tissue. We selected three inhibitors R-Ketorolac, ML141 and EHT 1864 to carry out an in silico investigation of the binding of these drugs to Cdc42 and to Rac1 (R-ketorolac and ML141 for Cdc42 as well as R-ketorolac and EHT 1864 for Rac1) and their effect on the migration and infiltration of GBM. These three inhibitors have a rather different structure (Figure 1E) both in size and in chemical properties. R-Ketorolac contains a carboxylic moiety, which, being negatively charged at physiological pH, will enter into cells - and inside GBM - much more slowly that ML141, who is neutral, and of EHT 1864, who is positively charged. R-ketorolac is known to affect the activity of both Rac1 and Cdc42, with the following half inhibitory concentrations (IC50): R-ketorolac 0.57 μM and 1.01 μM for Rac1 and Cdc42, respectively [18]. Conversely, ML141 and EHT 1864 are exclusive inhibitors of Cdc42 (IC50 of 0.20 μM)[19] and Rac1 (IC50 1–5 μM) [1, 20], respectively. These values of IC50 refer to biochemical assay in which the target proteins and the inhibitors have been purified and are in a solution. In the next section we will examine the effect of these inhibitors on the migration of GBM and the effective concentrations are higher because of the more complex conditions.

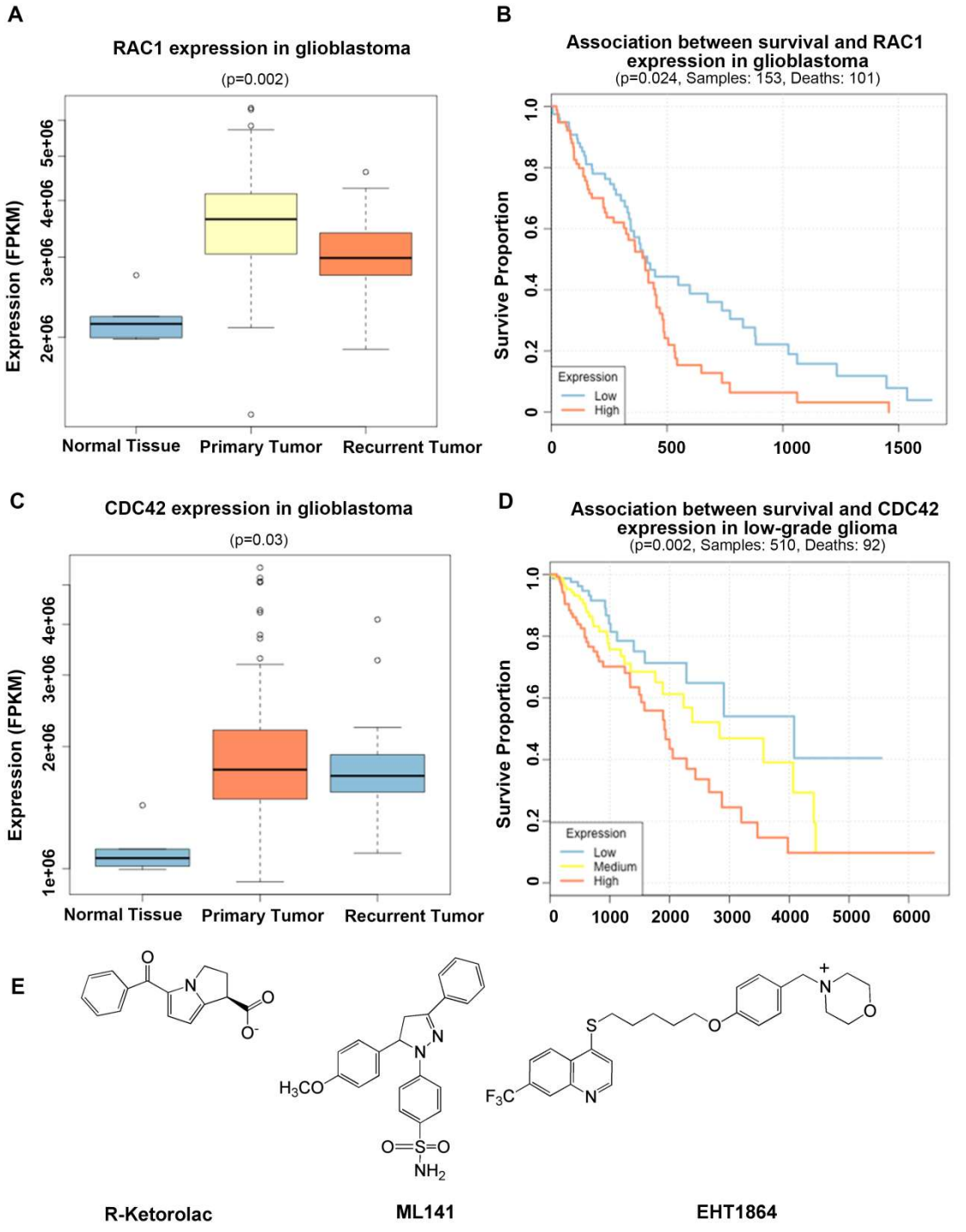

Figure 1 - Analysis of Rac1 and Cdc42 in GBM: differential expression and association to patient survival in The Cancer Genome Atlas (TCGA) data. A and C, Rac1 (A) and Cdc42 (C) is significantly overexpressed in glioma tumor samples, compared to matched normal brain tissue. P-value calculated using DESeq2. B. GBM patients with higher Rac1 expression are associated to higher risk than patients with lower Rac1 expression. D, Low-grade glioma patients with higher Cdc42 expression are associated to higher risk than patients with lower Cdc42 expression. P-value calculated using log-rank test. E, Sketch of R-Ketorolac, ML141 and EHT 1864 molecular structure.

The action of the inhibitors on GBM migration

We analysed GBM cell line U87 which is very often used for understanding properties of high grade GBM. Migration and infiltration were studied by the transwell assay (Figure 2 and 3) and by live cell imaging (Figure 4 and 5).The transwell migration assay is a standard method of measuring cell movement through an empty space. The transwell assay is based on the use of a hollow plastic chamber sealed at one end with a porous membrane. The chamber is suspended over a larger well which contains a specific medium. Migrating cells, i.e. infiltrating GBM are plated inside the chamber and allowed to migrate through the pores to the other side of the membrane. Migrated cells are fixed after a given time, stained and counted. Live cell imaging methods visualize individual cells in a dish and take an image every minute and in this way can follow the motility of individual cells. These two methods are complementary: live cell imaging require a substantial illumination of the cells under investigation and cannot be used for experiments lasting several days, while the transwell assay can be used over several days with only minor side effects on the investigated cells (Figure 2). The elongated and fusiform shapes in Figure 2 are the profile of the migrating U87 GBM in control conditions (first column) and in the presence of 1, 10 and 20 μM of EHT 1864 (second, third and fourth column). The assay was conducted for three days (first, second and third row in Figure 2). Visual inspection shows that more GBM cells are able to invade into the empty space at later days and that this migration is reduced by increasing amount of EHT 1864.

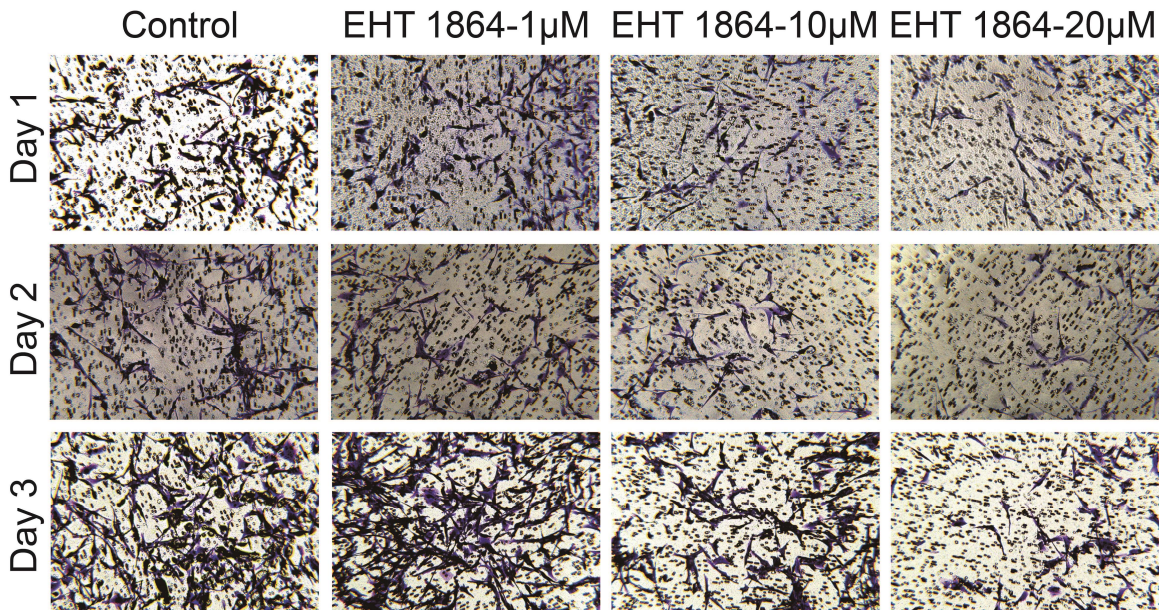

Figure 2 Rac1 inhibitor EHT 1864 reduces transwell migration of U87 GBM cells.Transwellassay was conducted for three days

(first, second and third row) in the presence of 0, 1, 10 and 20 μM of EHT 1864 (first, second, third and fourth column).

The number of GBM present in the empty space at different days obtained by crystal violet and calculated with image J, and we found that 1 μM EHT 1864 has a small effect on GBM migration but 20 μM EHT 1864 almost halved the number of migrating GBM both for the GBM cell line U87 on Day 2 and Day 3 (Figure 2).

We also computed the number of migrating cells per field at different days and in the presence of different amount of the tested inhibitors. Collected data from at least three different experiments show that 50 μM ML141 blocked almost completely migration at Day1 (Figure 3B), while the action of EHT 1864(Figure 3A) and of R-Ketorolac (Figure 3C) was more prominent at Day2. This observation is consistent with the more pronounced ability of ML141 to cross the lipid membrane and act on the interior of cells.

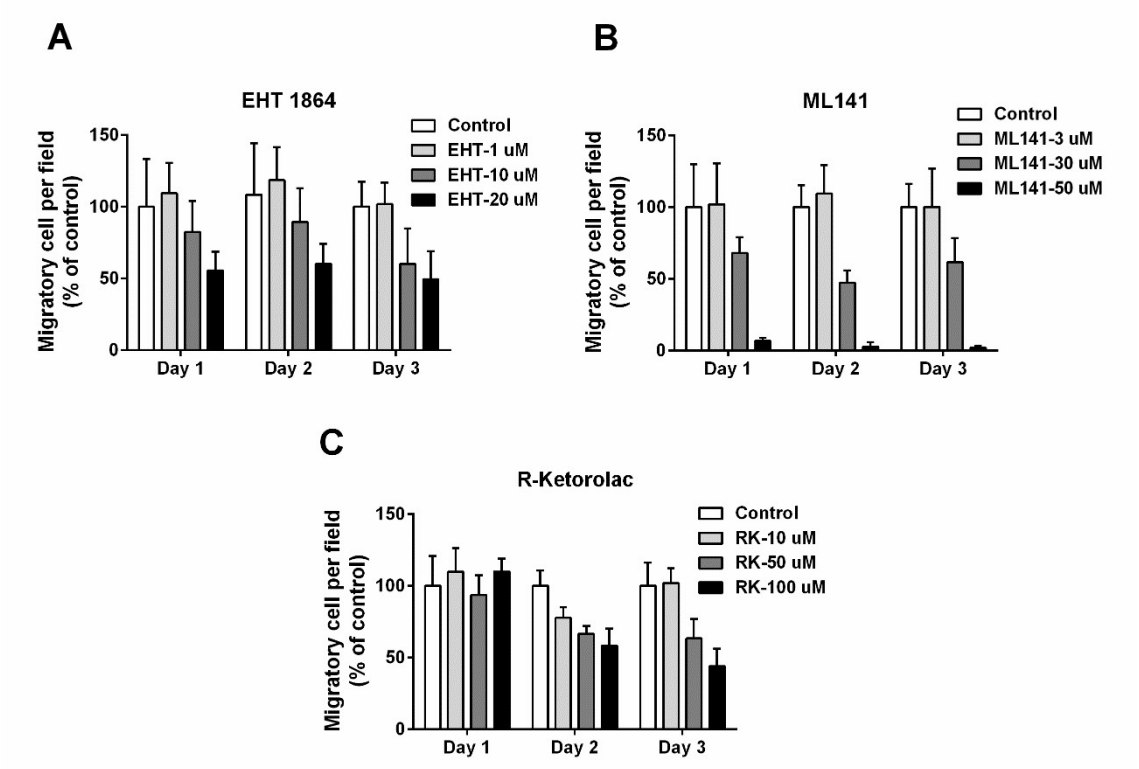

Figure 3 - Three inhibitors EHT 1864 (A), ML141 (B) and R-Ketorolac (C) inhibit U87 GBM cell migration in transwell assay depending on concentration and time of treatment.

At later days, such as Day3 we observed often a higher number of cells per field (comparing Day3 and Day2 for EHT 1864 in Figure 2) than at previous days because GBM replicates and the used inhibitors block migration and not replication. Collected data indicate that the concentration of the inhibitors blocking half of the GBM motility is approximately 20, 30 and 50 μM for EHT 1864, ML141 and R-Ketorolac, respectively.

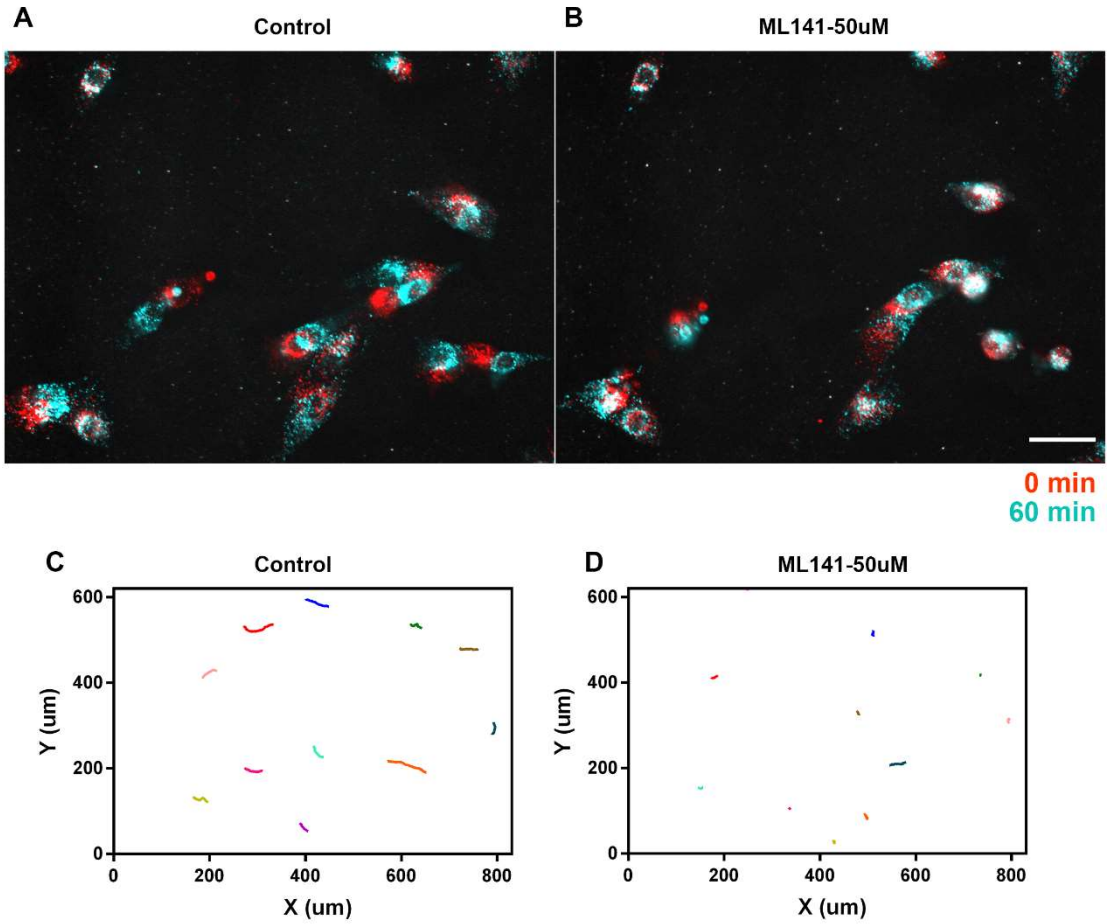

Figure 4 - ML141 inhibits U87 GBM cells motility analyzed with live cell imaging. A and B, Live cell imaging frames at different recording time points were merged before and after 50 μM of ML141 treatment. Red indicates cells at T=0 min, cyan indicates the same cells at T=60 min. When two channels are co-localized, they appear white and indicating immobilizing cells. C and D, Migration trajectories before and after 50 μM of ML141 treatmentwere reconstructed.

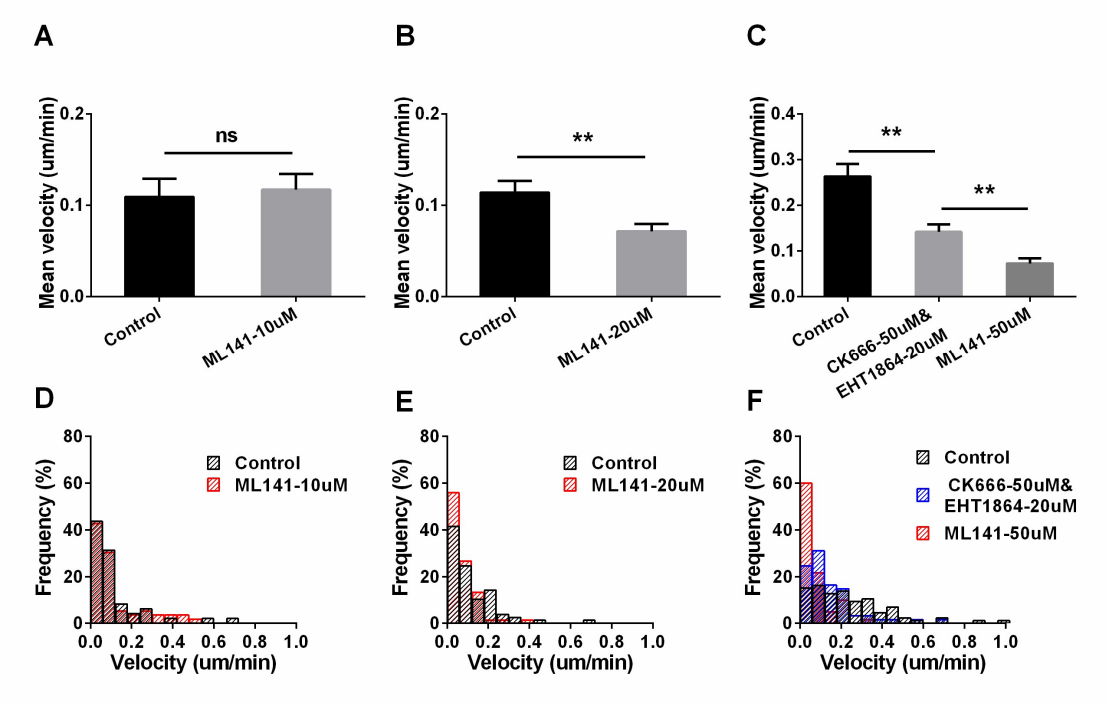

Figure 5–Effect of ML141 on velocities of U87 GBM cells. A-C, Mean velocity was significantly decreased by 20 μM (B) and 50 μM (C) of ML141. Data were shown as mean ± sem, **p<0.01. D-E, Velocity distribution of U87 GBM cells before and after 10 and 20 μM ML141 treatment.F Velocity distribution of U87 GBM cells before and after 50 μM ML141, and 50 μM CK666, an Arp2/3 inhibitor, and 20 μM of EHT1864treatment

We looked also to the action of these inhibitors with live cell imaging (Figure 4 and Figure 5) and we observed a very rapid action of ML141 on GBM motility: the addition of 50 μM halved the motility with some minutes and similarly EHT 1864 had a rather fast action. In contrast, we could not detect a fast action of R-Ketorolac, presumably because of the presence of the carboxylic group which limits its ability to cross the lipid membrane. The inhibitory action of R-Ketorolac is best seen with the transwell assay and requires at least 24 hours.

Live cell imaging allows the tracking over time of an individual migrating GBM and therefore provides an estimate of the mean velocity of migrating cells. As GBM cells replicate very efficiently, both the transwell assay and live cell imaging are not exempt of limitations: in the presence of a high replication activity the transwell assay can underestimate the effect of an inhibitor and the live cell imaging tracking can be confused during mitosis. Nevertheless, the combination of the two assays provides a reliable characterization of the effect of the used inhibitors on GBM motility.

Molecular mechanismof inhibition from molecular simulations

According to the experiments reported above the tested inhibitors (Figure 3), known to target the Rac1 and Cdc42 proteins were able to reduce the migration and/or the infiltration propensity of the U87 cell lines. As such, we employed docking and all atom explicitly solvated classical MD simulations to unveil the molecular mechanism of inhibition of the above mentioned inhibitors.

Identification of the inhibitor's binding pose via docking and Molecular Dynamics simulations

Since all drugs are known to exert a non-competitive inhibition mechanism (i.e. the do exert inhibition of the small-molecule inhibitor without competing with their natural cofactor (i.e. Guanine Triphosphate (GTP) cofactor), we have initially identified possible binding cavities, distinct from the GTP binding site, possibly able to host these small molecules. This search was done considering both the GTP and GDP-bound form of the proteins, which represent their active and inactive form, respectively. In the GDP-bound form of the proteins, we identified by using site detector algorithms two cavities (sites 1 and 2) on Cdc42 and only one cavity (Site 1) on Rac1 potentially able to bind the inhibitors. No cavity was instead present in the GTP bound form of the protein. In order, to assess the drug gability of these pockets, we docked the investigated inhibitors on site1, which flanks the GTP binding cavity. Remarkably only the R-enantiomer of Ketorolac and of ML141 could be docked in this site, consistently with experimental findings showing inhibitory activity on Rho GTPases, exclusively for this enantiomer. The binding stability of the drug was monitored by performing 100-400 ns long MD simulations for each drug/GTPase adduct. Site 2, identified exclusively for Cdc42, is rather small and flexible. As a result, all molecules docked in this site rapidly dissociated within the first 30 ns MD simulations. This first set of simulations unprecedentedly allowed to predict the binding pose of R-ketorolac and ML141 on Cdc42 and that of R-ketorolac and EHT 1864 on Rac1 (Figure 6). In the following we perform systematic analysis to unravel the molecular mechanism exerted by the used inhibitors on the small Rho GTPases.

Inhibition mechanism of Cdc42

We initially focused in dissecting the inhibition mechanism of the two investigated Cdc42 inhibitors (Figure 6A and B). Different non-competitive mechanisms may be operative for small Rho GTPases depending if the inhibitors exert their action by interfering with the GTP or GEF biding [20]. Our set of simulations predicts that the carboxylic moiety of R-ketorolac coordinates the Mg^{2+}ion. This coordination may weaken the interaction of the metal ion with the GDP phosphates. This coordination may facilitate their lease of GDP

cofactor release from Cdc42 and/or preventing the binding of a new GTP molecule in an optimal position to undergo a new cycle. Thus, consistently with experimental evidences, R-ketorolac, can be classified as a GTP binding inhibitor, possibly. Additionally, the aromatic ring of R-ketorolac lies in the vicinity of the switch II region, where the GEF proteins have been demonstrated to bind in crystallographic studies, possibly interfering with the binding of these proteins (Figure 6).

At variance of R-ketorolac, the binding pose of ML141predicted from docking and MD simulations reveals that the drug protrudes towards the Mg^{2+} ion site with its amine moiety (Figure 6B). Its interaction with the Mg^{2+} ion and with the pocket flanking the GDP binding site confirm its interference also with the GDP/GTP binding, as suggested experimentally. Also one of the aromatic ring of ML141 heads toward the small cavity lined by switch II also approaches the GEF binding pocket nearby the Phe56 residue (Figure 6).

We next inspected the impact of ketorolac and ML141 on the structural and functional properties of Cdc42, by monitoring the RMSF of the drug/protein adduct as compared to that of the Cdc42 protein *per se*. Ostensibly, the regions mostly affected by drug binding are those corresponding to switches I and II for ketorolac, whose flexibility surprisingly increase upon drug binding. In contrast, ML141 only slightly affects the switch I. In order to understand how drug binding could impact the internal motion of the protein we also computed the per-residue cross-correlation matrix (CCM). Positive regions of the CCM indicate dynamically coupled regions, associated to a lock step motion of the protein, while negative regions indicate the negatively correlated motion with the corresponding parts of the protein moving in an opposite manner [21]. The CCM of the GDP bound-Cdc42 shows a dynamical coupling of two functionally relevant regions, switch I and switch II, with switch I being moving in a lockstep motion with α1, α4, β6 and β1, while being negatively correlated with αi (Figure 7A) and switch II being negatively correlated with switch I, β1 and αi. This is consistent with an opening/closing motion of the switch I disclosed by the essential dynamics of the proteins (Figure 8), which capture the most relevant slow vibrational motion of the protein. The observed movement of the GDP-bound Cdc42 is most likely instrumental to the loading/release of the GTP/GDP cofactor, and to engage the interactions with the variety of protein effectors that mediate the small RhoGTPase signaling. To monitor the impact of the ketorolac and ML141 binding on these internal motion of Cdc42 we also computed the CCM of the drug-bound protein. This CCM, plotted as a difference with respect to the undrugged form of the protein (Figure 7B, C), reveals that both drugs dampen the overall internal motion of the Cdc42 (Figure

8) thus preventing the GTP/GDP exchange and Rho GTPase activation.

The computed binding free energy (ΔG_b) of both drugs to Cdc42 revealed that the binding of ketorolac to Cdc42 (ΔG_b, of -154 ± 5 kcal/mol) is energetically favored with respect to that of ML141 (ΔG_b, of -45 ± 6 kcal/mol). The electrostatic interactions between the negatively charged carboxyl moiety of ketorolac and the Mg^{2+} ion markedly contribute to the ΔG_b. In addition, residues Lys16 and Val36 stabilize drug binding by establishing electrostatic and hydrophobic interactions, respectively. We remark that the computed Gb are calculated rely on force fields and neglect the electronic rearrangements of the charge density induced by the Mg^{2+} ions (charge transfer and polarization effects) to the coordinating ligands. As a result, the calculated ΔG_b is most likely overestimated [22]. In addition to Lys16also Phe37, Ala59 and Tyr64 contribute to the G_b of ML141 by establishing hydrophobic interactions. Surprisingly, none of the two drugs establishes persistent H-bonds with their binding pocket.

As a further check we monitored if ML141 could bind at the Cdc42/GEF interface. Indeed, small molecules able of stabilizing the GEF/GTPase adduct may permanently inactivate the GTPase cycle. Among the GEF proteins known to bind to Cdc42 we selected Dock9 since an X-ray structure of this protein in complex with Cdc42 is available. Thus, ML141 was docked in a cavity at the interface of Cdc42/Dock9, and the resulting binding pose of ML141 resulted to be stable in MD simulations. The binding of ML141 had a limited impact on the Cdc42/Dock9 flexibility (i.e. does not markedly affected the RMSF of the two switch regions, which, in the adduct, are locked by Dock9). Upon ML141 binding an increase of positive correlation of the two Cdc42 switches is observed (Figure 7D), underlining a partial recovery of Cdc42 internal motion which, counteracts the stability of Dock9 binding. Consistently, the ΔG_b of ML141 at the Dock9/Cdc42 interface is smaller than in the single Cdc42 protein (ΔG_b= -28 ± 3 kcal/mol) being stabilized by hydrophobic and electrostatic interactions with residues Gln342, Glu403, respectively, from Dock9 and with hydrophobic interactions with Leu67 from Cdc42. This suggests that ML141most likely bind to site 1 of Cdc42 protein, in line with its activity as nucleotide binding inhibitors suggested experimentally.

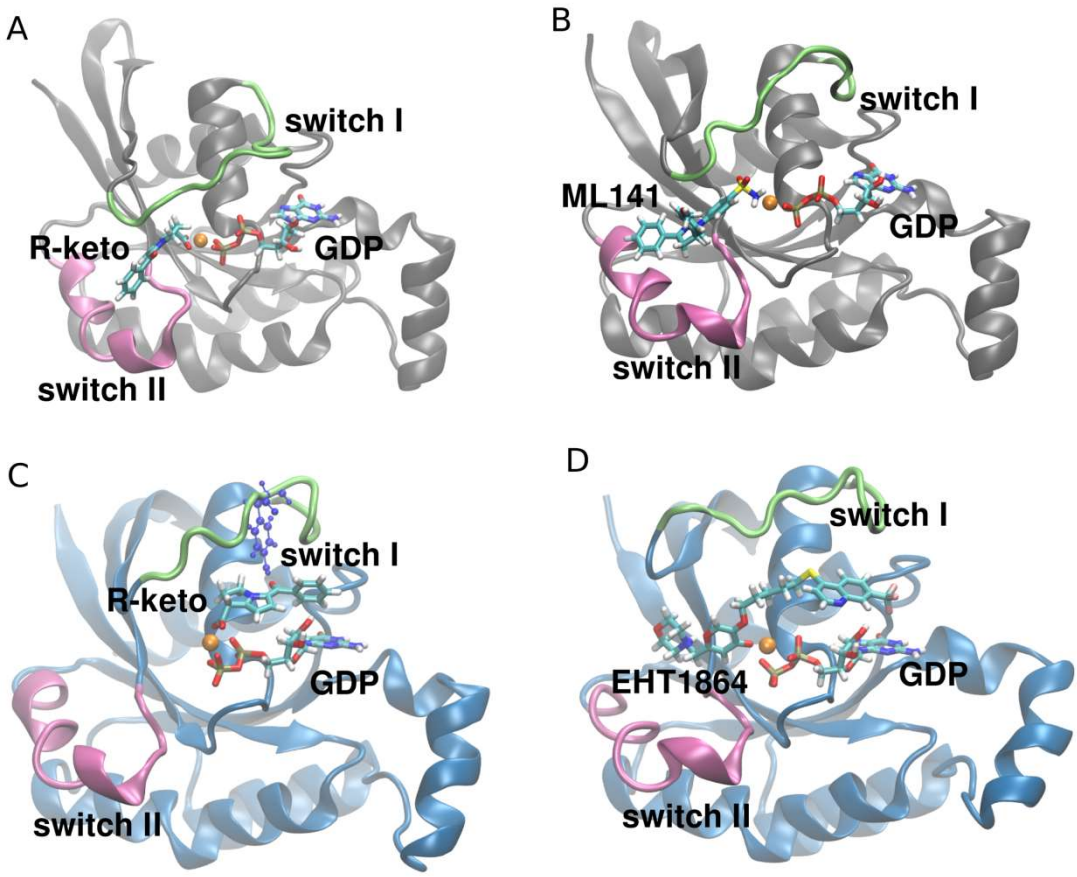

Figure 6 – Binding pose of R-ketorolac (R-keto, A) andR-ML141 (B) on Cdc42, R-keto (C) and EHT 1864, (D) on Rac1. Cdc42 and Rac1 are shown in gray and blue new cartoons, respectively, switch I (from residue 27 to residue 37) and II (from residue 59 to residue 73) in lime and mauve, respectively, Mg^{2+} ions is pictured in orange van deer Waals sphere and Guanine diphosphate (GDP) and the inhibitors are shown as licorice and colored by atom name. In C the hydrogen bond between R-keto and Tyr32 (depicted as blue balls and sticks) of Rac1 is shown.

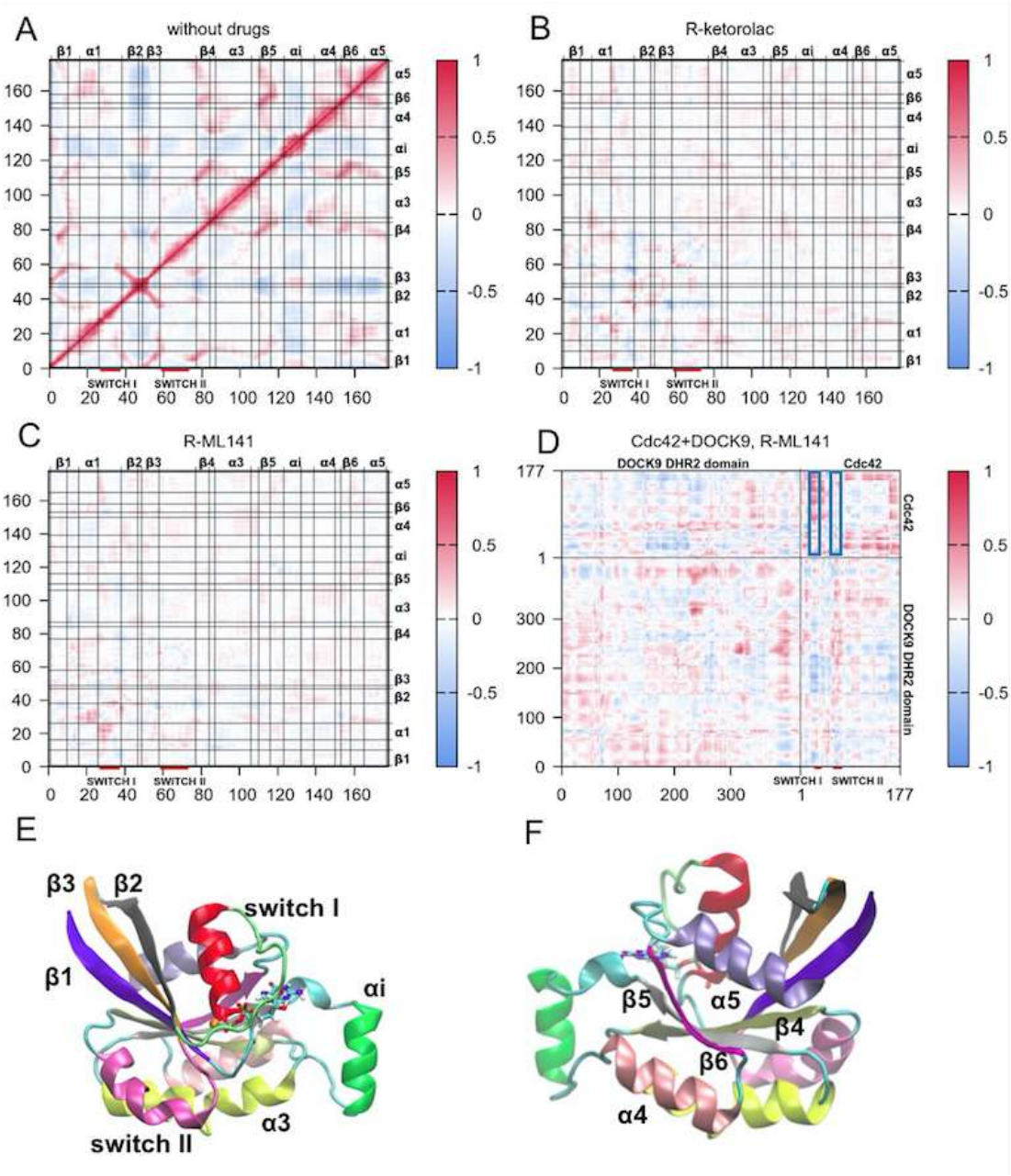

Figure 7 – Per-residue cross correlation matrix (CCM)of Guanine diphosphate (GDP)-bound Cdc42(A). Difference between the per-residue CCM of GDP-bound Cdc42 in complex with R-ketorolac (B) and ML141 (C) and Cdc42 and the CCM of GDP-bound Cdc42 without drug. Difference between the per-residue CCM of GDP-bound Cdc42 in upon binding of Dock9 and ML141 and the CCMof GDP-bound Cdc42 alone (D). The Pearson's cross correlation coefficients vary from -1 (anticorrelated motion, blue) to +1 (correlated motion, red). Horizontal and vertical lines define different regions of the protein: β1 (residues 1 to 10), α1 (residues 16 to 26), β2 (residues 38 to 47), β3 (residues 49 to 58), β4 (residues 77 to 84), α3 (residues 87 to 106), β5 (residues 110 to 116), αi (residues 123 to 132), α4 (residues 139 to 150), β6 (residues 153 to 158), α5 (residues 165 to 177). Domain partitioning of Cdc42 is shown in E and F. Residues corresponding to switch I and II are highlighted by red lines.

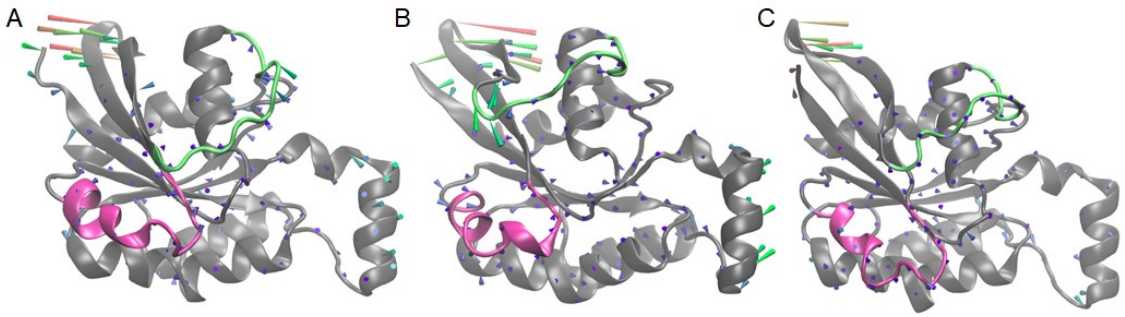

Figure 8 –Porcupine plot representing the essential dynamics of Cdc42 in the GDP- bound form (A), in complex with R-ketorolac (B), with R-ML141 (C). Cdc42 is depicted in gray new cartoons, with switch I and II highlighted in lime and mauve, respectively. The arrows indicate the direction of the motion, their length and color (from blue to red) is representative of the motion amplitude.

Inhibition Mechanism of Rac1

The same simulation protocol was also instrumental to elucidate the binding mode and the inhibition mechanism of R-ketorolac and EHT 1864 to Rac1. Also in this case docking and MD simulations predict that both drugs bind nearby the GDP binding site. R-ketorolac coordinates the Mg^{2+} ion with its carboxylic moiety, similarly to what observed in Cdc42, while EHT 1864 occupies the cavity between the GDP molecule and switch I (Figure 6). In spite of the structural similarity of Cdc42 and Rac1, the pocket lined by switch II is smaller in Rac1 that in Cdc42 due to the presence of Trp56 in the first as compared to Phe56 in the latter. As a result, the aromatic ring of R-ketorolacin Rac1 linesswitch I, being stabilized by π-stacking interaction with the GDP cofactor (Figure 6). Consistently with the binding poses observed, both drugs upon binding to Rac1 (Figure 6C and D) principally perturb switch I. Interestingly, the binding of the studied inhibitors locks the internal dynamics of the protein, hampering the opening/closing motion of the switch loops (Figure 9), upon ketorolac binding. Conversely, EHT 1864 does not interfere with the Rac1's internal dynamics. The CCM of both systems also highlights marked differences. While R-ketorolac introduces small changes in the per-residue CCM (Figure 10), EHT 1864 largely perturbs the protein dynamics increasing the negatively/positively coupled motions of switch I and II respectively (Figure 10).

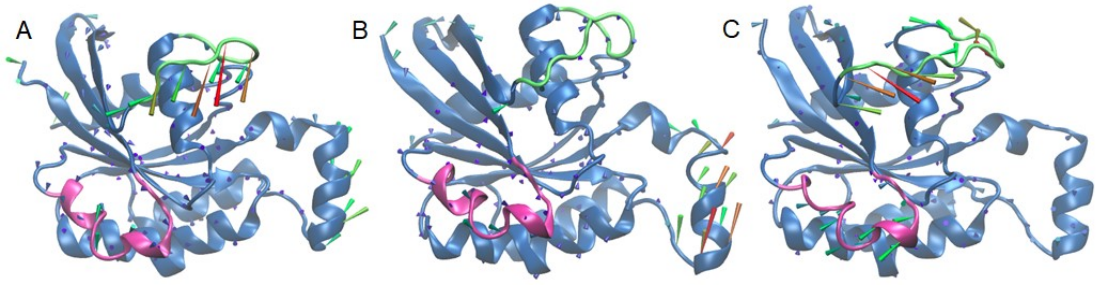

Figure 9 – Porcupine plot representing the essential dynamics of Rac1 in the free GDP bound form (A), in complex with

R-ketorolac (B), in complex with EHT 1864 (C). Cdc42 is depicted in blue new cartoons, with switch I and II highlighted in lime and mauve, respectively. The arrows indicate the direction of the motion, their length and color (from blue to red) is representative of the motion amplitude.

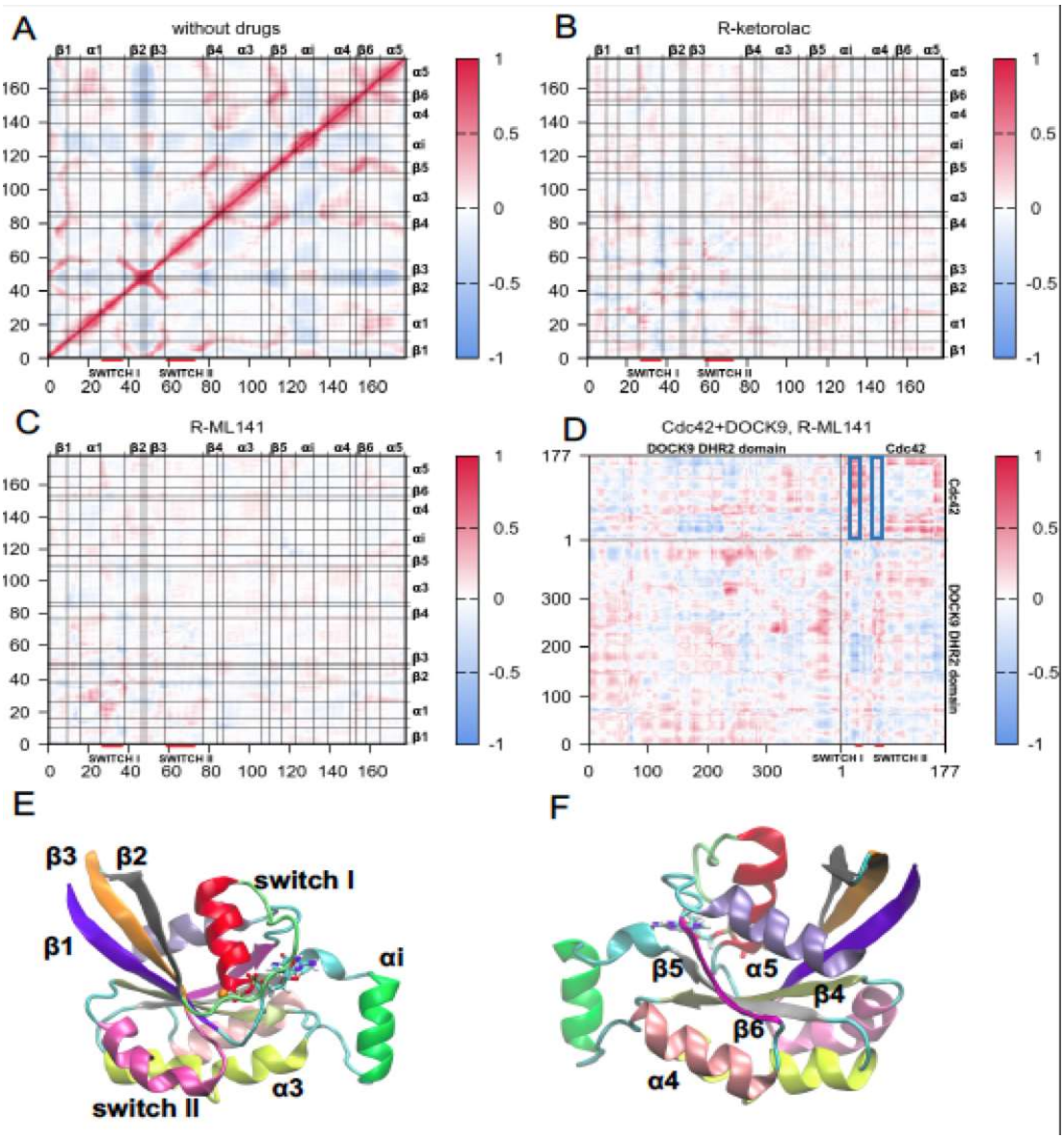

Figure 10 –Per-residue correlation matrix (CCM) for the GDP bound form of Rac1 (A). Difference between the per residue CCM of GDP-bound Rac1 in complex with R-ketorolac (B) and EHT 1864, charge +1 (C) and the same form of the protein without drugs. Difference between the per-residue CCM of GDP-bound Rac1 in complex with Dock2 andEHT 1864, charge +1, and the same form of the protein without drugs (D). The Pearson's cross correlation coefficients vary from -1 (blue, anti-correlated motion) to +1 (red, correlated motion). Horizontal and vertical lines define different regions of the protein: β1 (residues 1 to 10), α1 (residues 16 to 26), β2 (residues 38 to 47), β3 (residues 49 to 58), β4 (residues 77 to 84), α3 (residues 87 to 106), β5 (residues 110 to 116), αi (residues 123 to 132), α4 (residues 139 to 150), β6 (residues 153 to 158), α5 (residues 165 to 177). Domain partitioning of Rac1 is shown in E and F. Switch I and II are highlighted by red lines under the matrices.

The calculated ΔG_bs reveal that ketorolac binds more strongly than EH1864 to Rac1 (ΔG_b=-182 ± 7 kcal/mol

and ΔG_b=-62 ± 9 kcal/mol for R-ketorolac and EHT 1864, respectively) and that ketorolac has a larger binding affinity towards Rac1 than to Cdc42, consistently with its higher potency (lower IC_{50}) [20].Similarly to its binding pose in Cdc42, the binding of R-ketorolac is mostly due to the electrostatic interactions of its carboxyl moiety with the Mg^{2+} ions, being here further stabilized by electrostatic interactions with Tyr32, and by hydrophobic interactions with Cys18 and Pro29. Its binding pose is also stabilized by a persistent H-bond formed between the hydroxyl group of Tyr32 and its carbonyl oxygen. In contrast, the binding of EHT 1864, mostly establishes hydrophobic interactions with the binding pocket and electrostatic interactions between its amine moiety of the drug and Asp38.

As in the Cdc42 case, we also monitored if EHT 1864 could bind at the interface of Rac1 and a specific GEF, i.e. Dock2 for which a crystal structure was available. Docking simulations followed by MD simulation confirmed once more the presence of a druggable pocket at the Rac1/Dock2 interface. The binding of EHT 1864 at this site induces a slight increase of the switch I flexibility. Consistently, the CCM of the Rac1/EHT 1864 adduct registers an increase of the positive correlation (Figure 10) of this critical region. Therefore, the binding of EHT 1864 at the Rac1/Dock2 is not effective in blocking functional dynamics of protein, but rather destabilized the Rca1/Dock2 adduct. This is further confirmed by a decrease of the ΔG_b (-28 ± 6 kcal/mol) with respect to that of EHT 1864 binding toRac1. Constituently with its suggested activity as nucleotide binding inhibitor EHT 1864 most likely targets the Rac1 rather than the Rca1/Dock2 adduct.

Discussion

The present study illustrates the effect of three inhibitors Ketorolac, ML141 and EHT 1864 on the migration and motility of GBM and a detailed analysis based on all-atom simulations elucidates the binding pose and the mechanism of these inhibitors on two small GTPases, Cdc42 and Rac1, involved in cellular motility. The complementary use of the two approaches provides a better insight and it is important also to clearly understand their differences.

In vivo and in silico comparison

In the experimental analysis shown in Figure 2-5, the inhibitors are added to the extracellular medium bathing the GBM and therefore these drugs must cross the cellular membrane before interacting with Rac1 and Cdc42. Therefore, it is expected that the concentration of the inhibitors halving half of the migration $K_{1/2migration}$ to be different from the concentration inhibiting half of Rac1 and Cdc42 activity in *in vitro* conditions. From the transwell experiments performed in U87 GBM cell line we have estimated that $K_{1/2migration}$ to be approximately 20, 30 and 50 μM for EHT 1864, ML141 and R-Ketorolac, respectively. For EHT 1864, the corresponding values obtained in vitro conditions are 1-5μM[1],and 20 μM on MDA-MB-231 and MCF-7 breast cancer cells[23].For ML141, 2 μMin vitro conditions[24], 3 μM for 50% reduction on ovarian cancer cell migration[19]. R-ketorolac against Rac1 and Cdc42 in Hela cells with values of 0.57 μM and 1.01μM [25], respectively. The reduced efficacy of the compounds, as compared to in vitro tests and migration characteristics in other cell line types, suggest that other pathways may also be relevant to stop the infiltration and migration propensities of the GBM.

Switches, binding and docking sites in Cdc42 and Rac1

The set of docking and MD simulations performed supply a molecular basis for the inhibition mechanism exerted by the known GTPase inhibitors tested in this study. R-ketorolac, bearing a carboxylic moiety, coordinates the Mg^{2+} ions, in line with the high affinity of carboxylic moieties towards Mg^{2+} ions observed in protein enzymes.Its binding may reduce the binding strength of GDP towards the Mg^{2+}metal triggering GDP dissociation and inactivating the small Rho GTPase function by hampering the GDP/GTP exchange. Nevertheless, the binding of R-ketorolac is slightly different in Cdc42 and Rac1, where in the first both switch I and II regions are lined by the drug hampering the opening/closing motion of the cavity and possibly

affecting also the interactions with the GEF proteins in Cdc42. Conversely, when binding to Rac1 R-ketorolac exclusively affects the switch I, which is less involved in the GEFinteraction/stabilization. The discussed difference in the binding poses is also confirmed also by the predicted binding mode of ML141 and EHT 1864, the first heading towards the switch II cavity, while the second being mainly and mostly lined by switch I. WhileML141 engages strong interactions with the cavity and hampers the typical opening/closing motion of the switches I/II, which necessary to GTP/GDP upload/release. Conversely, in spite of its larger size EHT 1864 does not completely freeze the movement of Rac1. Being Rho GTPases at the cross road of an intricate signaling interactome and being their action co-adjuvated by several interacting partners, we have attempted at predicting if/how the binding of the studied inhibitors could differently affect the interactions with selected proteins. Notably, by superimposing the drug-bound form of Rac1/Cdc42 proteins with selected Rho GTPase partners, for which the crystal structure in complex with their partner GTPase is available, it emerges that R-ketorolac and EHT 1864 appears to counteract the binding of specific Rac1 protein partner, plexin B1 [26].P-Rex1 and Epithelial cell transforming protein 2 (ETC2)[27], among the others which are involved in GBM migration and invasive propensity, while affecting to a lower extent the interaction with a typical GEF such as Dock2. Conversely the binding of both R-ketorolac and ML141 appears to potentially have an impact even on GEF (Dock9) binding.

Specific actions of R-Ketorolac, ML141 and EHT 1864

Migration and motility in cells is regulated by a complex and highly interconnected network of proteins. Therefore, pharmacological inhibition of these proteins simultaneously could be of therapeutic benefit.

R-Ketorolac is an inhibitor both of Rac1 and Cdc42, while ML141 is more specific for Cdc42 and EHT 1864 inhibits Rac1 preferentially. According to previous research, in melanoma Rac1 is not only overexpressed but also mutated[28].The knockdown of Rac1 in melanoma cells depresses the formation of invadopodia [29], and in this case decreases its capacity to promote cancer metastasis. The already approved drug Ketorolac and in particular its R-enantiomer inhibits Rac1 and Cdc4 in ovarian cancer [30], and potentially contributes to the observed survival benefit. This observation suggest to use the same drug for treating glioma/GBM at their early stages also in the case of brain cancer.R-Ketorolac is a drug already approved by the US Food and Drug Administration (FDA) in 1989, while ML141 and EHT 1864 not yet at the moment. Therefore, to study the molecular mechanism and working concentration of these three inhibitors will benefit

the clinical promotion and use.

Materialsand methods

Cell culture

U87 GBM cells (#89081402, Sigma-Aldrich) were cultured in DMEM supplemented with 10% fetal bovine serum (FBS; Invitrogen, Life Technologies, Gaithersburg, MD), 1% PenStrep (100 U/ml penicillin and 100 µg/ml streptomycin; Invitrogen).The GFP-labelled U87 GBM cells were infected by a mix containing lentiviral vector, LV-GFP.All the cells were cultured in an incubator at 37°C, 5% CO_2, 95%relative humidity and medium was replaced every 3 days. Once 70–80% ofconfluence had been reached, the cells were re-plated at a density of$2.5\times10^3/cm^2$.

Transwell assay

5 × 10^5U87 GBM cells in DMEM medium (without FBS) were seeded to the top chambers of 12-well transwell plates (Millipore; 8 µm pore size), and 10% FBS DMEM medium was added to the well. Inhibitors were employed in both the chamber and the well. After incubation for indicated time, cells in the top of the chamber (non-migrating cells) were removed from the chambers, and cells in the bottom of the chamber (migrating cells) were fixed with 4% PFA for 20 min and stained with 5% crystal violet for 30 min in room temperature. The migrated cells were counted with a microscope.

Live-cell imaging

GFP labelled U87 GBM cells were plated at a density of 8.0×10^4 cells into 35-mm dishes with a glass bottom and cultured for 1 day. Live-cell imaging experiments were performed on an epi-fluorescence microscope (NikonTi2-E) equipped with a chamber incubator and light-emitting diode (LED) illumination (λ=490 nm for). During all imaging experiments, cells were kept at 37°C, 5% CO_2 and 95% humidity. Time-lapse images were taken with 50 ms of exposure time and one image was taken every 2 min. The videos were analysed using the Fiji plugin TrackMate [31], which allows the selection of regions of interest (ROIs) for every cell and obtain the average velocities for each cell.

Computational model building

The starting configurations for the building the models of the Cdc42 and Rac1 proteins were taken from the crystal structures deposited in the protein data bank (PDB) (PDBid 5CJP and 2YIN, for Cdc42 and Rac1, respectively). Conversely, in order to investigate the binding of the drug at the interface with the specific

GEF proteins, we used the crystal structures of Dock9/Cdc42 and Dock2/Rac1 complexes with Cdc42 and Rac1 deposited in the PDB (PDB id 2WMO and 2YIN). For each system the protein structures were prepared, and the protonation state of the ionizable residues was determined by using Schödinger software suite.

Since the investigated inhibitors are known to act via a non-competitive mechanism (i.e. they do not compete with the GTP substrate) we initially looked for possible binding pockets able to host the inhibitors studies here, following an already established computational protocol [32]. To this aim we used the SiteMap [33] and FT Map softwares [34].The search of druggable pockets was carried on the crystal structure of the proteins and on selected frames of the equilibrated molecular dynamics (MD) trajectories of each protein in the Guanine triphosphate (GTP) and Guanine diphosphate (GDP) bound state. As a result, we identified two possible druggable pockets on Cdc42 and one pocket on Rac1. Docking simulations of the experimentally tested inhibitors were then performed to find a binding pose of the drugs on these pockets, following an ensemble docking approach [35]. Namely, we used as target protein structures: (i) the crystal structure of Rac1 and Cdc42 in the free form and the protein structure in complex with their specific GEFs, (ii) a representative of the equilibrated part of the simulation trajectory selected by a cluster analysis; (iii) a visually selected trajectory frame of the GDP- bound form of the proteins in which the pockets were able to accommodate the studied inhibitors. Prior to performing docking simulations, each drug was prepared considering all possible protonation states. Docking simulations were done with the Glide program of the Schödinger suite.

As a result, the R-ketorolac was considered in its negative, R-ML141 in its neutral and EHT 1864 in its positive form, which is predicted to be the most abundant at physiological pH.

Molecular dynamics (MD) simulations

The topology of the system was built with the Amber2018 tool *tleap* using the amber ff1ILDN force field (FF) [36]. The parameters of the GTP and GDP cofactors and of the tested drugs were built according to the following procedure: each molecule was subjected to a structure minimization using the Jaguar program at density functional theory (DFT) B3LYP level of theory and the 6-31G** basis set. Next, electrostatic potential (ESP) derived charges were computed according to the Merz-Kolmann partitioning scheme using the Gaussian software (Gaussian 09, R. A. G. I., Wallingford CT, 2016).with the same basis set, and converted

in RESP charges with the resp module of amber tools 2018. For the other FF parameters the general amber force field (Gaff) was employed [37]. For the Mg^{2+} ion present in the active site we used the Aqvist parameters [38]. The systems were solvated by adding a layer of 10 Angstrom of TIP3P water molecules[39] and neutralized with Na^{+} ions, using the Joung and Cheatman parameters[40].This lead to a total number of 44662 atoms for GDP-bound Cdc42, 35813 atoms for GDP-bound Cdc42 in complex with R-ketorolac, 36611 atoms for GDP-bound Cdc42 in complex withML141; 92293 atoms for GDP-bound in complex with Cdc42 and Dock9 ; 92310 atoms for for GDP-bound Cdc42 in complex with ML141 and Dock9; 34986 atoms for GDP-bound Rac1, 34739 atoms for GDP-bound Rac1 +R-ketorolac, 34415 atoms for GDP-bound Rac1 in complex withEHT 1864; 95331 atoms for GDP-bound Rac1 in complex with Dock2 and 95156 atoms for GDP-bound Rac1 in complex with Dock2 + EHT 1864. Overall ten different systems were simulated and extensively analyzed in this study. The system topology was then converted to the GROMACS format with the acpype software [41].

A short minimization was run before annealing the system to 300K. The pressure was equilibrated to 1atm using the Berendsen barostat. In the simulations with the drugs, after equilibration the position of the drug in the binding site was restrained for 30 ns and subsequently a production run was started removing the constraint. For all simulations the pressure was kept to equilibrium value with the Parrinello-Rahman barostat [42] while the temperature was controlled with the velocity rescale thermostat [43]. The length of the simulations of Cdc42 and Rac1 without drugs is 440 ns.

Analysis

The root mean square deviation (RMSD), the root mean square fluctuation (RMSF), the principal component analysis (PCA) and the per residue correlation matrix were derived using both GROMACS2018[44]and Amber 18 programs [45]. In particular the GROMACS2018 tools were used to compute the RMSD (gmx rms) and RMSF (gmxrmsf), while the hydrogen (H)-bonds and cross correlation matrix were computed with the AMBER2018 tool *cpptraj*. A cluster analysis was performed with the GROMACS2018 cluster tool using the algorithm described in Daura's report *[46].* Only Cα atoms of each residue were considered to compute RMSD, RMSF and correlation matrix. To compute the RMSD the whole trajectory was used, while all other properties were evaluated on a stable (almost flat RMDS) final 100 ns part of the whole trajectory. The PCA was performed with the GROMACS 2018 tools (gmxcovar, gmxanaeig). To obtain the PCs we applied the

following protocol: the trajectory was first fitted on the reference structure to remove translational and rotational motion, and then the mass-weighted covariance matrix was computed for the Cα atoms and diagonalized [21]. The eigenvectors exhibiting the largest eigenvalues pinpoint the most relevant motions sampled during the simulation, which is also referred to as principal components (PCs) [47].

The motion along the first eigenvector (essential dynamics), i.e. the vector corresponding to the largest eigenvalue, is commonly referred as essential dynamics and represents the most relevant motion of the system. This was visualized with the VMD program, and arrows highlighting the direction of motion were drawn using the porcupineplot.tcl plugin of the VMD program.

Energetic analysis

Binding free energies between the proteins and selected ligands (ΔG_b) were calculated by using the Molecular Mechanics-Generalized Born Surface Area (MM-GBSA) method [48] with Amber18 also using the per-residue decomposition tool to gain a direct view of how each residue lining the binding site contributes to drug-binding. The value of the igb flag was set to 2 and a salt concentration of 0.1 M was used. MM-GBSA calculations were performed on 100 equally distant frames the last 100 ns part of the equilibrated MD trajectory, following a protocol used in previous studies. The conformational entropic contribution of the free energy was not considered, as this term usually does not improve the quality of the results [49]. For what concerns the energetic contribution of each residue in the protein we used a threshold of 1 kcal/mol, absolute value, above which one residue was considered as significant in favoring/disfavoring the binding of the drug.

Reference

1. M. Weller, P. Roth, M. Preusser, et al., *Vaccine-based immunotherapeutic approaches to gliomas and beyond.* Nat Rev Neurol, 2017. **13**(6): p. 363-374.
2. S.J. Bagley, A.S. Desai, G.P. Linette, et al., *CAR T-cell therapy for glioblastoma: recent clinical advances and future challenges.* Neuro Oncol, 2018. **20**(11): p. 1429-1438.
3. R.J. Diaz, S. Ali, M.G. Qadir, et al., *The role of bevacizumab in the treatment of glioblastoma.* J Neurooncol, 2017. **133**(3): p. 455-467.
4. A.A. Thomas, C.W. Brennan, L.M. DeAngelis, et al., *Emerging therapies for glioblastoma.* JAMA Neurol, 2014. **71**(11): p. 1437-1444.
5. R. Stupp, W.P. Mason, M.J. van den Bent, et al., *Radiotherapy plus concomitant and adjuvant temozolomide for glioblastoma.* N Engl J Med, 2005. **352**(10): p. 987-996.
6. K.P.L. Bhat, V. Balasubramaniyan, B. Vaillant, et al., *Mesenchymal differentiation mediated by NF-kappaB promotes radiation resistance in glioblastoma.* Cancer Cell, 2013. **24**(3): p. 331-346.
7. J. Behnan, G. Finocchiaro, and G. Hanna, *The landscape of the mesenchymal signature in brain tumours.* Brain, 2019. **142**(4): p. 847-866.
8. C.W. Pak, K.C. Flynn, and J.R. Bamburg, *Actin-binding proteins take the reins in growth cones.* Nat Rev Neurosci, 2008. **9**(2): p. 136-147.
9. T.R. Stankiewicz and D.A. Linseman, *Rho family GTPases: key players in neuronal development, neuronal survival, and neurodegeneration.* Front Cell Neurosci, 2014. **8**: p. 314.
10. W.A. Sayyad, P. Fabris, and V. Torre, *The Role of Rac1 in the Growth Cone Dynamics and Force Generation of DRG Neurons.* PLoS One, 2016. **11**(1): p. e0146842.
11. A.J. Ridley, H.F. Paterson, C.L. Johnston, et al., *The small GTP-binding protein rac regulates growth factor-induced membrane ruffling.* Cell, 1992. **70**(3): p. 401-410.
12. C.D. Nobes and A. Hall, *Rho, rac, and cdc42 GTPases regulate the assembly of multimolecular focal complexes associated with actin stress fibers, lamellipodia, and filopodia.* Cell, 1995. **81**(1): p. 53-62.
13. A.J. Ridley, *Rho GTPases and actin dynamics in membrane protrusions and vesicle trafficking.* Trends Cell Biol, 2006. **16**(10): p. 522-529.
14. A. Hall, *Rho family GTPases.* Biochem Soc Trans, 2012. **40**(6): p. 1378-1382.
15. S. Etienne-Manneville and A. Hall, *Rho GTPases in cell biology.* Nature, 2002. **420**(6916): p. 629-635.
16. X. Chi, S. Wang, Y. Huang, et al., *Roles of rho GTPases in intracellular transport and cellular transformation.* Int J Mol Sci, 2013. **14**(4): p. 7089-7108.
17. Y. Guo, S.R. Kenney, C.Y. Muller, et al., *R-Ketorolac Targets Cdc42 and Rac1 and Alters Ovarian Cancer Cell Behaviors Critical for Invasion and Metastasis.* Mol Cancer Ther, 2015. **14**(10): p. 2215-2227.
18. L. Hong, S.R. Kenney, G.K. Phillips, et al., *Characterization of a Cdc42 protein inhibitor and its use as a molecular probe.* J Biol Chem, 2013. **288**(12): p. 8531-8543.
19. A. Shutes, C. Onesto, V. Picard, et al., *Specificity and mechanism of action of EHT 1864, a novel small molecule inhibitor of Rac family small GTPases.* J Biol Chem, 2007. **282**(49): p. 35666-35678.
20. M.D.M. Maldonado and S. Dharmawardhane, *Targeting Rac and Cdc42 GTPases in Cancer.* Cancer Res, 2018. **78**(12): p. 3101-3111.
21. L. Casalino, G. Palermo, A. Spinello, et al., *All-atom simulations disentangle the functional dynamics underlying gene maturation in the intron lariat spliceosome.* Proc Natl Acad Sci U S A, 2018. **115**(26): p. 6584-6589.

22. L. Casalino, G. Palermo, N. Abdurakhmonova, et al., *Development of Site-Specific Mg(2+)-RNA Force Field Parameters: A Dream or Reality? Guidelines from Combined Molecular Dynamics and Quantum Mechanics Simulations.* J Chem Theory Comput, 2017. **13**(1): p. 340-352.
23. J. Molnar, C. Fazakas, J. Hasko, et al., *Transmigration characteristics of breast cancer and melanoma cells through the brain endothelium: Role of Rac and PI3K.* Cell Adh Migr, 2016. **10**(3): p. 269-281.
24. Z. Surviladze, A. Waller, J.J. Strouse, et al., *A Potent and Selective Inhibitor of Cdc42 GTPase*, in *Probe Reports from the NIH Molecular Libraries Program*. 2010: Bethesda (MD).
25. T.I. Oprea, L.A. Sklar, J.O. Agola, et al., *Novel Activities of Select NSAID R-Enantiomers against Rac1 and Cdc42 GTPases.* PLoS One, 2015. **10**(11): p. e0142182.
26. E. Angelopoulou and C. Piperi, *Emerging role of plexins signaling in glioma progression and therapy.* Cancer Lett, 2018. **414**: p. 81-87.
27. M. Chen, H. Pan, L. Sun, et al., *Structure and regulation of human epithelial cell transforming 2 protein.* Proc Natl Acad Sci U S A, 2020. **117**(2): p. 1027-1035.
28. M. Krauthammer, Y. Kong, B.H. Ha, et al., *Exome sequencing identifies recurrent somatic RAC1 mutations in melanoma.* Nat Genet, 2012. **44**(9): p. 1006-1014.
29. O.Y. Revach, S.E. Winograd-Katz, Y. Samuels, et al., *The involvement of mutant Rac1 in the formation of invadopodia in cultured melanoma cells.* Exp Cell Res, 2016. **343**(1): p. 82-88.
30. Y. Guo, S.R. Kenney, L. Cook, et al., *A Novel Pharmacologic Activity of Ketorolac for Therapeutic Benefit in Ovarian Cancer Patients.* Clin Cancer Res, 2015. **21**(22): p. 5064-5072.
31. J.Y. Tinevez, N. Perry, J. Schindelin, et al., *TrackMate: An open and extensible platform for single-particle tracking.* Methods, 2017. **115**: p. 80-90.
32. J. Sgrignani, M. Bon, G. Colombo, et al., *Computational approaches elucidate the allosteric mechanism of human aromatase inhibition: a novel possible route to Small-molecule regulation of CYP450s activities?* J Chem Inf Model, 2014. **54**(10): p. 2856-2868.
33. T.A. Halgren, *Identifying and characterizing binding sites and assessing druggability.* J Chem Inf Model, 2009. **49**(2): p. 377-389.
34. R. Brenke, D. Kozakov, G.Y. Chuang, et al., *Fragment-based identification of druggable 'hot spots' of proteins using Fourier domain correlation techniques.* Bioinformatics, 2009. **25**(5): p. 621-627.
35. A. Spinello, S. Martini, F. Berti, et al., *Rational design of allosteric modulators of the aromatase enzyme: An unprecedented therapeutic strategy to fight breast cancer.* Eur J Med Chem, 2019. **168**: p. 253-262.
36. J.A. Maier, C. Martinez, K. Kasavajhala, et al., *ff14SB: Improving the Accuracy of Protein Side Chain and Backbone Parameters from ff99SB.* J Chem Theory Comput, 2015. **11**(8): p. 3696-3713.
37. J. Wang, R.M. Wolf, J.W. Caldwell, et al., *Development and testing of a general amber force field.* J Comput Chem, 2004. **25**(9): p. 1157-1174.
38. J. Aqvist, *Ion-water interaction potentials derived from free energy perturbation simulations.* The Journal of Physical Chemistry, 1990. **94**(21): p. 8021-8024.
39. W.L. Jorgensen, J. Chandrasekhar, J.D. Madura, et al., *Comparison of simple potential functions for simulating liquid water.* The Journal of chemical physics, 1983. **79**(2): p. 926-935.
40. I.S. Joung and T.E. Cheatham, 3rd, *Determination of alkali and halide monovalent ion parameters for use in explicitly solvated biomolecular simulations.* J Phys Chem B, 2008. **112**(30): p. 9020-9041.
41. A.W. Sousa da Silva and W.F. Vranken, *ACPYPE - AnteChamber PYthon Parser interfacE.* BMC Res Notes, 2012. **5**: p. 367.

42. M. Parrinello and A. Rahman, *Crystal structure and pair potentials: A molecular-dynamics study.* Physical review letters, 1980. **45**(14): p. 1196.
43. G. Bussi, D. Donadio, and M. Parrinello, *Canonical sampling through velocity rescaling.* J Chem Phys, 2007. **126**(1): p. 014101.
44. D. Van Der Spoel, E. Lindahl, B. Hess, et al., *GROMACS: fast, flexible, and free.* J Comput Chem, 2005. **26**(16): p. 1701-1718.
45. A.B. Rubenstein, K. Blacklock, H. Nguyen, et al., *Systematic Comparison of Amber and Rosetta Energy Functions for Protein Structure Evaluation.* J Chem Theory Comput, 2018. **14**(11): p. 6015-6025.
46. X. Daura, K. Gademann, B. Jaun, et al., *Peptide folding: when simulation meets experiment.* Angewandte Chemie International Edition, 1999. **38**(1-2): p. 236-240.
47. J. Borisek, A. Saltalamacchia, A. Galli, et al., *Disclosing the Impact of Carcinogenic SF3b Mutations on Pre-mRNA Recognition Via All-Atom Simulations.* Biomolecules, 2019. **9**(10).
48. I. Massova and P.A. Kollman, *Combined molecular mechanical and continuum solvent approach (MM-PBSA/GBSA) to predict ligand binding.* Perspectives in drug discovery and design, 2000. **18**(1): p. 113-135.
49. J. Borisek, A. Saltalamacchia, A. Spinello, et al., *Exploiting Cryo-EM Structural Information and All-Atom Simulations To Decrypt the Molecular Mechanism of Splicing Modulators.* J Chem Inf Model, 2020. **60**(5): p. 2510-2521.

Chapter 3. Supplementary Materials

After the completion of my work submitted and accepted by Cancers I performed further experiments related to the following two issues:

1. The effect of the substrate on GBM cell motility.
2. The roles of Piezo1on the response of GBM cell to the substrate rigidity.

3.1 The Effect of the Substrate on GBM Cell Motility

Abstract

Cells exhibit complex responses to the extracellular environment. Matrigel matrix and poly-l-ornithine substrates are widely used for enhancing cell attachment. In this study, I want to compare the differences in the response of GBM cell to these two substrates. GBM cell cultured on glass was considered as the control. I found that:

- Cell viability and motility were different among these conditions.
- GBM cells changed their actin organization, adhesion dynamics during migration by regulating Rho GTPases and focal adhesion molecules.

It is conceivable that a better understanding of the interactions between cells and their substrates are prerequisite for drug screening.

Background

Nowadays, a number of therapeutic agents for GBM treatment have been reported, which mainly target the growth factor receptors and their downstream pathways, cell cycle, epigenetic modulators, angiogenesis, and antitumor immune responses [250-251]. However, only a low percentage of drugs can be approved to the market. Over the past two decades, research has established that environmental features affect several of processes, including cell spreading, adhesion, growth, proliferation, apoptosis, migration, differentiation and organoid formation, cancer progression and response to drugs. Cell exhibits complex responses to the microenvironment, especially during cell migration. The majority strategy for drug discovery is based on cell culture. The inappropriate substrate of cell culture may contribute to the high failure rate in drug discovery. In this study, I cultured GBM cell U87 and U251 on glass and matrigel matrix or poly-l-ornithine substrate to investigate how these substrates affect GBM cell. I focus my attention on the alterations of gene expression, cell proliferation and motility. Furthermore, I want to compare the differences in actin organization, actomyosin contractility and cell adhesions dynamics during GBM cell migration among these substrates.

Preliminary Results

1 - GBM Cell Viability of Different Substrates

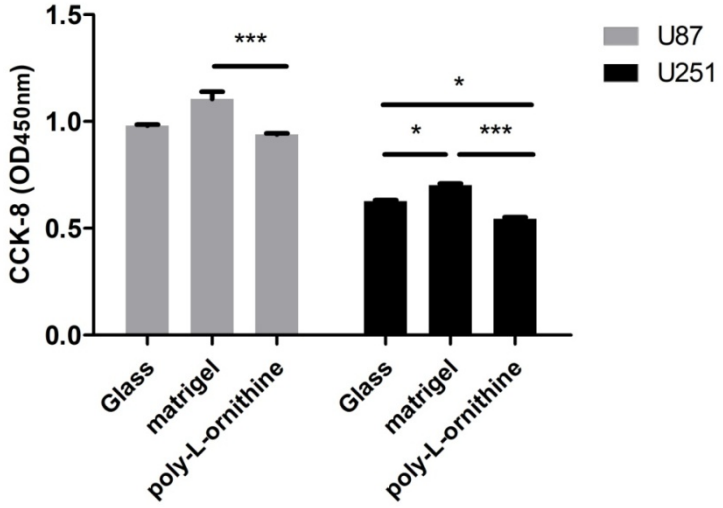

Figure 1. Two main categories of substrates were used, the naturally-occurring substrate, matrigel matrix and the synthetic substrate, poly-l-ornithine. Glass surface was used as control. Matrigel matrix and poly-l-ornithine are widely used as a coating to enhance cell attaching and adhering to plastic and glass surfaces. Two types of typical GBM cell lines, U87 (GBM multiforme grade IV) and U251 (GBM-astrocytoma grade III-IV) were used. CCK-8 assay was used to detect the cell viability in the entire group, and GBM cell viability was dramatically higher in matrigel than that of the poly-l-ornithine group (Figure 1). Cell viability of U87 and U251 GBM cells was evaluated using the CCK-8 assay after culturing on matrigel matrix and poly-l-ornithine coated plastic for 12h. Cell cultured on the glass surface was used as control. ***: $p<0.001$, *: $p<0.05$

2 - GBM Motility on Different Substrates

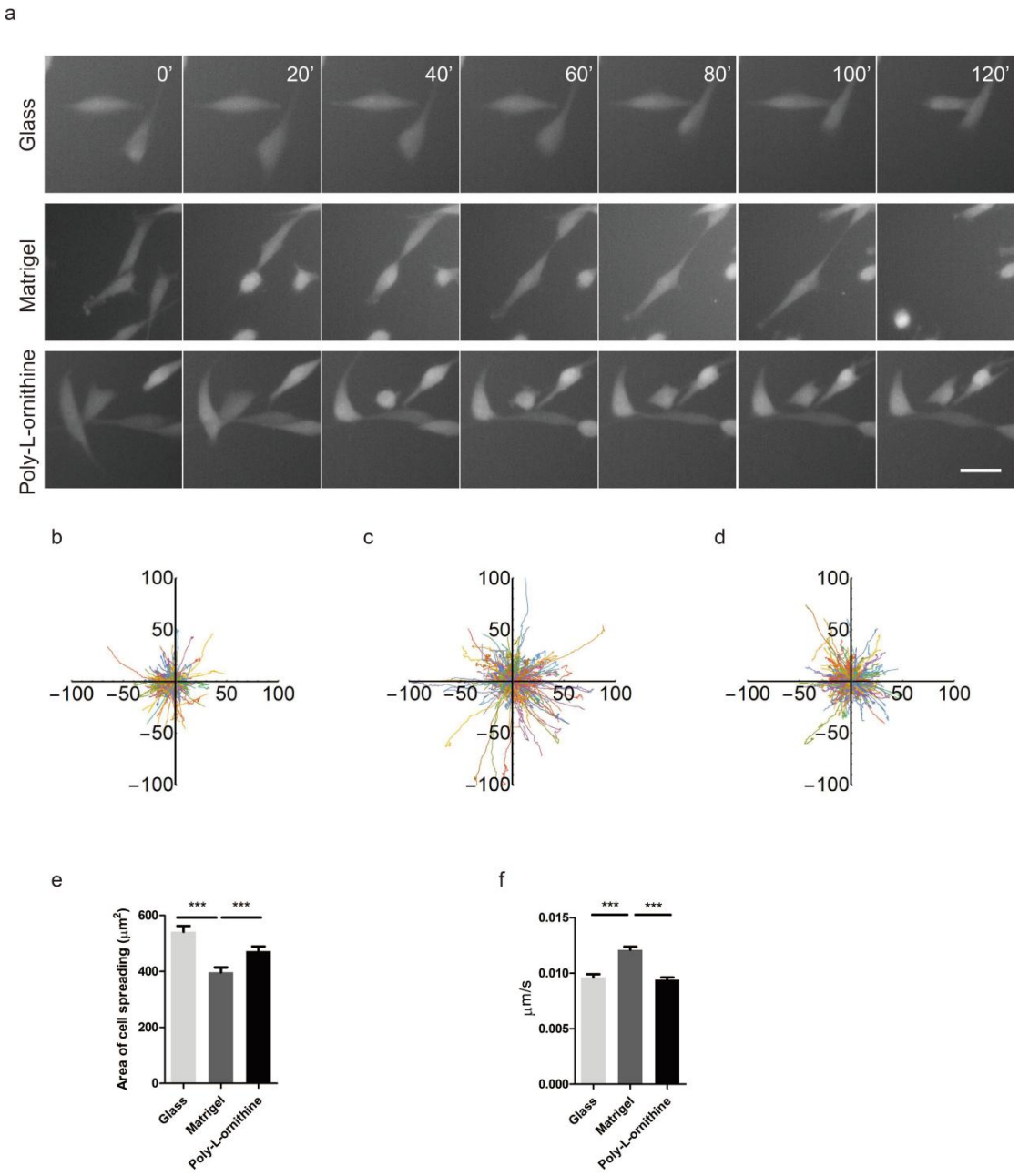

Figure 2. U87 cell movement was detected in three conditions using live cell imaging. A stable U87-GFP cell line was established to visualize GBM movements. Analysis of the movies revealed that cells on matrigel matrix substrate quickly change their type during migration (Figure 2a). Trajectories of individual cells were used to quantify motility differences following different substrate culture (Figure 2b-d). The cell moved significantly faster in the matrigel matrix group than the other two groups (Figure 2f), accompanying the smallest spreading area (Figure 2e). (a) U87-GFP cell was cultured on matrigel and poly-l-ornithine coated

surface and recorded for 2h using the time-lapse recording. (b-d) Cell trajectories of U87-GFP cells growth on glass (b), matrigel matrix (c) and poly-l-ornithine (d) for 2h; each color represents the trajectory of an individual cell, and the starting positions of each cell were registered to the center of the plot. (e) U87-GFP cell spreading areas were quantified using the ImageJ program (NIH). (f) The mean velocity of the U87-GFP cell in each group was recorded for 2h and analyzed using the ImageJ program (NIH). Scale bar: 50μm. Cell number: 274 cells in the glass group, 272 cells in the matrigel matrix group and 278 cells in the poly-l-ornithine group.

3 - Actin Stress Fibers Organization of GBM Cell Grown on Different Substrates

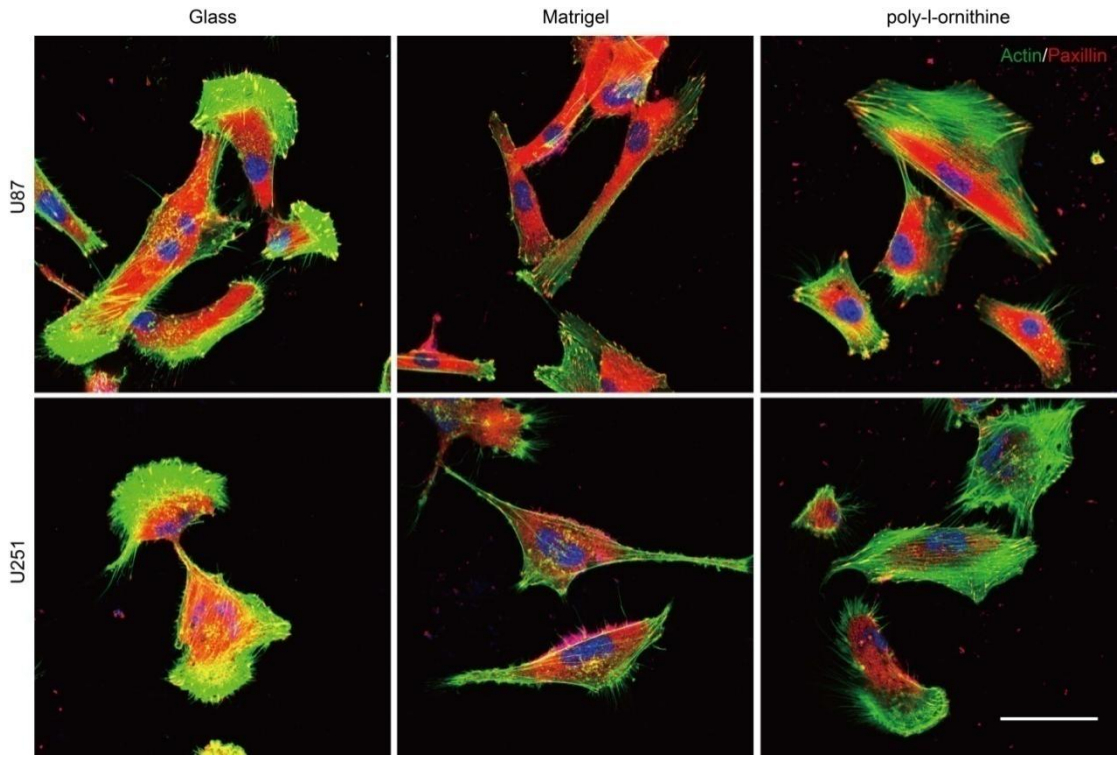

Figure 3. Cells use protrusions for movement. When GBM cellswere cultured on glass and poly-l-ornithine substrate, most of the U87 and U251 cells exhibited epithelial-like morphology and formed a large protrusion with actin stress fibers (Figures 3 left panel and right panel, green). However, when GBM cellswere cultured on matrigel matrix substrate, cells shrank their cell body and formed a small protrusion with less actin stress fibers (Figures 3 middle panel, green). Confocal sections of U87 and U251 cells cultured on glass, matrigel matrix and poly-l-ornithine substrate and stained with Phalloidin (green) and Paxillin (red). Scale bar: 50μm.

4 - Dynamics of Cell Adhesion over Different Substrates

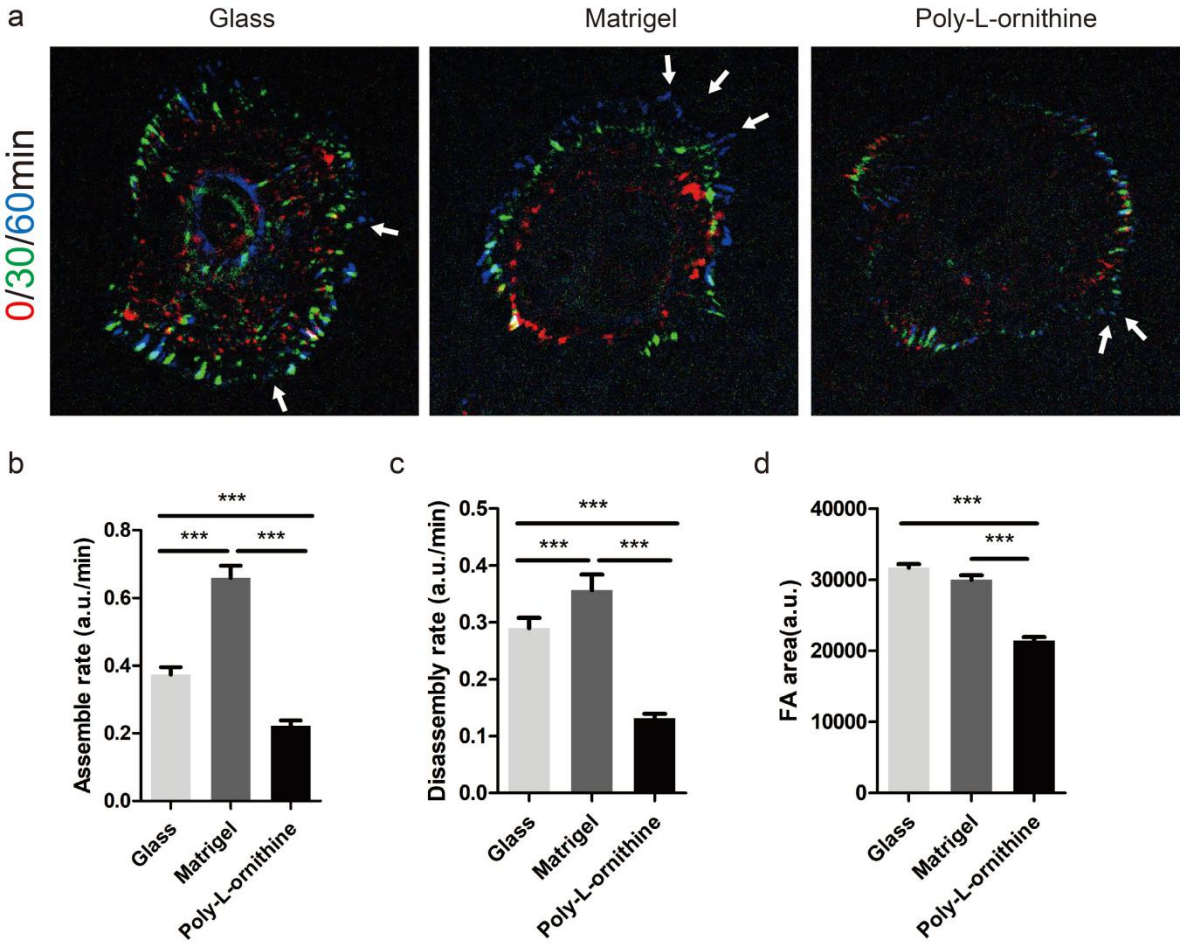

Figure 4. Cell adhesions form at the cell front and disassemble at both the front and rear of the cell. These events are crucial for cell migration. Paxillin-GFP expressed U87 cells were seeded on the three substrates and observed the assembly and disassembly of Paxillin spots using live cell imaging (Figure 4a, Videos S4-6). Recordings lasted approximately 60min, and one frame was digitized every 2min. Data showed that both the assembly and disassembly rates in the matrigel matrix group were the fastest, these rates in the glass group were lower than that of the matrigel matrix group, and the poly-l-ornithine group had the lowest rates (Figure 4b-c). The area of adhesions of the glass and matrigel matrix group was significantly larger than that of the poly-l-ornithine group (Figure 4d). Furthermore, during migration, cell adhesions tended to assemble in one direction on both the matrigel matrix and poly-l-ornithine group (Figure 4a). However, the cell adhesions on the glass surface exhibited a random growth (Figure 4a). (a) Paxillin expressed U87 cells were imaged by time-lapse microscopy at 2min intervals for 60min. The red Paxillin spots were recorded at

0min, the green Paxillin spots were recorded at 30min, and the blue Paxillin spots were recorded at 60min. The closed arrow indicates the tendency of adhesions assembly. Histograms represent the adhesion assembly rate (b), disassembly rate (c) and adhesion area (d). Recordings are showed in Videos S4-6. Tracking cell adhesion numbers: 260 in the glass group, 242 in the matrigel matrix group and 161 in the poly-l-ornithine group.

5 - Rho GTPases and Focal Adhesion Molecules in GBM Cells

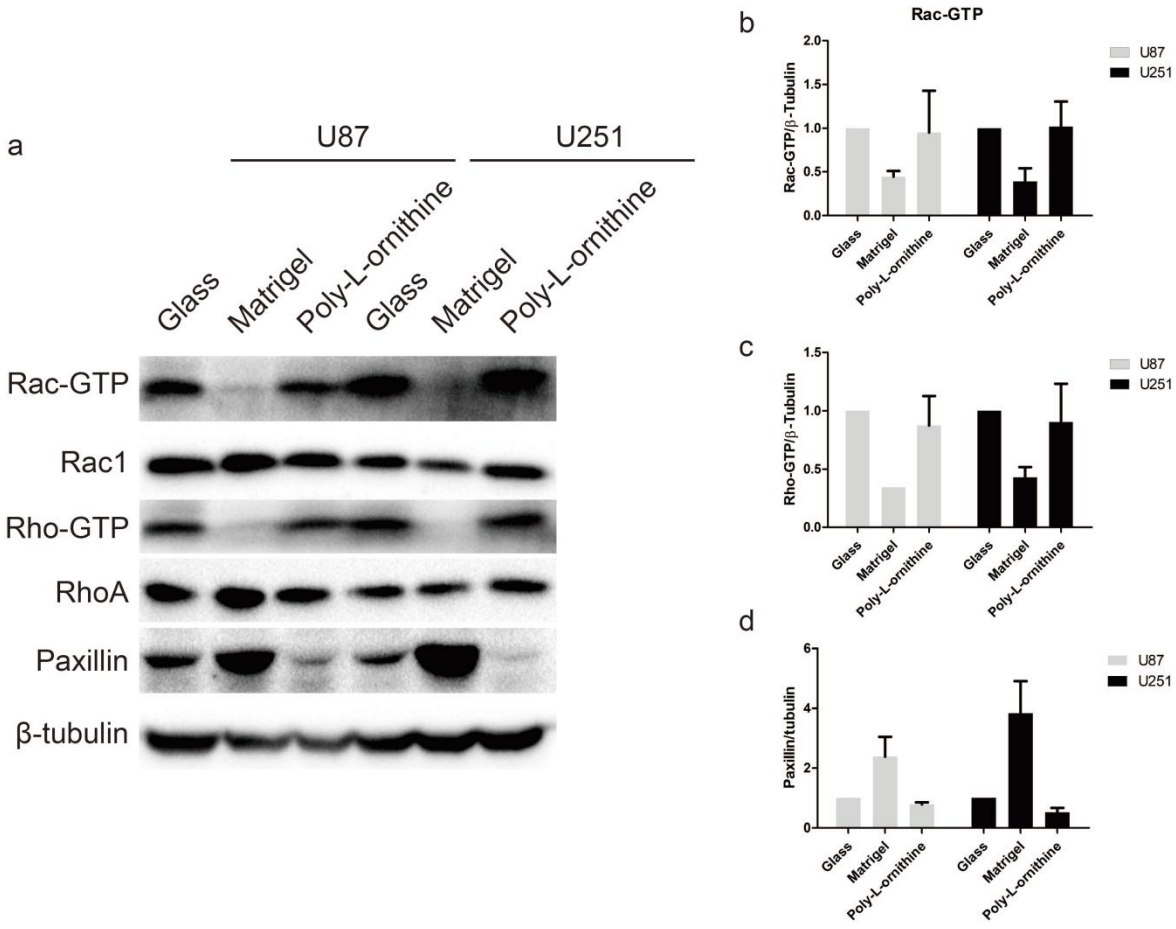

Figure 5. In mesenchymal cell migration, cells use filopodia and lamellipodia protrusions to push the cell forward [52, 108-109]. Filopodia are finger-like protrusions that contain parallel bundles of actin filaments in the direction of the protrusion. Lamellipodia are thin branched actin sheets, which can both protrude and retract. It is reported that Rho GTPases family member Cdc42 and Rac1 play important roles in these two structures, respectively. RhoA can promote myosin II activity with the help of ROCK and plays functions in both cell front and rear [106-107]. Our results showed that the levels of Rac-GTP and Rho-GTP of both the glass and poly-l-ornithine groups were much higher than that of the matrigel matrix group (Figure 5a, b-c). However, the level of Paxillin exhibited an inverse tendency (Figure 5a, d). (a) Western blot analysis for detecting the levels of Rac-GTP, Rho-GTP, Rac1, RhoA and Paxillin in U87 and U251 that cultured on glass, matrigel matrix and poly-l-ornithine substrates. (b-d) Histograms of the expression levels of Rac-GTP, Rho-GTP and Paxillin compared to β-tubulin.

Conclusion

In the present study, I confirm that when cells were cultured on three culture substrates: glass, matrigelmatrix and poly-l-ornithine, GBM cells can respond to the environment changes in various biological ways, including alterations in cell viability, cell morphology and migration. GBM cell was also found differences inactin stress fibers organization and adhesion dynamics of different substrates. The levels of active Rho GTPases, Rac-GTP and RhoA-GTP, and focal adhesion adapter protein, Paxillin, were different among these substrates.

In conclusion, both matrigel matrix and poly-l-ornithine are wildly used to enhance cell attachment, especially for primary cells. I find that even these commonly used substrates can introduce cell responses in a multiple and fast way. Cell-based assays are a simple, fast and cost-effective way for the drug discovery process. Drug development is a lengthy and costly process; however, the failure rate in drug discovery nowadays is still very high. Understanding how cell benefits from the different substrates and choosing the right one will help us get the most out of our experiments.

Next step, I want to use the RNA sequencing technique to detect the differentially expressed (DE) genes of GBM cell in different substrates and predict which signal pathways are mainly involved in GBM cell response to those differences. Further, I want to use RT-PCR or western blot to confirm the most interesting moleculesobtained from RNA sequencing.

Materials and Methods

Cell Lines

Human GBM cell lines U87, U251 (all from ATCC) and U87 stably transfected with LV_Pgk1p-mCherry were cultured at 37 °C, 5% CO2 in DMEM medium supplemented with 10% FBS and penicillin/streptomycin. Cell cultures were routinely subcultured every two days by trypsinization using standard procedures.

Immunofluorescent Staining

Cells were fixed with 4% PFA for 20min and permeabilized with 0.1% TritonX-100 for 20min. Cells were then incubated with primary antibody and second antibody. The following primary antibodies were used: anti-myosin IIa (1:200, CST) and anti-Paxillin (1:200, Abcam). Phalloidin (1:2000, Invitrogen) was used to detect F-actin.

Cell Proliferation Assay

5×10^3 cells were plated in 96-well plates. After 12 hours' culture, cells were transfected with Rac1-siRNA and NC-siRNA and cultured for another 48 hours. Cell growth was measured by colorimetric CCK-8 assay (Sigma-Aldrich Co, St Louis, MO, USA).

Cell Transfection and Live cell Imaging

Cells were plated at a density of 1×10^5 cells/ml into 35 mm confocal dishes and incubated overnight. Transient transfection of Paxillin-GFP was carried out with Lipofectamine™ 2000 (Invitrogen) using the protocol provided by the manufacturer. 24 hours after transfection, cells were used for live cell imaging assay.

For live cell imaging assay, cells were maintained in a 37℃, 5% CO2 in chambers in culture medium on an inverted microscope (Nikon, UK) with a motorized stage (Prior Scientific, UK) controlled by NIS-Elements software (Nikon, UK). Stable U87-GFP cells were used to detect the cell shape and velocity changes on glass, matrigel and poly-L-orinithine. Time-lapse image series were acquired at 1min intervals using a 20×1.4 NA objective lens (Nikon). Paxillin-GFP fluorescence time-lapse image series were acquired at 2min intervals using a 40×1.4 NA objective lens (Nikon).

Tracking Assays and Data analysis

Tracking of cell migration was performed over a period of 2 hours. Individual cells were tracked by repeated selection of cells in movie frames and manual tracing of migration pathways with image J software.

Individual cell adhesions tracking were performed similarly to cell tracking procedure. We then fit the curves of 'adhesion assembly' or 'adhesion disassembly' by Origin software using Slogistic1 function, and got the k/-k value as the rate of assembly or disassembly.

Western Blot

Cells were plated at a density of 2×10^6 cells/well in 10cm and grown to 70-80% confluence. After cultured on glass, matrigel and poly-L-orinithine for 48h, cells were washed with cold PBS and lysed in lysis buffer supplemented with a protease inhibitor cocktail (Sigma-Aldrich Co). Equal amounts of total protein were boiled for 5min in 5×sample buffer and fractionated by 12% SDS-PAGE. Samples were then transferred to PVDF membranes (Millipore). Immunoblots were detected using ECL System (Millipore) with horseradish peroxidase-conjugated secondary antibodies (Sigma). The following first antibodies were used: anti-Rac1 (Abcam), anti-RhoA (Millipore), anti-Rac-GTP, anti-Rho-GTP, anti-Paxillin (Cell Signaling Technology).

Statistical Analysis

Difference between groups was assessed by Student's t-test, one-way ANOVA or two-way ANOVA test. Graphpad Prism was used for all statistical analyses. The difference of cell mobility, adhesion dynamics and cell spreading area was evaluated by one-way ANOVA followed by Kruskal-Wallis test. The results are presented as the mean ± SEM of at least three independent experiments.

3.2 The roles of Piezo1 on GBM cell Response to Substrate

Background

Abnormal organization and modification of ECM molecules are observed in tumor ECM. The mechanical properties of the ECM can transmit to cell (mechanotransduction) and direct many cellular properties. In this study, I cultured GBM cells on collagen I coated-substrates with different rigidity. GBM cell altered their proliferation, morphology and motility when responding to substrate rigidity. Mechanosensitive ion channel (MSC) Piezo1 is reported overexpressed in glioma and associated with glioma aggression. However, how this molecule regulating glioma progression is still unclear. I found that Piezo1 upregulated on the stiff substrate compare to the soft one. Using GsMT×4 to block the activation of Piezo1 channel, GBM cell significantly reduced their velocity during migration. The results also showed that Rho GTPases and focal adhesion molecules were involved in GBM dynamics.

Preliminary Results

1 - Substrate Rigidity Alters GBM Cell Proliferation, Morphology and Cytoskeletal Organization and Cell Adhesion Formation.

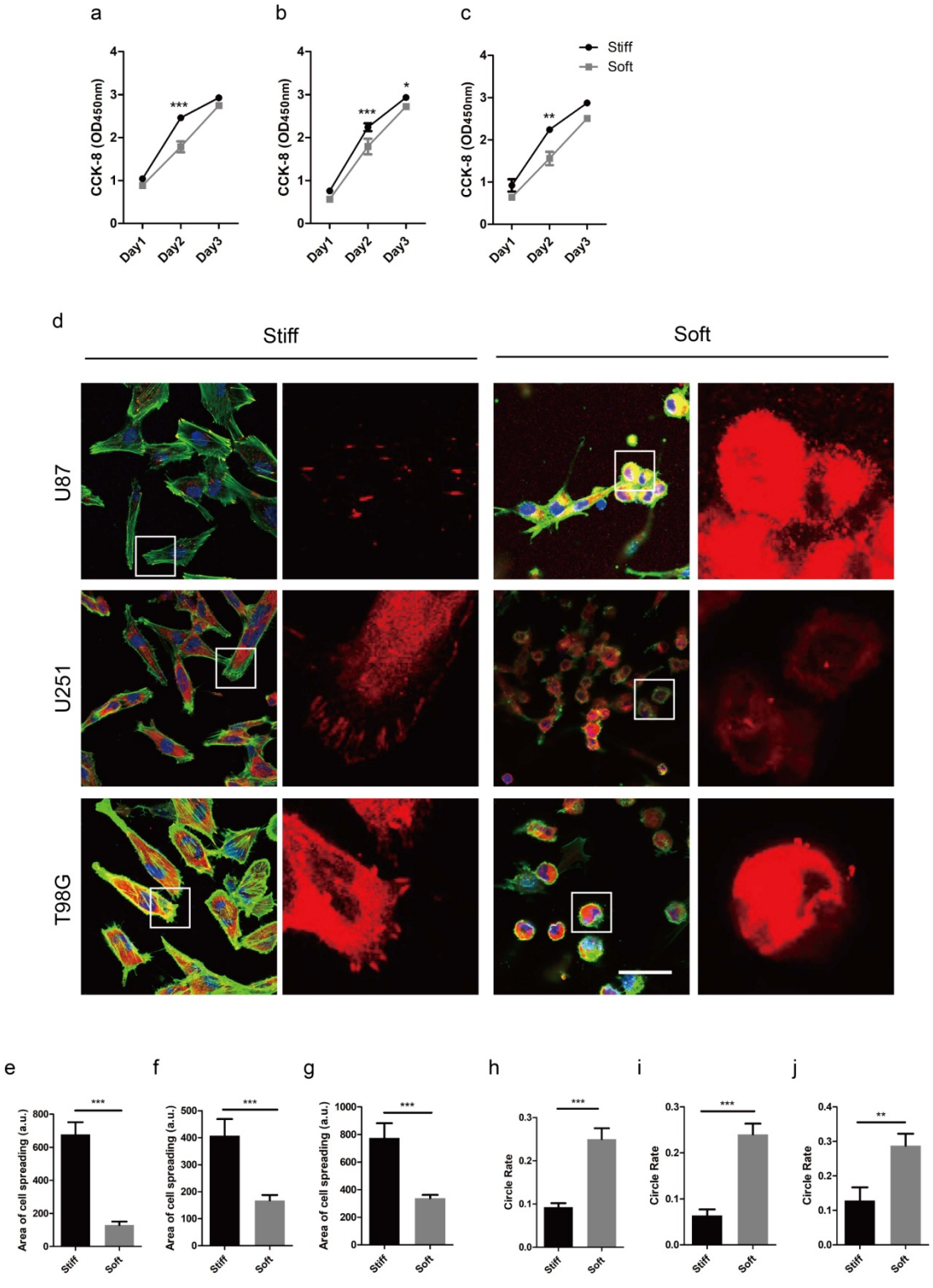

Figure 1. GMB cell U87, U251 and T98G were cultured on soft collagen substrate and stiff collagen substrate, respectively. Substrate rigidity significantly changed the proliferation rate of GBM cells (Figure1a-c). GBM cell cultured on the rigid substrate was typically well-spread with actin stress fibers and Paxillin-positive adhesions (Figure 1d-j). Cell cultured on the soft substrate was mostly shrunk into a round shape, with cortical rings of F-actin and small, punctuate Paxillin spots (Figure 1d-j). (a-c) The proliferation of GBM cells in different rigidity of the substrates was detected by CCK-8 assay. (d) Substrate rigidity altered GBM cell morphology, cytoskeletal organization and cell adhesion formation. (e-g) The cell spread area of GBM cell that cultured in stiff and soft substrate. (h-j) The circle rate of GBM cells that cultured in stiff and soft substrate. U87, U251 and T98G cells were stained for F-actin (green), nuclear DNA (blue) and the focal adhesion protein Paxillin (red). Scale bar: 50 μm

2 - The Rigidity of the Substrateregulates the Levels of Piezo1 and Migration-Related Molecules

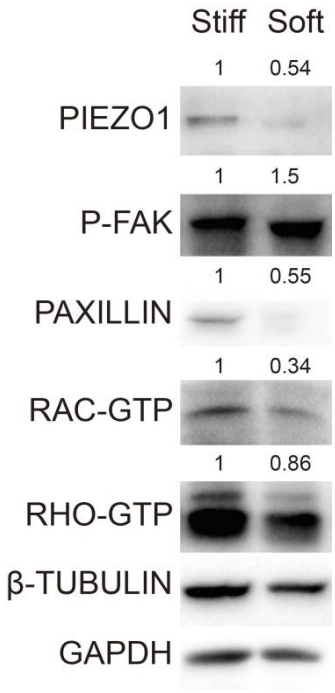

Figure 2. MSC Piezo1 isreported overexpressed in glioma and associated with glioma aggression [161]. To investigate whether Piezo1 is involved in the sensing ECM rigidity in GBM cell, the expression of Piezo1 was detected by western blotting. The results showed that Piezo1 was upregulated in the stiff substrate compare to the soft substrate (Figure 2). Furthermore, the levels of activated Rho GTPases, Rho-GTP, and Rac-GTPwere also upregulated in stiff substrate accompany a higher level of the focal adhesion adaptor protein, Paxillin (Figure 2). However, the phosphorylation level of FAK was downregulated in the stiff substrate.The expression of Piezo1, P-FAK, Paxillin, Rac-GTP and Rho-GTP was detected by western blotting, the expression of β-Tubulin and GAPDH was detected as control.

3 - Inhibition of Piezo1 Decreases the Motility of GBM Cells

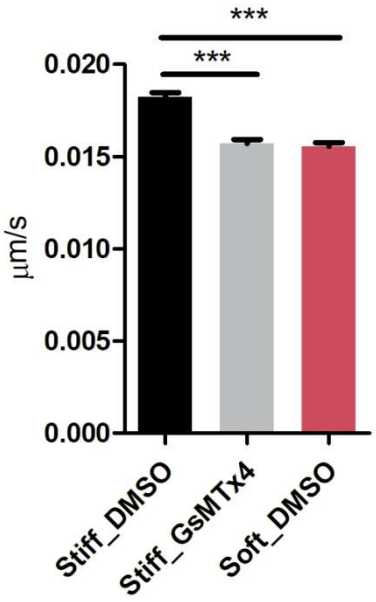

Figure 3. As mentioned above, alterations were found in cell migration-related molecules during their response to ECM stiffness changes. Cell motility is critical for tumor invasion. To investigate whether ECM stiffness could affect the velocity of GBM movement, the random motility of the U87-GFP cell was recorded by live cell imaging. Mean velocity fell dramatically with decreasing substrate rigidity. Using 5μm GsMT×4 to block the activation of Piezo1 channel, cell movement significantly slowed down on stiff substrate. U87-GFP cells were recorded for 2h. After 2h recording, cells were incubated with GsMT×4 and recorded for another 2h. The mean velocity of U87-GFP cells was recorded for 2h and analyzed using the ImageJ program (NIH). Recordings of the U87-GFP cell movement are shown in VideosS1, S2 and S3.

4 - Inhibition of Piezo1 Decreases the Motility of GBM Cells

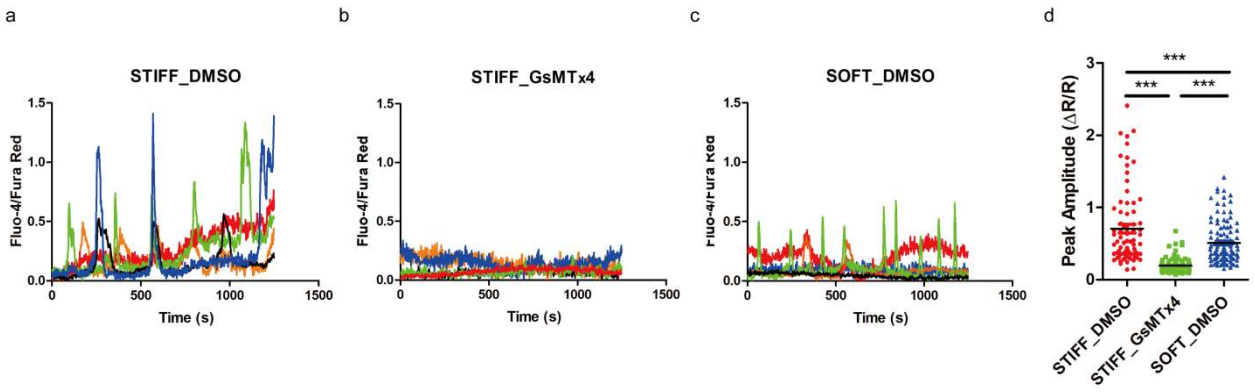

Figure 4. Piezo1 is a nonselective cation channel and is permeable to extracellular calcium (Ca^{2+}) influx. To investigate whether Piezo1 regulating GBM cell movement is mediated by the extracellular Ca^{2+} influx, the Ca^{2+} flux of GBM cell was then detected by Fluo-4 and Fura Red staining. GBM cells showed strong Ca^{2+} signals on the stiff substrate and weak Ca^{2+} signals on the soft substrate. However, inhibiting Piezo1 by GsMT×4 reduced the Ca^{2+} signals on the stiff substrate in GBM cells. (a-c) Ca^{2+} signals were detected by Flou4 and Fura Red staining. Typical curves of Ca^{2+} signals in stiff substrate with (a) and without (b) Piezo1 activation, and in soft substrate (c) were shown by the ratio between Fluo-4 and Fura Red. The peak amplitude of Ca^{2+} signals were recorded for 20 min and analyzed using the ImageJ program (NIH). Recordings of the U87-GFP Ca^{2+} flux are shown in VideosS4, S5 and S6.

Conclusion

So far, I confirm that GBM cells responded to ECM rigidity by changing their proliferation and morphology. The motility of GBM cells also changed according to the ECM rigidity. MSC Piezo1 was upregulated in the stiff substrate, accompany with the upregulation of Rac-GTP, Rho-GTP and Paxillin. Furthermore, Blocked Piezo1 by GsMT×4 reduced the GBM cell velocity of both soft and stiff substrate.

In conclusion, GBM cells can respond to substrate mechanical properties, changing cell proliferation, morphology and motility. Substrate rigidity induced cell movement can inhibit by the inhibition of Piezo1, which indicates that MSC Piezo1 plays a very significant role in cell mechanotransduction.

To further confirm that Piezo1 is involved in the substrate rigidity induced GBM cell movement, first I want to use the Piezo1 agonist, yoda1, to investigate whether the activity of Piezo1 can increase GBM motility and the expression of migration-related molecules. Further investigate the roles of Piezo1 on GBM cell response to substrate rigidity by gene knockdown and overexpression. Next I want to explore the downstream signals involved in Piezo1 mechanical behavior in GBM cell and try to find out the pathway of upregulating Piezo1 in stiff substrate.

Materials and Methods

Cell Lines

Human GBM cell lines U87, U251 and T98G (all from ATCC) and U87 stably transfected with LV_Pgk1p-GFP were cultured at 37 °C, 5% CO2 in DMEM medium supplemented with 10% FBS and penicillin/streptomycin. Cell cultures were routinely subcultured every two days by trypsinization using standard procedures.

Stiff substrates were generated by coating tissue culture dishes with 50 μg/ml bovine collagen type I (Sigma) in PBS. After incubatingfor 1 h at 37°C, the remaining solution was aspirated, and the dish was rinsed with PBS before seeding cells. Soft substrates were generated by polymerizing a bovine collagen type I gel (2.5 mg/ml; Sigma) on tissue culture dishes. A collagen gel solution was made by mixing 8 parts of collagen solution with 1 part of 10× PBS and adjusting the pH to approximately 7 with NaOH (0.1 N).Afterincubatedat 37°C until completion of the gelation, cells were then seededdirectly on top of the gels.

Immunofluorescent Staining

Cells were fixed with 4% PFA for 20min and permeabilized with 0.1% TritonX-100 for 20min. Cells were then incubated with primary antibody and second antibody. The following primary antibodies were used: anti-Paxillin (1:200, Abcam). Phalloidin (1:2000, Invitrogen) was used to detect F-actin.

Cell Proliferation Assay

5×10^3 cells were plated in 96-well plates coated with soft and stiff collagenI, respectively. Cell growth was measured by colorimetric CCK-8 assay (Sigma-Aldrich Co, St Louis, MO, USA) after culture of 12h, 36h and 60h.

Live Cell Imaging

For live cell imaging assay, cells were maintained in a 37°C, 5% CO2 in chambers in culture medium on an inverted microscope (Nikon, UK) with a motorized stage (Prior Scientific, UK) controlled by NIS-Elements software (Nikon, UK). Stable U87-GFP cells were used to detect the velocity changes on different rigidity of substrates. Time-lapse image series were acquired at 1min intervals using a 20×1.4 NA objective lens (Nikon).

Tracking Assays and Data Analysis

Tracking of cell migration was performed over a period of 2 hours. Individual cells were tracked by repeated selection of cells in movie frames and manual tracing of migration pathways with imageJ software.

Western Blot

Cells were plated at a density of 2×10^6 cells/well in 6cm and grown to 70-80% confluence. After cultured on soft and stiff substrates for 24h, cells were washed with cold PBS and lysed in lysis buffer supplemented with a protease inhibitor cocktail (Sigma-Aldrich Co). Equal amounts of total protein were boiled for 5min in 5×sample buffer and fractionated by 12% SDS-PAGE. Samples were then transferred to PVDF membranes (Millipore). Immunoblots were detected using ECL System (Millipore) with horseradish peroxidase-conjugated secondary antibodies (Sigma). The following first antibodies were used: anti-Rac-GTP, anti-Rho-GTP, anti-Paxillin (Cell Signaling Technology), anti-p-FAK, anti-β-Tubulin (Cell Signaling Technology), anti-GAPDH (Cell Signaling Technology).

Ca^{2+} imaging

1×10^5 cells were plated in 35mm chamber (a glass-bottom Petri dish). Cells were incubated with fluo-4 AM (final concentration 4 mM) and Fura Red AM (final concentration 5 mM) at 37°C for 30min in Ringer solution with 0.2% pluronic F-127. Removed the dye's solution and washed 3 times with Ringer solution and incubated at 37°C for another 30 min. Time-lapse image series were acquired at 2s intervals using a 20×1.4 NA objective lens (Leica).

Statistical Analysis

Difference between groups was assessed bystudent's t-test, one-way ANOVA or two-way ANOVA test. Graphpad Prism was used for all statistical analyses. The difference of CCK-8 was evaluated by one-way ANOVA followed by the Kruskal-Wallis test. The differencesincell area and circle rate were evaluated by student's t-test. The difference in cell mobility was evaluated by two-way ANOVA. The results are presented as the mean ± SEM of at least three independent experiments.

Chapter 4. Conclusion and Future Perspectives

The work presented in my Ph. D. thesis demonstrates that the Rho GTPases and the mechanical properties of tumor cellsare linked.

The Rho GTPase family member Rac1 ismostly expressed in gliomas, and its levelcorrelates with patient survival outcome. In section 2.1, I proved that Rac1 plays essential roles in GBM cell migration. Using siRNA to knockdown the mRNA level of Rac1 or using EHT 1846 to inhibit the activation of Rac1 dramatically reduced GBM cell motility.Cells use protrusions for their movement, and the activation of Rac1 essentially participates in lamellipodia formation during mesenchymal migration. Lack of Rac1 changed GBM cells from a well-spread cell body with lamellipodia like protrusion into a thin cell body with long protrusion.

Furthermore, actin stress fibers were dismissed, and paxillin positive-adhesions changed into small pots in the long protrusion of the Rac1 depleting cell. In the lamella and lamellipodia, actomyosin can provide contractileforce and promote cell adhesiondisassembly. I found an abnormal myosinIIa location and cell adhesion dynamics accompany reduced phosphorylation of Erk1/2 when inhibiting the activation of Rac1, which indicates that Rac1 also directly or indirectly regulates the downstream step of cell migration. Additionally, GBM cell changes their rigidity and viscosity in response to Rac1 inhibition, suggesting that cell mechanical properties can be used for further cancer research, such as drug discovery and novel biomarker.

References

1. Louis, D.N., et al., *The 2016 World Health Organization Classification of Tumors of the Central Nervous System: a summary.* Acta Neuropathol, 2016. **131**(6): p. 803-20.
2. *Global, regional, and national burden of brain and other CNS cancer, 1990-2016: a systematic analysis for the Global Burden of Disease Study 2016.* Lancet Neurol, 2019. **18**(4): p. 376-393.
3. Braganza, M.Z., et al., *Ionizing radiation and the risk of brain and central nervous system tumors: a systematic review.* Neuro Oncol, 2012. **14**(11): p. 1316-24.
4. Coble, J.B., et al., *Occupational exposure to magnetic fields and the risk of brain tumors.* Neuro Oncol, 2009. **11**(3): p. 242-9.
5. Kheifets, L., et al., *A pooled analysis of extremely low-frequency magnetic fields and childhood brain tumors.* Am J Epidemiol, 2010. **172**(7): p. 752-61.
6. Wang, P., et al., *Wireless Phone Use and Risk of Adult Glioma: Evidence from a Meta-Analysis.* World Neurosurg, 2018. **115**: p. e629-e636.
7. Yang, M., et al., *Mobile phone use and glioma risk: A systematic review and meta-analysis.* PLoS One, 2017. **12**(5): p. e0175136.
8. Baan, R., et al., *Carcinogenicity of radiofrequency electromagnetic fields.* Lancet Oncol, 2011. **12**(7): p. 624-6.
9. Farrell, C.J. and S.R. Plotkin, *Genetic causes of brain tumors: neurofibromatosis, tuberous sclerosis, von Hippel-Lindau, and other syndromes.* Neurol Clin, 2007. **25**(4): p. 925-46, viii.
10. Ostrom, Q.T., et al., *Epidemiology of Intracranial Gliomas.* Prog Neurol Surg, 2018. **30**: p. 1-11.
11. Amirian, E.S., et al., *Approaching a Scientific Consensus on the Association between Allergies and Glioma Risk: A Report from the Glioma International Case-Control Study.* Cancer Epidemiol Biomarkers Prev, 2016. **25**(2): p. 282-90.
12. Schwartzbaum, J., et al., *Association between prediagnostic IgE levels and risk of glioma.* J Natl Cancer Inst, 2012. **104**(16): p. 1251-9.
13. Giulioni, M., et al., *Epilepsy associated tumors: Review article.* World J Clin Cases, 2014. **2**(11): p. 623-41.
14. Forsyth, P.A. and J.B. Posner, *Headaches in patients with brain tumors: a study of 111 patients.* Neurology, 1993. **43**(9): p. 1678-83.
15. Kirby, S. and R.A. Purdy, *Headaches and brain tumors.* Neurol Clin, 2014. **32**(2): p. 423-32.
16. Brindle, K.M., et al., *Brain Tumor Imaging.* J Clin Oncol, 2017. **35**(21): p. 2432-2438.
17. Bangiyev, L., et al., *Adult brain tumor imaging: state of the art.* Semin Roentgenol, 2014. **49**(1): p. 39-52.
18. Nabors, L.B., et al., *Central nervous system cancers.* J Natl Compr Canc Netw, 2013. **11**(9): p. 1114-51.
19. Ostrom, Q.T., et al., *CBTRUS Statistical Report: Primary Brain and Other Central Nervous System Tumors Diagnosed in the United States in 2012-2016.* Neuro Oncol, 2019. **21**(Suppl 5): p. v1-v100.
20. Sandmann, T., et al., *Patients With Proneural Glioblastoma May Derive Overall Survival Benefit From the Addition of Bevacizumab to First-Line Radiotherapy and Temozolomide: Retrospective Analysis of the AVAglio Trial.* J Clin Oncol, 2015. **33**(25): p. 2735-44.
21. Aldape, K., et al., *Glioblastoma: pathology, molecular mechanisms and markers.* Acta Neuropathol, 2015. **129**(6): p. 829-48.
22. Yan, H., et al., *IDH1 and IDH2 mutations in gliomas.* N Engl J Med, 2009. **360**(8): p. 765-73.
23. Molinaro, A.M., et al., *Genetic and molecular epidemiology of adult diffuse glioma.* Nat Rev Neurol, 2019. **15**(7): p. 405-417.
24. Reifenberger, G., et al., *Advances in the molecular genetics of gliomas - implications for classification and therapy.* Nat Rev Clin Oncol, 2017. **14**(7): p. 434-452.
25. Lassman, A.B., et al., *Safety and efficacy of depatuxizumab mafodotin + temozolomide in patients with EGFR-amplified, recurrent glioblastoma: results from an international phase I multicenter trial.* Neuro Oncol, 2019. **21**(1): p. 106-114.
26. Cloughesy, T., et al., *Randomized, Double-Blind, Placebo-Controlled, Multicenter Phase II Study of Onartuzumab Plus*

Bevacizumab Versus Placebo Plus Bevacizumab in Patients With Recurrent Glioblastoma: Efficacy, Safety, and Hepatocyte Growth Factor and O(6)-Methylguanine-DNA Methyltransferase Biomarker Analyses. J Clin Oncol, 2017. **35**(3): p. 343-351.

27. Cloughesy, T.F., et al., *Phase II study of cabozantinib in patients with progressive glioblastoma: subset analysis of patients with prior antiangiogenic therapy.* Neuro Oncol, 2018. **20**(2): p. 259-267.
28. Ellingson, B.M., et al., *Volumetric response quantified using T1 subtraction predicts long-term survival benefit from cabozantinib monotherapy in recurrent glioblastoma.* Neuro Oncol, 2018. **20**(10): p. 1411-1418.
29. Tabernero, J., et al., *Phase I Dose-Escalation Study of JNJ-42756493, an Oral Pan-Fibroblast Growth Factor Receptor Inhibitor, in Patients With Advanced Solid Tumors.* J Clin Oncol, 2015. **33**(30): p. 3401-8.
30. Speranza, M.C., et al., *BKM-120 (Buparlisib): A Phosphatidyl-Inositol-3 Kinase Inhibitor with Anti-Invasive Properties in Glioblastoma.* Sci Rep, 2016. **6**: p. 20189.
31. Taylor, J.W., et al., *Phase-2 trial of palbociclib in adult patients with recurrent RB1-positive glioblastoma.* J Neurooncol, 2018. **140**(2): p. 477-483.
32. Lohmann, B., et al., *Interferon-beta sensitizes human glioblastoma cells to the cyclin-dependent kinase inhibitor, TG02.* Oncol Lett, 2020. **19**(4): p. 2649-2656.
33. Agrawal, R., et al., *p53 and miR-210 regulated NeuroD2, a neuronal basic helix-loop-helix transcription factor, is downregulated in glioblastoma patients and functions as a tumor suppressor under hypoxic microenvironment.* Int J Cancer, 2018. **142**(9): p. 1817-1828.
34. England, B., T. Huang, and M. Karsy, *Current understanding of the role and targeting of tumor suppressor p53 in glioblastoma multiforme.* Tumour Biol, 2013. **34**(4): p. 2063-74.
35. Kolb, E.A., et al., *Initial testing (stage 1) of eribulin, a novel tubulin binding agent, by the pediatric preclinical testing program.* Pediatr Blood Cancer, 2013. **60**(8): p. 1325-32.
36. Roth, P., et al., *Proteasome inhibition for the treatment of glioblastoma.* Expert Opin Investig Drugs, 2020: p. 1-9.
37. Garcia-Romero, N., et al., *Bevacizumab dose adjustment to improve clinical outcomes of glioblastoma.* BMC Med, 2020. **18**(1): p. 142.
38. Tipping, M., J. Eickhoff, and H. Ian Robins, *Clinical outcomes in recurrent glioblastoma with bevacizumab therapy: An analysis of the literature.* J Clin Neurosci, 2017. **44**: p. 101-106.
39. Scaringi, C., et al., *Integrin inhibitor cilengitide for the treatment of glioblastoma: a brief overview of current clinical results.* Anticancer Res, 2012. **32**(10): p. 4213-23.
40. Brandes, A.A., et al., *A Phase II randomized study of galunisertib monotherapy or galunisertib plus lomustine compared with lomustine monotherapy in patients with recurrent glioblastoma.* Neuro Oncol, 2016. **18**(8): p. 1146-56.
41. Herbertz, S., et al., *Clinical development of galunisertib (LY2157299 monohydrate), a small molecule inhibitor of transforming growth factor-beta signaling pathway.* Drug Des Devel Ther, 2015. **9**: p. 4479-99.
42. Wick, W., U. Naumann, and M. Weller, *Transforming growth factor-beta: a molecular target for the future therapy of glioblastoma.* Curr Pharm Des, 2006. **12**(3): p. 341-9.
43. Glavatskyi, O.Y., et al., *Temozolomide in glioblastoma treatment: 15-year clinical experience and analysis of its efficacy.* Exp Oncol, 2020. **42**(2): p. 148-156.
44. Lee, E.Q., et al., *Phase II study of panobinostat in combination with bevacizumab for recurrent glioblastoma and anaplastic glioma.* Neuro Oncol, 2015. **17**(6): p. 862-7.
45. Alvarez, A.A., et al., *The effects of histone deacetylase inhibitors on glioblastoma-derived stem cells.* J Mol Neurosci, 2015. **55**(1): p. 7-20.
46. Kim, Y.H., et al., *Survival benefit of levetiracetam in patients treated with concomitant chemoradiotherapy and adjuvant chemotherapy with temozolomide for glioblastoma multiforme.* Cancer, 2015. **121**(17): p. 2926-32.
47. Harder, B.G., et al., *Developments in Blood-Brain Barrier Penetrance and Drug Repurposing for Improved Treatment of*

Glioblastoma. Front Oncol, 2018. **8**: p. 462.
48. Elmaci, I. and M.A. Altinoz, *Targeting the cellular schizophrenia. Likely employment of the antipsychotic agent pimozide in treatment of refractory cancers and glioblastoma.* Crit Rev Oncol Hematol, 2018. **128**: p. 96-109.
49. Weyerhauser, P., S.R. Kantelhardt, and E.L. Kim, *Re-purposing Chloroquine for Glioblastoma: Potential Merits and Confounding Variables.* Front Oncol, 2018. **8**: p. 335.
50. Barbieri, F., et al., *Repurposed Biguanide Drugs in Glioblastoma Exert Antiproliferative Effects via the Inhibition of Intracellular Chloride Channel 1 Activity.* Front Oncol, 2019. **9**: p. 135.
51. Chin, C., et al., *Immunotherapy and Epigenetic Pathway Modulation in Glioblastoma Multiforme.* Front Oncol, 2018. **8**: p. 521.
52. Ridley, A.J., *Life at the leading edge.* Cell, 2011. **145**(7): p. 1012-22.
53. Rossman, K.L., C.J. Der, and J. Sondek, *GEF means go: turning on RHO GTPases with guanine nucleotide-exchange factors.* Nat Rev Mol Cell Biol, 2005. **6**(2): p. 167-80.
54. Van Aelst, L. and C. D'Souza-Schorey, *Rho GTPases and signaling networks.* Genes Dev, 1997. **11**(18): p. 2295-322.
55. Garcia-Mata, R. and K. Burridge, *Catching a GEF by its tail.* Trends Cell Biol, 2007. **17**(1): p. 36-43.
56. Bernards, A. and J. Settleman, *GAP control: regulating the regulators of small GTPases.* Trends Cell Biol, 2004. **14**(7): p. 377-85.
57. Roberts, P.J., et al., *Rho Family GTPase modification and dependence on CAAX motif-signaled posttranslational modification.* J Biol Chem, 2008. **283**(37): p. 25150-63.
58. DerMardirossian, C. and G.M. Bokoch, *GDIs: central regulatory molecules in Rho GTPase activation.* Trends Cell Biol, 2005. **15**(7): p. 356-63.
59. Hodge, R.G. and A.J. Ridley, *Regulating Rho GTPases and their regulators.* Nature Reviews Molecular Cell Biology, 2016. **17**(8): p. 496-510.
60. Kazanietz, M.G. and M.J. Caloca, *The Rac GTPase in Cancer: From Old Concepts to New Paradigms.* Cancer Res, 2017. **77**(20): p. 5445-5451.
61. Jaffe, A.B. and A. Hall, *Rho GTPases: biochemistry and biology.* Annu Rev Cell Dev Biol, 2005. **21**: p. 247-69.
62. Evers, E.E., et al., *Rho family proteins in cell adhesion and cell migration.* Eur J Cancer, 2000. **36**(10): p. 1269-74.
63. Chimini, G. and P. Chavrier, *Function of Rho family proteins in actin dynamics during phagocytosis and engulfment.* Nat Cell Biol, 2000. **2**(10): p. E191-6.
64. Etienne-Manneville, S. and A. Hall, *Rho GTPases in cell biology.* Nature, 2002. **420**(6916): p. 629-35.
65. Raftopoulou, M. and A. Hall, *Cell migration: Rho GTPases lead the way.* Dev Biol, 2004. **265**(1): p. 23-32.
66. Svensmark, J.H. and C. Brakebusch, *Rho GTPases in cancer: friend or foe?* Oncogene, 2019. **38**(50): p. 7447-7456.
67. Martinez-Quiles, N., et al., *WIP regulates N-WASP-mediated actin polymerization and filopodium formation.* Nat Cell Biol, 2001. **3**(5): p. 484-91.
68. Ho, H.Y., et al., *CR16 forms a complex with N-WASP in brain and is a novel member of a conserved proline-rich actin-binding protein family.* Proc Natl Acad Sci U S A, 2001. **98**(20): p. 11306-11.
69. Eden, S., et al., *Mechanism of regulation of WAVE1-induced actin nucleation by Rac1 and Nck.* Nature, 2002. **418**(6899): p. 790-3.
70. Zigmond, S.H., *Formin-induced nucleation of actin filaments.* Curr Opin Cell Biol, 2004. **16**(1): p. 99-105.
71. Ghosh, M., et al., *Cofilin promotes actin polymerization and defines the direction of cell motility.* Science, 2004. **304**(5671): p. 743-6.
72. Dawe, H.R., et al., *ADF/cofilin controls cell polarity during fibroblast migration.* Curr Biol, 2003. **13**(3): p. 252-7.
73. Svitkina, T.M. and G.G. Borisy, *Arp2/3 complex and actin depolymerizing factor/cofilin in dendritic organization and treadmilling of actin filament array in lamellipodia.* J Cell Biol, 1999. **145**(5): p. 1009-26.
74. Ohashi, K., et al., *Rho-associated kinase ROCK activates LIM-kinase 1 by phosphorylation at threonine 508 within the activation loop.* J Biol Chem, 2000. **275**(5): p. 3577-82.

75. Riento, K. and A.J. Ridley, *Rocks: multifunctional kinases in cell behaviour.* Nat Rev Mol Cell Biol, 2003. **4**(6): p. 446-56.
76. Devreotes, P. and A.R. Horwitz, *Signaling networks that regulate cell migration.* Cold Spring Harb Perspect Biol, 2015. **7**(8): p. a005959.
77. Cassimeris, L., *The oncoprotein 18/stathmin family of microtubule destabilizers.* Curr Opin Cell Biol, 2002. **14**(1): p. 18-24.
78. Daub, H., et al., *Rac/Cdc42 and p65PAK regulate the microtubule-destabilizing protein stathmin through phosphorylation at serine 16.* J Biol Chem, 2001. **276**(3): p. 1677-80.
79. Arimura, N., et al., *Phosphorylation of collapsin response mediator protein-2 by Rho-kinase. Evidence for two separate signaling pathways for growth cone collapse.* J Biol Chem, 2000. **275**(31): p. 23973-80.
80. Palazzo, A.F., et al., *mDia mediates Rho-regulated formation and orientation of stable microtubules.* Nat Cell Biol, 2001. **3**(8): p. 723-9.
81. Fukata, M., et al., *Rac1 and Cdc42 capture microtubules through IQGAP1 and CLIP-170.* Cell, 2002. **109**(7): p. 873-85.
82. Wen, Y., et al., *EB1 and APC bind to mDia to stabilize microtubules downstream of Rho and promote cell migration.* Nat Cell Biol, 2004. **6**(9): p. 820-30.
83. Watanabe, T., et al., *Interaction with IQGAP1 links APC to Rac1, Cdc42, and actin filaments during cell polarization and migration.* Dev Cell, 2004. **7**(6): p. 871-83.
84. Miralles, F., et al., *Actin dynamics control SRF activity by regulation of its coactivator MAL.* Cell, 2003. **113**(3): p. 329-42.
85. Coso, O.A., et al., *The small GTP-binding proteins Rac1 and Cdc42 regulate the activity of the JNK/SAPK signaling pathway.* Cell, 1995. **81**(7): p. 1137-46.
86. Gallagher, E.D., et al., *RhoA binds to the amino terminus of MEKK1 and regulates its kinase activity.* J Biol Chem, 2004. **279**(3): p. 1872-7.
87. Jaffe, A.B., A. Hall, and A. Schmidt, *Association of CNK1 with Rho guanine nucleotide exchange factors controls signaling specificity downstream of Rho.* Curr Biol, 2005. **15**(5): p. 405-12.
88. Perona, R., et al., *Activation of the nuclear factor-kappaB by Rho, CDC42, and Rac-1 proteins.* Genes Dev, 1997. **11**(4): p. 463-75.
89. Joyce, D., et al., *Integration of Rac-dependent regulation of cyclin D1 transcription through a nuclear factor-kappaB-dependent pathway.* J Biol Chem, 1999. **274**(36): p. 25245-9.
90. Welsh, C.F., et al., *Timing of cyclin D1 expression within G1 phase is controlled by Rho.* Nature Cell Biology, 2001. **3**(11): p. 950-957.
91. Roovers, K. and R.K. Assoian, *Effects of rho kinase and actin stress fibers on sustained extracellular signal-regulated kinase activity and activation of G1 phase cyclin-dependent kinases.* Mol Cell Biol, 2006. **26**(13): p. 5203.
92. Roovers, K., et al., *Nuclear translocation of LIM kinase mediates Rho-Rho kinase regulation of cyclin D1 expression.* Dev Cell, 2003. **5**(2): p. 273-84.
93. Chou, M.M., J.M. Masuda-Robens, and M.L. Gupta, *Cdc42 promotes G1 progression through p70 S6 kinase-mediated induction of cyclin E expression.* J Biol Chem, 2003. **278**(37): p. 35241-7.
94. Olson, M.F., H.F. Paterson, and C.J. Marshall, *Signals from Ras and Rho GTPases interact to regulate expression of p21Waf1/Cip1.* Nature, 1998. **394**(6690): p. 295-9.
95. Hu, W., C.J. Bellone, and J.J. Baldassare, *RhoA stimulates p27(Kip) degradation through its regulation of cyclin E/CDK2 activity.* J Biol Chem, 1999. **274**(6): p. 3396-401.
96. Sherr, C.J. and J.M. Roberts, *CDK inhibitors: positive and negative regulators of G1-phase progression.* Genes Dev, 1999. **13**(12): p. 1501-12.
97. Pines, J., *The cell cycle kinases.* Semin Cancer Biol, 1994. **5**(4): p. 305-13.
98. Rosenblatt, J., et al., *Myosin II-dependent cortical movement is required for centrosome separation and positioning during mitotic spindle assembly.* Cell, 2004. **117**(3): p. 361-72.

99. Gotta, M., M.C. Abraham, and J. Ahringer, *CDC-42 controls early cell polarity and spindle orientation in C. elegans.* Curr Biol, 2001. **11**(7): p. 482-8.
100. Yasuda, S., et al., *Cdc42 and mDia3 regulate microtubule attachment to kinetochores.* Nature, 2004. **428**(6984): p. 767-71.
101. Glotzer, M., *Animal cell cytokinesis.* Annu Rev Cell Dev Biol, 2001. **17**: p. 351-86.
102. Komatsu, S., et al., *Effects of the regulatory light chain phosphorylation of myosin II on mitosis and cytokinesis of mammalian cells.* J Biol Chem, 2000. **275**(44): p. 34512-20.
103. Yamashiro, S., et al., *Citron kinase, a Rho-dependent kinase, induces di-phosphorylation of regulatory light chain of myosin II.* Mol Biol Cell, 2003. **14**(5): p. 1745-56.
104. Gibson, M.C. and N. Perrimon, *Apicobasal polarization: epithelial form and function.* Curr Opin Cell Biol, 2003. **15**(6): p. 747-52.
105. Plant, P.J., et al., *A polarity complex of mPar-6 and atypical PKC binds, phosphorylates and regulates mammalian Lgl.* Nat Cell Biol, 2003. **5**(4): p. 301-8.
106. Nobes, C.D. and A. Hall, *Rho, rac, and cdc42 GTPases regulate the assembly of multimolecular focal complexes associated with actin stress fibers, lamellipodia, and filopodia.* Cell, 1995. **81**(1): p. 53-62.
107. Ridley, A.J., et al., *Cell migration: integrating signals from front to back.* Science, 2003. **302**(5651): p. 1704-9.
108. Pollard, T.D. and G.G. Borisy, *Cellular motility driven by assembly and disassembly of actin filaments.* Cell, 2003. **112**(4): p. 453-65.
109. Henson, J.H., et al., *Two components of actin-based retrograde flow in sea urchin coelomocytes.* Mol Biol Cell, 1999. **10**(12): p. 4075-90.
110. Palecek, S.P., et al., *Integrin-ligand binding properties govern cell migration speed through cell-substratum adhesiveness.* Nature, 1997. **385**(6616): p. 537-540.
111. Case, L.B. and C.M. Waterman, *Integration of actin dynamics and cell adhesion by a three-dimensional, mechanosensitive molecular clutch.* Nat Cell Biol, 2015. **17**(8): p. 955-63.
112. Riveline, D., et al., *Focal contacts as mechanosensors: externally applied local mechanical force induces growth of focal contacts by an mDia1-dependent and ROCK-independent mechanism.* J Cell Biol, 2001. **153**(6): p. 1175-86.
113. Hu, K., et al., *Differential transmission of actin motion within focal adhesions.* Science, 2007. **315**(5808): p. 111-5.
114. Parsons, J.T., A.R. Horwitz, and M.A. Schwartz, *Cell adhesion: integrating cytoskeletal dynamics and cellular tension.* Nature Reviews Molecular Cell Biology, 2010. **11**(9): p. 633-643.
115. Webb, D.J., et al., *FAK-Src signalling through paxillin, ERK and MLCK regulates adhesion disassembly.* Nat Cell Biol, 2004. **6**(2): p. 154-61.
116. Turner, C.E., K.A. West, and M.C. Brown, *Paxillin-ARF GAP signaling and the cytoskeleton.* Curr Opin Cell Biol, 2001. **13**(5): p. 593-9.
117. Hoefen, R.J. and B.C. Berk, *The multifunctional GIT family of proteins.* J Cell Sci, 2006. **119**(Pt 8): p. 1469-75.
118. Deakin, N.O. and C.E. Turner, *Distinct roles for paxillin and Hic-5 in regulating breast cancer cell morphology, invasion, and metastasis.* Mol Biol Cell, 2011. **22**(3): p. 327-41.
119. Tomar, A. and D.D. Schlaepfer, *Focal adhesion kinase: switching between GAPs and GEFs in the regulation of cell motility.* Curr Opin Cell Biol, 2009. **21**(5): p. 676-83.
120. Shutes, A., et al., *Atypical mechanism of regulation of the Wrch-1 Rho family small GTPase.* Curr Biol, 2004. **14**(22): p. 2052-6.
121. Alan, J.K., et al., *Regulation of the Rho family small GTPase Wrch-1/RhoU by C-terminal tyrosine phosphorylation requires Src.* Mol Cell Biol, 2010. **30**(17): p. 4324-38.
122. Dart, A.E., et al., *PAK4 promotes kinase-independent stabilization of RhoU to modulate cell adhesion.* J Cell Biol, 2015. **211**(4): p. 863-79.
123. Saras, J., P. Wollberg, and P. Aspenstrom, *Wrch1 is a GTPase-deficient Cdc42-like protein with unusual binding characteristics and cellular effects.* Exp Cell Res, 2004. **299**(2): p. 356-69.

124. Troeger, A. and D.A. Williams, *Hematopoietic-specific Rho GTPases Rac2 and RhoH and human blood disorders.* Exp Cell Res, 2013. **319**(15): p. 2375-83.
125. Dorn, T., et al., *RhoH is important for positive thymocyte selection and T-cell receptor signaling.* Blood, 2007. **109**(6): p. 2346-55.
126. Gu, Y., et al., *RhoH, a hematopoietic-specific Rho GTPase, regulates proliferation, survival, migration, and engraftment of hematopoietic progenitor cells.* Blood, 2005. **105**(4): p. 1467-75.
127. Chae, H.D., et al., *Cross-talk between RhoH and Rac1 in regulation of actin cytoskeleton and chemotaxis of hematopoietic progenitor cells.* Blood, 2008. **111**(5): p. 2597-605.
128. Sanchez-Aguilera, A., et al., *Involvement of RhoH GTPase in the development of B-cell chronic lymphocytic leukemia.* Leukemia, 2010. **24**(1): p. 97-104.
129. Riou, P., P. Villalonga, and A.J. Ridley, *Rnd proteins: multifunctional regulators of the cytoskeleton and cell cycle progression.* Bioessays, 2010. **32**(11): p. 986-92.
130. Oinuma, I., et al., *Rnd1 and Rnd3 targeting to lipid raft is required for p190 RhoGAP activation.* Mol Biol Cell, 2012. **23**(8): p. 1593-604.
131. Wennerberg, K., et al., *Rnd proteins function as RhoA antagonists by activating p190 RhoGAP.* Curr Biol, 2003. **13**(13): p. 1106-15.
132. Madigan, J.P., et al., *Regulation of Rnd3 localization and function by protein kinase C alpha-mediated phosphorylation.* Biochem J, 2009. **424**(1): p. 153-61.
133. Boureux, A., et al., *Evolution of the Rho family of ras-like GTPases in eukaryotes.* Mol Biol Evol, 2007. **24**(1): p. 203-16.
134. Rivero, F., et al., *The Dictyostelium discoideum family of Rho-related proteins.* Nucleic Acids Res, 2001. **29**(5): p. 1068-79.
135. Chang, F.K., et al., *DBC2 is essential for transporting vesicular stomatitis virus glycoprotein.* J Mol Biol, 2006. **364**(3): p. 302-8.
136. Sahai, E. and C.J. Marshall, *RHO-GTPases and cancer.* Nat Rev Cancer, 2002. **2**(2): p. 133-42.
137. Reuther, G.W., et al., *Leukemia-associated Rho guanine nucleotide exchange factor, a Dbl family protein found mutated in leukemia, causes transformation by activation of RhoA.* J Biol Chem, 2001. **276**(29): p. 27145-51.
138. Ingram, D.A., et al., *Hyperactivation of p21(ras) and the hematopoietic-specific Rho GTPase, Rac2, cooperate to alter the proliferation of neurofibromin-deficient mast cells in vivo and in vitro.* J Exp Med, 2001. **194**(1): p. 57-69.
139. Ridley, A.J., et al., *The small GTP-binding protein rac regulates growth factor-induced membrane ruffling.* Cell, 1992. **70**(3): p. 401-10.
140. Kim, S.K., *Cell polarity: new PARtners for Cdc42 and Rac.* Nat Cell Biol, 2000. **2**(8): p. E143-5.
141. Engers, R., et al., *Rac affects invasion of human renal cell carcinomas by up-regulating tissue inhibitor of metalloproteinases (TIMP)-1 and TIMP-2 expression.* J Biol Chem, 2001. **276**(45): p. 41889-97.
142. Zhuge, Y. and J. Xu, *Rac1 mediates type I collagen-dependent MMP-2 activation. role in cell invasion across collagen barrier.* J Biol Chem, 2001. **276**(19): p. 16248-56.
143. Matsumoto, Y., et al., *Small GTP-binding protein, Rho, both increased and decreased cellular motility, activation of matrix metalloproteinase 2 and invasion of human osteosarcoma cells.* Jpn J Cancer Res, 2001. **92**(4): p. 429-38.
144. Coste, B., et al., *Piezo1 and Piezo2 are essential components of distinct mechanically activated cation channels.* Science, 2010. **330**(6000): p. 55-60.
145. Ge, J., et al., *Architecture of the mammalian mechanosensitive Piezo1 channel.* Nature, 2015. **527**(7576): p. 64-9.
146. Saotome, K., et al., *Structure of the mechanically activated ion channel Piezo1.* Nature, 2018. **554**(7693): p. 481-486.
147. Zhao, Q., et al., *Structure and mechanogating mechanism of the Piezo1 channel.* Nature, 2018. **554**(7693): p. 487-492.
148. Albuisson, J., et al., *Dehydrated hereditary stomatocytosis linked to gain-of-function mutations in mechanically activated PIEZO1 ion channels.* Nat Commun, 2013. **4**: p. 1884.
149. Lukacs, V., et al., *Impaired PIEZO1 function in patients with a novel autosomal recessive congenital lymphatic dysplasia.* Nat Commun, 2015. **6**: p. 8329.

150. Coste, B., et al., *Gain-of-function mutations in the mechanically activated ion channel PIEZO2 cause a subtype of Distal Arthrogryposis.* Proc Natl Acad Sci U S A, 2013. **110**(12): p. 4667-72.
151. Quade, A., et al., *Microangiopathy and mild mixed neuromyopathic alterations in a patient with homozygous PIEZO-2 mutation.* Neuromuscul Disord, 2018. **28**(12): p. 1006-1011.
152. Gudipaty, S.A., et al., *Mechanical stretch triggers rapid epithelial cell division through Piezo1.* Nature, 2017. **543**(7643): p. 118-121.
153. Eisenhoffer, G.T., et al., *Crowding induces live cell extrusion to maintain homeostatic cell numbers in epithelia.* Nature, 2012. **484**(7395): p. 546-9.
154. Li, J., et al., *Piezo1 integration of vascular architecture with physiological force.* Nature, 2014. **515**(7526): p. 279-282.
155. Hung, W.C., et al., *Confinement Sensing and Signal Optimization via Piezo1/PKA and Myosin II Pathways.* Cell Rep, 2016. **15**(7): p. 1430-1441.
156. Albarran-Juarez, J., et al., *Piezo1 and Gq/G11 promote endothelial inflammation depending on flow pattern and integrin activation.* J Exp Med, 2018. **215**(10): p. 2655-2672.
157. Sugisawa, E., et al., *RNA Sensing by Gut Piezo1 Is Essential for Systemic Serotonin Synthesis.* Cell, 2020. **182**(3): p. 609-624 e21.
158. Koser, D.E., et al., *Mechanosensing is critical for axon growth in the developing brain.* Nat Neurosci, 2016. **19**(12): p. 1592-1598.
159. Velasco-Estevez, M., et al., *Inhibition of Piezo1 attenuates demyelination in the central nervous system.* Glia, 2020. **68**(2): p. 356-375.
160. Solis, A.G., et al., *Mechanosensation of cyclical force by PIEZO1 is essential for innate immunity.* Nature, 2019. **573**(7772): p. 69-74.
161. Chen, X., et al., *A Feedforward Mechanism Mediated by Mechanosensitive Ion Channel PIEZO1 and Tissue Mechanics Promotes Glioma Aggression.* Neuron, 2018. **100**(4): p. 799-815 e7.
162. Qu, S., et al., *Effect of Piezo1 Overexpression on Peritumoral Brain Edema in Glioblastomas.* AJNR Am J Neuroradiol, 2020. **41**(8): p. 1423-1429.
163. Qu, S., S. Li, and Z. Hu, *Upregulation of Piezo1 Is a Novel Prognostic Indicator in Glioma Patients.* Cancer Manag Res, 2020. **12**: p. 3527-3536.
164. Schaefer, L. and R.M. Schaefer, *Proteoglycans: from structural compounds to signaling molecules.* Cell Tissue Res, 2010. **339**(1): p. 237-46.
165. Jarvelainen, H., et al., *Extracellular matrix molecules: potential targets in pharmacotherapy.* Pharmacol Rev, 2009. **61**(2): p. 198-223.
166. Rozario, T. and D.W. DeSimone, *The extracellular matrix in development and morphogenesis: a dynamic view.* Dev Biol, 2010. **341**(1): p. 126-40.
167. Smith, M.L., et al., *Force-induced unfolding of fibronectin in the extracellular matrix of living cells.* PLoS Biol, 2007. **5**(10): p. e268.
168. Friedland, J.C., M.H. Lee, and D. Boettiger, *Mechanically activated integrin switch controls alpha5beta1 function.* Science, 2009. **323**(5914): p. 642-4.
169. Mott, J.D. and Z. Werb, *Regulation of matrix biology by matrix metalloproteinases.* Curr Opin Cell Biol, 2004. **16**(5): p. 558-64.
170. Cruz-Munoz, W. and R. Khokha, *The role of tissue inhibitors of metalloproteinases in tumorigenesis and metastasis.* Crit Rev Clin Lab Sci, 2008. **45**(3): p. 291-338.
171. Lucero, H.A. and H.M. Kagan, *Lysyl oxidase: an oxidative enzyme and effector of cell function.* Cell Mol Life Sci, 2006. **63**(19-20): p. 2304-16.
172. Butcher, D.T., T. Alliston, and V.M. Weaver, *A tense situation: forcing tumour progression.* Nat Rev Cancer, 2009. **9**(2): p. 108-22.
173. Levental, K.R., et al., *Matrix crosslinking forces tumor progression by enhancing integrin signaling.* Cell, 2009. **139**(5): p. 891-906.
174. Payne, S.L., M.J. Hendrix, and D.A. Kirschmann, *Paradoxical roles for lysyl oxidases in cancer--a prospect.* J Cell Biochem, 2007.

101(6): p. 1338-54.
175. Conklin, M.W., et al., *Aligned collagen is a prognostic signature for survival in human breast carcinoma.* Am J Pathol, 2011. **178**(3): p. 1221-32.
176. Xing, F., J. Saidou, and K. Watabe, *Cancer associated fibroblasts (CAFs) in tumor microenvironment.* Front Biosci (Landmark Ed), 2010. **15**: p. 166-79.
177. Benzina, O., et al., *Changes induced by peripheral nerve injury in the morphology and nanomechanics of sensory neurons.* J Biomed Opt, 2013. **18**(10): p. 106014.
178. Kuznetsova, T.G., et al., *Atomic force microscopy probing of cell elasticity.* Micron, 2007. **38**(8): p. 824-33.
179. Darling, E.M., et al., *Viscoelastic properties of human mesenchymally-derived stem cells and primary osteoblasts, chondrocytes, and adipocytes.* J Biomech, 2008. **41**(2): p. 454-64.
180. Azeloglu, E.U., J. Bhattacharya, and K.D. Costa, *Atomic force microscope elastography reveals phenotypic differences in alveolar cell stiffness.* J Appl Physiol (1985), 2008. **105**(2): p. 652-61.
181. Isermann, P. and J. Lammerding, *Nuclear mechanics and mechanotransduction in health and disease.* Curr Biol, 2013. **23**(24): p. R1113-21.
182. Swift, J. and D.E. Discher, *The nuclear lamina is mechano-responsive to ECM elasticity in mature tissue.* J Cell Sci, 2014. **127**(Pt 14): p. 3005-15.
183. Swaminathan, V., et al., *Mechanical stiffness grades metastatic potential in patient tumor cells and in cancer cell lines.* Cancer Res, 2011. **71**(15): p. 5075-80.
184. Cross, S.E., et al., *Nanomechanical analysis of cells from cancer patients.* Nat Nanotechnol, 2007. **2**(12): p. 780-3.
185. Kavallaris, M., *Microtubules and resistance to tubulin-binding agents.* Nat Rev Cancer, 2010. **10**(3): p. 194-204.
186. Schilsky, R.L., *Personalized medicine in oncology: the future is now.* Nat Rev Drug Discov, 2010. **9**(5): p. 363-6.
187. Bellin, R.M., et al., *Defining the role of syndecan-4 in mechanotransduction using surface-modification approaches.* Proc Natl Acad Sci U S A, 2009. **106**(52): p. 22102-7.
188. Beningo, K.A., et al., *Traction forces of fibroblasts are regulated by the Rho-dependent kinase but not by the myosin light chain kinase.* Arch Biochem Biophys, 2006. **456**(2): p. 224-31.
189. Elosegui-Artola, A., et al., *Mechanical regulation of a molecular clutch defines force transmission and transduction in response to matrix rigidity.* Nat Cell Biol, 2016. **18**(5): p. 540-8.
190. McClatchey, A.I., *ERM proteins at a glance.* J Cell Sci, 2014. **127**(Pt 15): p. 3199-204.
191. Huveneers, S. and E.H. Danen, *Adhesion signaling - crosstalk between integrins, Src and Rho.* J Cell Sci, 2009. **122**(Pt 8): p. 1059-69.
192. Sawada, Y., et al., *Force sensing by mechanical extension of the Src family kinase substrate p130Cas.* Cell, 2006. **127**(5): p. 1015-26.
193. Guilluy, C., et al., *The Rho GEFs LARG and GEF-H1 regulate the mechanical response to force on integrins.* Nat Cell Biol, 2011. **13**(6): p. 722-7.
194. Tominaga, T., et al., *Diaphanous-related formins bridge Rho GTPase and Src tyrosine kinase signaling.* Mol Cell, 2000. **5**(1): p. 13-25.
195. Gupton, S.L., et al., *mDia2 regulates actin and focal adhesion dynamics and organization in the lamella for efficient epithelial cell migration.* J Cell Sci, 2007. **120**(Pt 19): p. 3475-87.
196. Wu, X., et al., *FAK-mediated src phosphorylation of endophilin A2 inhibits endocytosis of MT1-MMP and promotes ECM degradation.* Dev Cell, 2005. **9**(2): p. 185-96.
197. Franco, S.J., et al., *Calpain-mediated proteolysis of talin regulates adhesion dynamics.* Nat Cell Biol, 2004. **6**(10): p. 977-83.
198. Ezratty, E.J., M.A. Partridge, and G.G. Gundersen, *Microtubule-induced focal adhesion disassembly is mediated by dynamin and focal adhesion kinase.* Nat Cell Biol, 2005. **7**(6): p. 581-90.

199. van Helvert, S., C. Storm, and P. Friedl, *Mechanoreciprocity in cell migration.* Nature Cell Biology, 2018. **20**(1): p. 8-20.
200. Plotnikov, S.V., et al., *Force fluctuations within focal adhesions mediate ECM-rigidity sensing to guide directed cell migration.* Cell, 2012. **151**(7): p. 1513-27.
201. Elosegui-Artola, A., et al., *Rigidity sensing and adaptation through regulation of integrin types.* Nat Mater, 2014. **13**(6): p. 631-7.
202. Medjkane, S., et al., *Myocardin-related transcription factors and SRF are required for cytoskeletal dynamics and experimental metastasis.* Nat Cell Biol, 2009. **11**(3): p. 257-68.
203. Dupont, S., et al., *Role of YAP/TAZ in mechanotransduction.* Nature, 2011. **474**(7350): p. 179-83.
204. Ho, C.Y., et al., *Lamin A/C and emerin regulate MKL1-SRF activity by modulating actin dynamics.* Nature, 2013. **497**(7450): p. 507-11.
205. Small, J.V., et al., *The lamellipodium: where motility begins.* Trends Cell Biol, 2002. **12**(3): p. 112-20.
206. Sharma, V.P., et al., *Reconstitution of in vivo macrophage-tumor cell pairing and streaming motility on one-dimensional micro-patterned substrates.* Intravital, 2012. **1**(1): p. 77-85.
207. Mim, C. and V.M. Unger, *Membrane curvature and its generation by BAR proteins.* Trends Biochem Sci, 2012. **37**(12): p. 526-33.
208. Galic, M., et al., *External push and internal pull forces recruit curvature-sensing N-BAR domain proteins to the plasma membrane.* Nat Cell Biol, 2012. **14**(8): p. 874-81.
209. Wilson, K., et al., *Mechanisms of leading edge protrusion in interstitial migration.* Nat Commun, 2013. **4**: p. 2896.
210. Charras, G.T., et al., *Reassembly of contractile actin cortex in cell blebs.* J Cell Biol, 2006. **175**(3): p. 477-90.
211. Beningo, K.A., M. Dembo, and Y.L. Wang, *Responses of fibroblasts to anchorage of dorsal extracellular matrix receptors.* Proc Natl Acad Sci U S A, 2004. **101**(52): p. 18024-9.
212. Tozluoglu, M., et al., *Matrix geometry determines optimal cancer cell migration strategy and modulates response to interventions.* Nat Cell Biol, 2013. **15**(7): p. 751-62.
213. Sanz-Moreno, V., et al., *Rac activation and inactivation control plasticity of tumor cell movement.* Cell, 2008. **135**(3): p. 510-23.
214. Bergert, M., et al., *Cell mechanics control rapid transitions between blebs and lamellipodia during migration.* Proc Natl Acad Sci U S A, 2012. **109**(36): p. 14434-9.
215. Harada, T., et al., *Nuclear lamin stiffness is a barrier to 3D migration, but softness can limit survival.* J Cell Biol, 2014. **204**(5): p. 669-82.
216. Ivkovic, S., et al., *Direct inhibition of myosin II effectively blocks glioma invasion in the presence of multiple motogens.* Mol Biol Cell, 2012. **23**(4): p. 533-42.
217. Paul, C.D., P. Mistriotis, and K. Konstantopoulos, *Cancer cell motility: lessons from migration in confined spaces.* Nat Rev Cancer, 2017. **17**(2): p. 131-140.
218. Darling, E.M. and D. Di Carlo, *High-Throughput Assessment of Cellular Mechanical Properties.* Annu Rev Biomed Eng, 2015. **17**: p. 35-62.
219. Binnig, G., C.F. Quate, and C. Gerber, *Atomic force microscope.* Phys Rev Lett, 1986. **56**(9): p. 930-933.
220. Stupp, R., et al., *Radiotherapy plus concomitant and adjuvant temozolomide for glioblastoma.* N Engl J Med, 2005. **352**(10): p. 987-96.
221. Stupp, R., et al., *Effects of radiotherapy with concomitant and adjuvant temozolomide versus radiotherapy alone on survival in glioblastoma in a randomised phase III study: 5-year analysis of the EORTC-NCIC trial.* Lancet Oncol, 2009. **10**(5): p. 459-66.
222. Chan, A.Y., et al., *Roles of the Rac1 and Rac3 GTPases in human tumor cell invasion.* Oncogene, 2005. **24**(53): p. 7821-9.
223. Parri, M. and P. Chiarugi, *Rac and Rho GTPases in cancer cell motility control.* Cell Commun Signal, 2010. **8**: p. 23.
224. Chi, X., et al., *Roles of rho GTPases in intracellular transport and cellular transformation.* Int J Mol Sci, 2013. **14**(4): p. 7089-108.
225. Blanchoin, L., et al., *Direct observation of dendritic actin filament networks nucleated by Arp2/3 complex and WASP/Scar proteins.* Nature, 2000. **404**(6781): p. 1007-11.
226. Goley, E.D. and M.D. Welch, *The ARP2/3 complex: an actin nucleator comes of age.* Nat Rev Mol Cell Biol, 2006. **7**(10): p.

713-26.
227. Takenawa, T. and H. Miki, *WASP and WAVE family proteins: key molecules for rapid rearrangement of cortical actin filaments and cell movement.* J Cell Sci, 2001. **114**(Pt 10): p. 1801-9.
228. Ridley, A.J., *Rho GTPases and actin dynamics in membrane protrusions and vesicle trafficking.* Trends Cell Biol, 2006. **16**(10): p. 522-9.
229. Malliri, A., et al., *Mice deficient in the Rac activator Tiam1 are resistant to Ras-induced skin tumours.* Nature, 2002. **417**(6891): p. 867-71.
230. Kissil, J.L., et al., *Requirement for Rac1 in a K-ras induced lung cancer in the mouse.* Cancer Res, 2007. **67**(17): p. 8089-94.
231. Gastonguay, A., et al., *The role of Rac1 in the regulation of NF-kappaB activity, cell proliferation, and cell migration in non-small cell lung carcinoma.* Cancer Biol Ther, 2012. **13**(8): p. 647-56.
232. Yang, W.H., et al., *RAC1 activation mediates Twist1-induced cancer cell migration.* Nat Cell Biol, 2012. **14**(4): p. 366-74.
233. Shutes, A., et al., *Specificity and mechanism of action of EHT 1864, a novel small molecule inhibitor of Rac family small GTPases.* J Biol Chem, 2007. **282**(49): p. 35666-78.
234. Remmerbach, T.W., et al., *Oral cancer diagnosis by mechanical phenotyping.* Cancer Res, 2009. **69**(5): p. 1728-32.
235. Liu, J., et al., *X-linked inhibitor of apoptosis protein (XIAP) mediates cancer cell motility via Rho GDP dissociation inhibitor (RhoGDI)-dependent regulation of the cytoskeleton.* J Biol Chem, 2011. **286**(18): p. 15630-40.
236. Olson, M.F. and E. Sahai, *The actin cytoskeleton in cancer cell motility.* Clin Exp Metastasis, 2009. **26**(4): p. 273-87.
237. Yamazaki, D., S. Kurisu, and T. Takenawa, *Regulation of cancer cell motility through actin reorganization.* Cancer Sci, 2005. **96**(7): p. 379-86.
238. Jordan, M.A. and L. Wilson, *Microtubules and actin filaments: dynamic targets for cancer chemotherapy.* Curr Opin Cell Biol, 1998. **10**(1): p. 123-30.
239. Dia, V.P. and P. Pangloli, *Epithelial-to-Mesenchymal Transition in Paclitaxel-Resistant Ovarian Cancer Cells Is Downregulated by Luteolin.* J Cell Physiol, 2017. **232**(2): p. 391-401.
240. Taatjes, D.J., et al., *Atomic force microscopy: High resolution dynamic imaging of cellular and molecular structure in health and disease.* J Cell Physiol, 2013. **228**(10): p. 1949-55.
241. Fletcher, D.A. and R.D. Mullins, *Cell mechanics and the cytoskeleton.* Nature, 2010. **463**(7280): p. 485-92.
242. Zhang, T., *Cytoplasmic motion induced by cytoskeleton stretching and its effect on cell mechanics.* Mol Cell Biomech, 2011. **8**(3): p. 169-93.
243. Yango, A., et al., *Measuring the viscoelastic creep of soft samples by step response AFM.* Soft Matter, 2016. **12**(40): p. 8297-8306.
244. Xiao, M., et al., *A Fully 3D Interconnected Graphene-Carbon Nanotube Web Allows the Study of Glioma Infiltration in Bioengineered 3D Cortex-Like Networks.* Adv Mater, 2018. **30**(52): p. e1806132.
245. Even-Ram, S., et al., *Myosin IIA regulates cell motility and actomyosin-microtubule crosstalk.* Nat Cell Biol, 2007. **9**(3): p. 299-309.
246. Vicente-Manzanares, M., et al., *Regulation of protrusion, adhesion dynamics, and polarity by myosins IIA and IIB in migrating cells.* J Cell Biol, 2007. **176**(5): p. 573-80.
247. Levental, I., P.C. Georges, and P.A. Janmey, *Soft biological materials and their impact on cell function.* Soft Matter, 2007. **3**(3): p. 299-306.
248. Wozniak, M.A. and C.S. Chen, *Mechanotransduction in development: a growing role for contractility.* Nat Rev Mol Cell Biol, 2009. **10**(1): p. 34-43.
249. Jaalouk, D.E. and J. Lammerding, *Mechanotransduction gone awry.* Nat Rev Mol Cell Biol, 2009. **10**(1): p. 63-73.
250. Gusyatiner, O. and M.E. Hegi, *Glioma epigenetics: From subclassification to novel treatment options.* Semin Cancer Biol, 2018. **51**: p. 50-58.
251. Lefranc, F., *Editorial: on the road to multi-modal and pluri-disciplinary treatment of glioblastomas.* Acta Neurochir (Wien), 2009.

151(2): p. 109-12.
252. Xu, J., et al., *Rac1 Promotes Cell Motility by Controlling Cell Mechanics in Human Glioblastoma.* Cancers (Basel), 2020. **12**(6).
253. Yang, C., et al., *Mechanical memory and dosing influence stem cell fate.* Nat Mater, 2014. **13**(6): p. 645-52.
254. Stowers, R.S., et al., *Matrix stiffness induces a tumorigenic phenotype in mammary epithelium through changes in chromatin accessibility.* Nat Biomed Eng, 2019. **3**(12): p. 1009-1019.
255. Provenzano, P.P., et al., *Collagen density promotes mammary tumor initiation and progression.* BMC Med, 2008. **6**: p. 11.
256. Mammoto, T., et al., *Role of collagen matrix in tumor angiogenesis and glioblastoma multiforme progression.* Am J Pathol, 2013. **183**(4): p. 1293-1305.
257. Walker, C., E. Mojares, and A. Del Rio Hernandez, *Role of Extracellular Matrix in Development and Cancer Progression.* Int J Mol Sci, 2018. **19**(10).
258. Park, J.S., et al., *Mechanical regulation of glycolysis via cytoskeleton architecture.* Nature, 2020. **578**(7796): p. 621-626.
259. Humphrey, J.D., E.R. Dufresne, and M.A. Schwartz, *Mechanotransduction and extracellular matrix homeostasis.* Nat Rev Mol Cell Biol, 2014. **15**(12): p. 802-12.